A Polyphasic Taxonomy Approach in the Identification of a New Strain of *Penicillium thymicola*

Allison O'Rourke

A Thesis Submitted in Partial Fulfillment
of the Requirements for the Degree of

Master of Chemistry

Department of Chemistry and Biomolecular Sciences
Faculty of Science
University of Ottawa

Supervisors: Dr. Christopher N. Boddy
Dr. David P. Overy

Examining Board: Dr. François-Xavier Campbell-Valois
Dr. Cory Harris

Abstract

Fungal taxonomy has been a consistent challenge in mycology for many decades. This is partly the result of phenotypic instability of fungi across different environments and generations, wherein a species may alter their morphology and secondary metabolite profile in response to their growth conditions. Thus, the use of a polyphasic approach to fungal taxonomy can be used to ensure the proper categorisation of fungal species. The polyphasic approach to fungal taxonomy applies a combination of taxonomic techniques in the identification of a fungal species, including macro- and micromorphological characteristics, phylogenetics and genetic barcoding, and secondary metabolite expression. Presented in this thesis is a polyphasic approach to taxonomize a newly isolated strain of *Penicillium thymicola*, isolated as an actinomycete culture contaminant in a chemical biology research laboratory. Throughout the analysis, the isolated strain is compared with a previously characterized strain of *P. thymicola*, DAOMC 180753. In our approach, three different fungal taxonomy techniques are applied to compare the two *P. thymicola* strains to each other and to the previously established *P. thymicola* type strain description. The fungal strains' macro- and micromorphological phenotypes were analyzed on six different media types, a phylogenetic analysis was performed using accepted *Penicillium sp.* barcode gene sequences, and their metabolomic profiles were characterised via UPLC-HRMS. Based on these investigations, it was determined that the newly isolated strain was, in fact, a strain of *P. thymicola*. However, the previously characterised strain DAOMC 180753 diverged from the official species description in both the morphological and metabolomic analyses, which were the result of either strain degeneration or species misidentification.

Dedication

Voor mijn moeder Jennifer en zus Emily

Zonder jullie beiden zou niets wat ik heb gedaan mogelijk zijn geweest

Acknowledgements

I have been massively fortunate to work with two incredible groups of scientists during my graduate degree, without whom this body of work would not have been possible.

I want to first express my unending gratitude to Chris Boddy, my first supervisor, for his unconditional support of my work, his expert scientific guidance, and for laughing at my jokes. I can't fully put into words (shocking, I know) how your encouragement and steadfast belief in my abilities has altered the course of my life. Thank you. I am less grateful for the diet coke addiction that I will now have to shake. To Jordan, my first mentor as an undergrad, and now my forever friend, thank you for your advice and for all our hot girl walks. Without you, I could not have survived grad school. To Ishaan, thank you for working with me on the bacteria projects that unfortunately did not make the cut – you are a great scientist, and I am so excited to see where you go in life. To the other past and present members of the Boddy Lab, thank you for 3 years of friendship and incredibly high-stakes games of pool.

To the Overy Lab, thank you for making me feel like family for the past 10 months. To Dave Overy, thank you for taking a chance on my project, for your unbelievably vast penicillium expertise and for your constant support. I am forever indebted to you for taking my half-baked penicillium project and turning it into coherent science. To Tom, thank you for your assistance with my genome assembly, and your incredibly Witt-ey humour. To Jonathan, thank you for being a wizard with a microscope and assisting me with the stunning images in this thesis. I want to also thank Amanda for running my samples on the UPLC-HRMS. To Carmen, thank you for everything because we both know that without you, I'd still be crying over R errors. To you and Anne, I simply promise that I will NEVER attempt to extract DNA from a eukaryotic organism ever again. Ever.

To my mom and sister, who have listened to me talk about "the lab" for too many years at this point, thank you for being the two constants in my life. I know you both think I "do proteins" (it hasn't been proteins in 3 years), but nothing I have ever accomplished would have been possible without you. I love you both endlessly. To Dr. Alain St-Amant, thank you for the unwavering belief you have had in me since my second year – I would not have made it here without having

you in my corner. To my other dear friends from inside and outside the lab, thank you for your support throughout these years – you are also my family.

Finally, if I cannot be remembered for my body of work, may I at least be remembered for the Danny Devito throw pillow.

Table of Contents

List of Tables

List of Figures

List of Symbols, Nomenclature and Abbreviations

A: Adenylation domain

Ant: Anthranilic Acid

antiSMASH: antibiotics & Secondary Metabolite Analysis Shell

BGC: Biosynthetic Gene Cluster

BLAST: Basic Local Alignment Search Tool

bp: Base pair(s)

BUSCO: Benchmarking Universal Single-Copy Orthologue tool

C: Condensation domain

CCFC: Canadian Collection of Fungal Cultures

CMD: Calmodulin

CREA: Creatine Sucrose Agar

CYA: Czapek Yeast Agar

CYANY: Czapek Yeast Agar + Nystatin

ddNTPs: 2',3'-dideoxynucleotide triphosphates

DG18: Dichloran Glycerol

gDNA: Genomic DNA

GOI: Gene Of Interest

HRMS: High Resolution Mass Spectrometry

HRMS/MS: High Resolution Mass Spectrometry/Mass Spectrometry

IARC: International Agency for Research on Cancer

ICTF: International Committee on the Taxonomy of Fungi

ISP2: International Streptomyces Project 2 Media

ITS: Internal Transcribed Spacer

JGI: Joint Genome Institute

MEA: Malt Extract Agar

MIBiG: Minimum Information about a Biosynthetic Gene cluster

MIC: Minimum Inhibitory Concentration

MQ: MiliQ

m/z: Mass-to-charge ratio

NCBI: National Center for Biotechnology Information

NEB: New England Biolabs

NGS: Next Generation Sequencing

NRPS: Non-Ribosomal Peptide Synthetase

OMA: Oatmeal Agar

PC: Principal Component

PCA: Principal Component Analysis

PCR: Polymerase Chain Reaction

Ppant: 4'-phosphopantetheine arm

RCDPS: Arginine-containing cyclodipeptide synthase

RPB2: RNA Polymerase II second largest subunit

rRNA: Ribosomal RNA

RT: Retention Time

ssDNA: Single-stranded DNA

T: Thiolation domain

TE: Thioesterase domain

TLC: Thin Layer Chromatography

UPLC: Ultraperformance Liquid Chromatography

XIC: Extracted Ion Chromatogram

YES: Yeast Extract Sucrose

YESNY: Yeast Extract Sucrose + Nystatin

Chapter 1: The Evolution of Fungal Taxonomy and Insights into *Penicillium* Species of Fungi

1.1 Applications of Fungi in Nature

Fungi are ubiquitous in nature and continuously interact with other living organisms in their environment. Fungi can be both 'friend and foe': certain fungal species act as crop pathogens that negatively impact natural resources, leading to food spoilage, while others can produce clinically and industrially relevant compounds. Fungal species that impact agricultural production include *Fusarium graminearum,* which infests cereal crops[1] and *Penicillium digitatum,* which causes green mould disease in oranges.[2] While the pathogenicity of some species paints fungi in a negative light, many other species are beneficial to society. The most notable example is *Penicillium rubens,* which revolutionized modern medicine by producing the first clinically effective antibiotic, penicillin, discovered by Alexander Fleming in 1928.[3] Other fungal species also provide significant benefit to the food industry, such as *Pencillium caseicolum*[4], used in Camembert cheese, *Penicillium roqueforti,*[5] used in Roqueforti cheese. The widespread utilisation of fungal species across various sectors of society stems from the abundant and unique secondary metabolites they produce, making fungi an important source of industrially and clinically relevant compounds. As such, they also present unique research opportunities for the discovery of novel compounds and the elucidation of their biosynthesis.

1.2 The History of Taxonomical Classification in Mycology

Fungi were first formally recognized as a distinct group of organisms by Linnaeus within the category of '*Regnum Vegetabile*' in the late 1700s.[6] The field of fungal taxonomy originated with the seemingly simple goal of organizing fungal species into groups based on shared visual characteristics, or their morphology.[7] Even though this strategy initially succeeded at differentiating ascomycete from basidiomycete species, it unfortunately resulted in the misallocation of numerous genetically unrelated fungal species due to their shared phenotypic characteristics.[7] Although colony texture and colour were once used as the basis of fungal taxonomy, they have since been determined to be subjective criteria unrelated to a fungal species' evolution.[8] The problem of fungal misidentification was further exacerbated by the dual nature of certain fungal species, as some species possess distinct sexual and asexual reproductive states. The field of taxonomy is continuously evolving, but our need as researchers to have accurate means of identifying the microorganisms we study remains constant.

1.3 One Fungus = One Name

The Amsterdam Declaration represents a crucial turning point in the world of fungal taxonomy. Prior to this symposium held by the International Committee on the Taxonomy of Fungi (ICTF) in April 2011, pleomorphic fungal species, or fungi who possess both sexual and asexual reproductive states, existed under a dual nomenclature system wherein their teleomorph (sexual) and anamorph (asexual) states were each given a unique name.[9–11] This was because it was assumed that the teleomorph state of a fungal species was superior to the anamorph state when analysing evolutionary relationships of fungi.[12] The use of this dual nomenclature system resulted in naming chaos in mycology, a problem which continues to exist today. The Declaration by the

ICTF enacted the official transition to a single-name nomenclature system for all fungi.[9] The names of the teleomorph states of fungi were given priority in naming, except for in cases where the anamorphic name is more widely recognized, the most notable example being the continued use of the anamorph name *Penicillium* instead of the teleomorph *Talaromyces*. Despite the Amsterdam Declaration having been passed over a decade ago, the legacy of dual nomenclature in fungal taxonomy lives on. A notable modern problem with a fungal species existing under two different names is brought about with the use of databases such as GenBank to compile and compare fungal DNA sequences.[11] One barcode gene sequence may be filed under two or more completely different names in these databases, altering the data users are collecting and compiling, and making it challenging to access relevant genetic information.

1.4 The Polyphasic Approach to Fungal Taxonomy

The classical approach to fungal taxonomy that relied solely on morphology has since been expanded, giving rise to the polyphasic approach to fungal taxonomy. This practice employs multiple taxonomic strategies such as an organism's secondary metabolite profile (chemotype) and genetic markers and phylogenetics (genotype), in addition to phenotypic characteristics like colony morphology and conidial micromorphology (**Figure 1.4.1**).[13–15] Although this polyphasic approach was initially proposed by Vandamme *et al.* in 1996[16] for the taxonomy of bacterial species, this approach has since been successfully implemented in fungal taxonomy.[13,14] The integration of each unique taxonomic feature of a given fungal species in polyphasic taxonomy provides a higher level of robustness than the traditional morphological approach, enhancing the robustness of the taxonomic conclusions.[13–15]

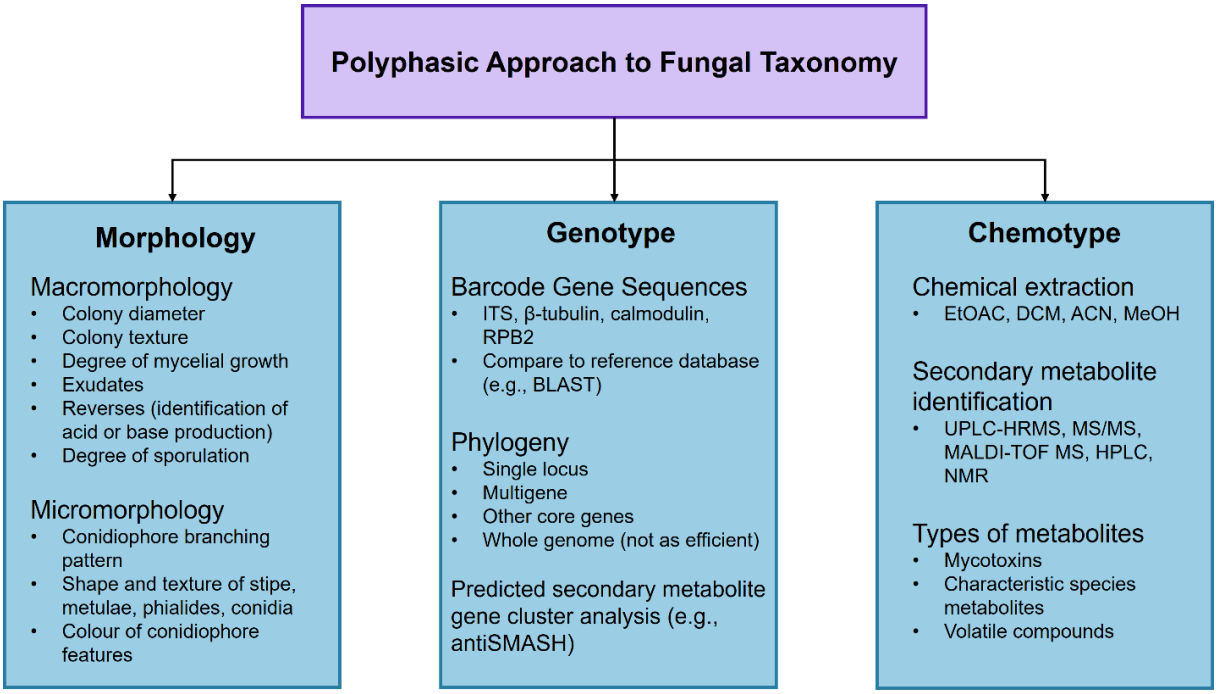

Figure 1.4.1 - Features of consideration in a polyphasic approach to fungal taxonomy. Adapted from Visage *et al.* (2014)[17] and Vandamme *et al.* (1996).[16] The polyphasic approach to taxonomy includes but is not limited to: morphological traits, genotype information, phylogenetic classification, and elements of chemotaxonomy.

1.5 The Phylum Ascomycota

Fungi comprise the second largest kingdom of eukaryotes, second only to Kingdom Animalia. This diverse kingdom of life definitionally includes unicellular and multicellular organisms that develop from spores and incorporate glucans and chitin in their cell walls, distinguishing their species from plants and animals alike.[18] Within this kingdom, Ascomycota is the largest phylum, comprising approximately 64,000 identified species.[19] Ascomycetes may act as mutualists, parasites, or pathogens of animals, plants, and other fungi.[20] Despite many species being identified only in their anamorphic state,[20] ascomycetes derive their name from the

characteristic formation of ascospores within an internal sac called an ascus in their sexual state, giving the species the colloquial name of 'sac fungi'.[21]

The phylum Ascomycota is predominantly comprised of filamentous fungi, but also includes yeasts that proliferate in both terrestrial and aquatic environments.[22] Filamentous ascomycetes germinate from spores and grow into colonies that consist of a system of cylindrical hyphal filaments called the mycelia.[21] Ascomycete hyphae have crosswalls called septa, which separate the compartments of the mycelia.[21] Hyphae grow through apical elongation, where cell wall material is continuously delivered to the apex, allowing the hyphal tip to continuously extend.[23,24] The apical growth of fungal hyphae allows fungal colonies to broaden their reach by extending hyphal filaments into their immediate environment. This tactic is exceptionally useful because it allows fungi to continue foraging for nutrients when the environment surrounding the parent mycelium is exhausted.[25] Spores from aerial hyphae may then be carried across great distances, increasing the fungus' proliferation.

1.6 Fungal Secondary Metabolism

Fungi are renowned as some of the most prolific producers of secondary metabolites in the natural world.[26] While primary metabolites are highly conserved in all organisms, secondary metabolites are incredibly structurally diverse compounds, giving rise to many unique natural products. Secondary and primary metabolism differ in their necessity for a microorganism's growth and proliferation, particularly in a nutrient-complete laboratory environment. Primary metabolism involves the production of metabolites that are essential for the growth and proliferation of an organism.[27] Secondary metabolism produces compounds that, while not absolutely required for the survival of the producing organism, are actively involved in fungal

development and how a species interacts with other organisms.[28,29] In nature, secondary metabolites play an active role in countering abiotic and biotic stress encountered in an organism's environment.[30] Secondary metabolites are assembled from condensation reactions with primary metabolite building blocks such as amino acids, carbohydrates (particularly pentoses and hexoses), short-chain fatty acids, and isoprene derivatives.[31,32] In fungi, secondary metabolism is often associated with the process of sporulation, the point at which fungi produce sexual or asexual spores.[33,34]

Fungal secondary metabolism is regulated on multiple levels of specificity, and certain pathways may be regulated globally and/or via pathway-specific regulators.[35–37] The genes that encode enzymes responsible for the biosynthesis of secondary metabolites and their regulation are often clustered together within the organism's genome, referred to as biosynthetic gene clusters (BGCs).[38] Transcription factors make up an important part of both global and pathway-specific biosynthesis regulation. Global transcription factors are encoded by genes not belonging to any specific BGC, whereas pathway-specific regulators are typically situated within the BGC they regulate.[39] The biosynthesis of secondary metabolites is also highly impacted by certain stimuli in the microorganism's environment – notably the pH, temperature, competition with other organisms, and the amount of light exposure received.[40–42] Thus, the composition of a growing microorganism's substrate is significant, particularly when looking at the nature and concentration of the carbon and nitrogen sources. When specifically considering filamentous fungi, the nutrient availability in the immediate environment can be determined by the organism and their metabolism adjusted to optimise energy usage, growth, and reproduction.[43]

1.7 The Genus *Penicillium*

Fungi of the genus *Penicillium* are ever-present in nature, inhabiting diverse habitats such as Antarctica,[44,45] deep-sea sediments,[46] and acidic environments, where they demonstrate impressive heavy metal resistance.[47,48] At present, researchers have isolated and identified over 350 species of *Penicillium* from nature, with this number evolving as new species are discovered, old ones are re-categorized, and/or duplicate species are removed from the official classification.[17] Most species of *Penicillium* are saprophytic organisms that accumulate nutrients through the decomposition of organic materials, thus a large portion of identified species are isolated from soil samples.[49] In addition to being saprophytes, a variety of *Penicillium* species are also fungal necrotrophs,[50] releasing a broad-range of sometimes host-specific toxins into their substrate.[51] Many *Penicillium* species also display halotolerance, allowing these species to proliferate in highly saline environments.[52]

1.8 Taxonomical Classification of *Penicillium sp.*

The name *Penicillium* is derived from the latin term '*penicillum*', meaning 'brush', attributed to the genus by J. H. F. Link in 1809, wherein he described the morphology of *Penicillium* colonies as 'tufts' of spores.[53] In this monograph, Link identified and described the first three known *Penicillium* species: *P. candidum, P. glaucum,* and *P. expansum.*[53] Since the discovery of the first *Penicillium* species of fungi, the total number of species in this genus has waxed and waned as identification methods have evolved and become more precise. Taxonomically, the genus *Penicillium* is a member of the *Eurotiomycete* class, the *Eurotiales* order, and the family *Aspergillaceae* (**Figure 1.8.1**). Due to the evident challenges present in *Penicillium* taxonomy and the observations of intraspecies morphological variations, Charles

Thom outlined standard operating practices for the classification and identification of *Aspergillus* and *Penicillium* species in 1954.[54] Thom's adamance for this meticulous and rigorous approach to working with fungi has been echoed by the modern-day heroes of *Penicillium* taxonomy: Robert A. Samson and J. I. Pitt[55], Jens C. Frisvad[8,14], and Toru Okuda.[56]

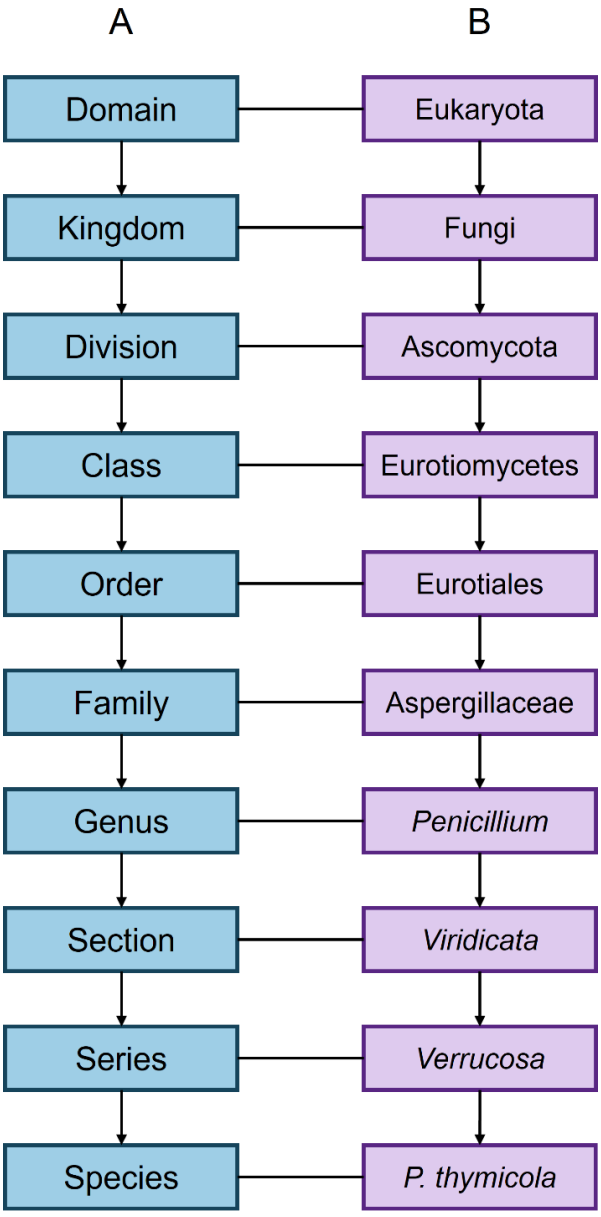

Figure 1.8.1 - Scientific classification system for *Penicillium sp.* and for *Penicillium thymicola*. A. General division of the scientific classification system in taxonomy from Domain to Species. **B.** Division of scientific classification for the species *Penicillium thymicola.*

While morphological characteristics were initially used to classify *Penicillium* species for nearly 180 years following Link's initial discovery, the emergence of new taxonomic characteristics and tools, such as DNA sequencing technology in the 1990s, gave researchers the ability to increase the precision of mycological taxonomy. These new techniques include secondary metabolite profiling,[8,57] using accepted fungal barcode DNA sequences (e.g., internal transcribed spacer (ITS)[58] and β-tubulin[17]) and phylogenetic analyses.[59] Unfortunately, these new and combined strategies have not always been enough to eliminate the challenges in species identification in the *Penicillium* genus. Outdated and varied lists of the accepted species coupled with the incomplete or inaccurate databases continue to pose problems for mycologists aiming to add new species to the already massive amount of information found in databases.[17]

1.9 *Penicillium thymicola*

Penicillium thymicola is a relatively uncommon species of the *Penicillium* genus, first described by Frisvad and Samson in 2004.[14] This species of fungi was aptly named after its herb of origin, thyme, but has since also been isolated from other herbs, sorghum, and soil.[14] Geographically, this fungal species has been found in the Czech Republic, Greece, Sudan, the United States of America, and Canada.[14,60] Like various other *Penicillium* species, *P. thymicola* is halotolerant and can proliferate in environments with high salinity.[14,61] *P. thymicola* is also psychrotolerant, thus can propagate at low temperatures, such as the standard refrigerator temperature of 4°C.[14,62]

1.10 *Penicillium thymicola* Known Metabolites

Of the hundreds of known secondary metabolites produced by the genus *Penicillium*, only a handful are confirmed to be synthesized by *Penicillium thymicola*. The secondary metabolites that have been identified from the *P. thymicola* type strain, IBT 5891, are shown in **Figure 1.10.1 A** and include alantrypinone[63], anacine[14], daldinin D[64], fumiquinazolines F and T[63,65], PC-2[14], pestafolide A[65], serantrypinone,[64] verrucolone[14], and 2-methylisoborneol.[14] In the official species description of *P. thymicola,* Frisvad and Samson stipulate that the presence of alantrypinone and fumiquinazoline F are diagnostic metabolites of this species.[14] Beyond *P. thymicola* IBT 5891, the strain *P. thymicola* DAOMC 180753, isolated from Canadian cheddar cheese in 1980, was found to produce ochratoxins A and B, in addition to PC-2, fumiquinazoline F, and alantrypinone by Nguyen and colleagues in 2016 (**Figure 1.10.1 B**).[60] Prior to this work, ochratoxins were known to be produced by various *Aspergillus* and *Penicililum* species of fungi, but this was the first and only research to describe its production in *Penicillium thymicola*.

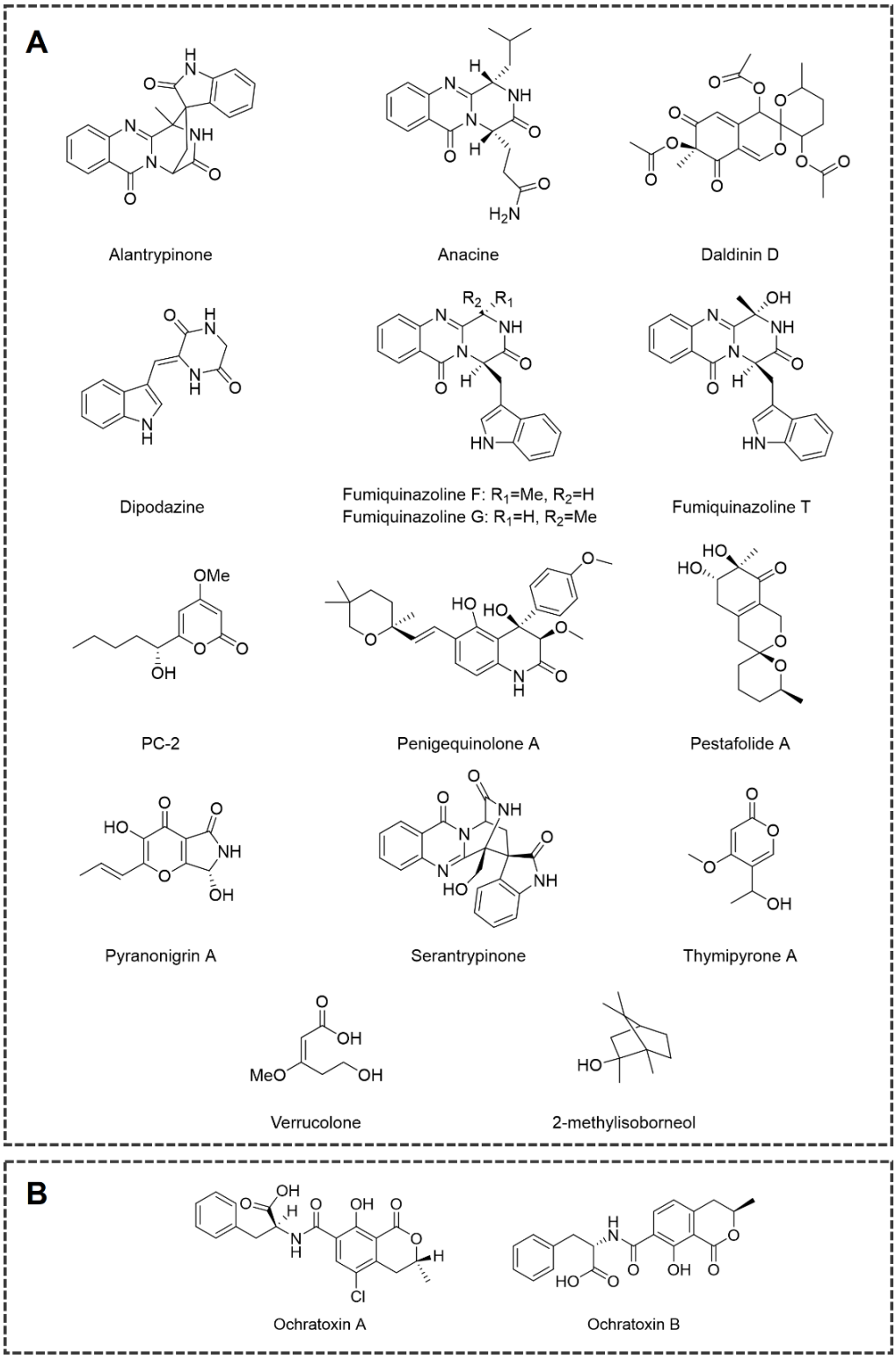

Figure 1.10.1 - *Penicillium thymicola* known metabolites. A. Metabolites isolated from *P. thymicola* IBT 5891. From left to right: alantrypinone, anacine, daldinin D, dipodazine, fumiquinazoline F and G,

fumiquinazoline T, PC-2, penigequinolone A, pestafolide A, pyranonigrin A, serantrypinone, thymipyrone A, verrucolone, and 2-methylisoborneol. **B.** Ochratoxins A and B, isolated from *P. thymicola* DAOMC 180753 in 2016.

1.11 Exudation in Fungi

Organisms employ numerous different mechanisms to store, discard, and use the metabolites they produce to maintain homeostasis. Referred to as 'guttation' in plant species, fungi are capable of excrete water and water-soluble metabolites from their hypha.[66,67] These droplets, known as exudates, are mainly composed of secondary metabolites, carboxylic acids, carbohydrates, and to a lesser degree, fatty and amino acids.[68] The phenomenon of fungal exudation has been described since the 19th century.[69] The specific environmental conditions required for a fungus to produce exudate varies between species and are known to only occur during a specific period in the fungal growth cycle.[66] Interestingly, there are descriptions of fungi that readily produce exudate in a laboratory setting but have not been found to do so in nature. This brings about a great mycological question: why do fungi produce exudate?

There are three main hypotheses that aim to answer this question. No single theory can explain the phenomenon in all exudate-producing fungi, thus several of these theories may be accurate at any given time, depending on the sample. In 1991, Jennings posited that a fungus may produce exudate to retain moisture in young aerial hyphae for a more consistent and rapid growth rate.[70] Using mathematical modeling of water volume in conjunction with fungal growth rates, Jennings described how water retention allows the fungus to maintain turgor, even in conditions with an unfavourable water potential.[70] More recently, fungal exudates have been proposed to act as a metabolite reservoir due to the sheer number of compounds, notably carbohydrates and fatty acids, present in them.[71–73] In their study published in 2010, Hutwimmer *et al.* demonstrated that a combination of more than one carbon source and well-metabolized, non-preferred sugars, could

promote exudation in *Metarhizium anisopliae.*[74] In addition to culture composition, temperature can impact the occurrence of this phenomenon, as exudates were primarily produced in cultures incubated in temperatures ranging from 20-30ºC.[74] In *Sclerotinia schlerotiorum*, the excretion of nutrients collected in fungal exudates, such as sugar alcohols, trehalose, and lauric and heptadecanoic acid was thought to regulate internal physiological mechanisms and accompany the development of structures like fungal sclerotia.[75,76]

1.12 Nystatin as an Antifungal

Nystatin is a member of the polyene macrolide antimicrobial group, a fungicidal family that also includes the frequently used antifungal amphotericin.[77] Polyene antifungals are characterised by the presence of four to eight conjugated double bonds within a macrolactone ring, as demonstrated in the chemical structure of nystatin, shown in **Figure 1.12.1**.[78–80] Nystatin is an amphipathic compound and its mechanism of action involves the formation of an antifungal-sterol complex in the host organism's cell membrane, which is thought to be facilitated by its unique chemical structure. The antifungal-sterol complex creates a barrel-like channel through the cell's plasma membrane, increasing its permeability to small molecules, thus causing the leakage of cell constituents, disruption of cellular metabolism, and eventually, cell death.[80–82] There has been scant research into the antifungal effects of nystatin on filamentous fungi, particularly with regards to *Penicillium* species. Stanley and English (1965) found that the presence of nystatin at a minimum inhibitory concentration (MIC) in liquid media lengthened the lag phase of growth in four *Aspergillus sp.,* which eventually would be rectified by the nystatin in the media breaking down.[83] While Stanely and English described their results within the context of an era where it was believed that nystatin resistance in filamentous fungi was an incredibly rare occurrence, our

modern-day age of antimicrobial resistance calls this assertion into question. Within the last decade, clinicians and researchers alike are taking notice of filamentous fungi exhibiting resistance to polyene macrolide antifungals, and the occurrence of fungal species altering their responses to the most effective antifungal agents must not be ignored.[84–86]

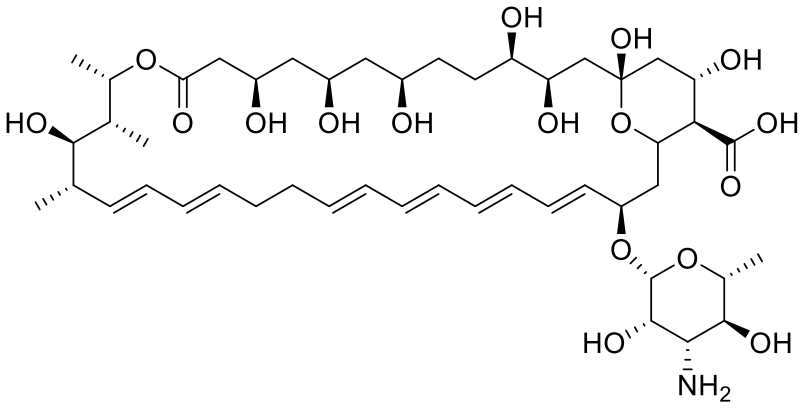

Nystatin
$C_{47}H_{75}NO_{17}$
Exact Mass: 925,50

Figure 1.12.1 - Nystatin Chemical Structure.

1.13 Thesis Overview

A novel fungal strain was isolated from a chemical biology research laboratory at the University of Ottawa, in Ottawa, ON Canada in 2022. The fungal strain was originally identified as a contaminant from a *Streptomyces sp.* culture, and was found to be resistant to common antifungals, such as nystatin. The infusion of nystatin in the growth medium triggered phenotypic changes in the antifungal-resistant colonies, including the production of fungal exudates and delayed sporulation. Due to the interesting response in growth from the fungal species,

understanding the isolate's taxonomic classification and investigating its secondary metabolite profile during its exposure to nystatin became the focus of this research thesis. Preliminary taxonomic identification of the fungal species via sequencing of the β-tubulin gene and BLAST database search by the Overy Lab suggested that this species was a strain of *Penicillium thymicola*. In this thesis, we explore the differences between a previously characterized strain of *P. thymicola,* DAOMC 180753, and the novel strain, CHEM 5317 using a polyphasic approach: a classical taxonomy approach based on morphology (Chapter 2), a phylogenetic evaluation (Chapter 3), and a chemotaxonomic approach using untargeted metabolomics (Chapter 4). The work of this thesis aims to exemplify the necessity of utilising taxonomic approach that implements multiple strategies when working with *Penicillium* species of fungi.

Chapter 2: Morphological Analysis and Comparison of new *P. thymicola* Isolate to Previously Characterized Strain DAOMC 180753

2.1 Introduction

2.1.1 Morphology as a Taxonomic Approach

Historically, the utilisation of macro- and micromorphological characteristics in fungal taxonomy was the first-line approach used by mycologists, and as such, is considered to be the classical approach to fungal taxonomy.[8] Various physical characteristics of fungal colonies have been employed to categorize species with similar features. The following macromorphological traits are typically considered when using a morphological approach to fungal taxonomy: diameter of colonies that have been three-point inoculated on solid media, colony texture, colour of conidia and mycelium, presence of soluble pigments, presence of exudates, colony reverses, and the degree of growth and acid or base production on Creatine Sucrose Agar (CREA).[17]

2.1.2 *Penicillium sp.* Macromorphology

Penicillium species of fungi can be easily recognized by the characteristic blue-green hue of their mycelium.[87] In addition, the colonies of *Penicillium sp.* may exhibit one of a variety of textures. Differences in colony textures in *Penicillium sp.* of fungi are the result of the manner in which the species' conidiophores are interwoven on the micromorphological level (**Figure 2.1.1**).[87] Colony textures may be described as velutinous, lanose, funiculose, fasciculate or synnematous.[87] A velutinous colony texture is soft and plush due to conidiophores emerging erect from the substrate (**Figure 2.1.1 A i**), a lanose colony texture is due to the conidiophores

intertwining in long aerial hyphae (**2.1.1 A ii**), a funiculose colony texture is the result of prostrate bundled hyphae (**Figure 2.1.1 A iii**), and a fasciculate or synnematous colony texture is the result of conidiophores forming loosely or compactly bundled hyphae (**Figure 2.1.1 A iv-vi**).[87]

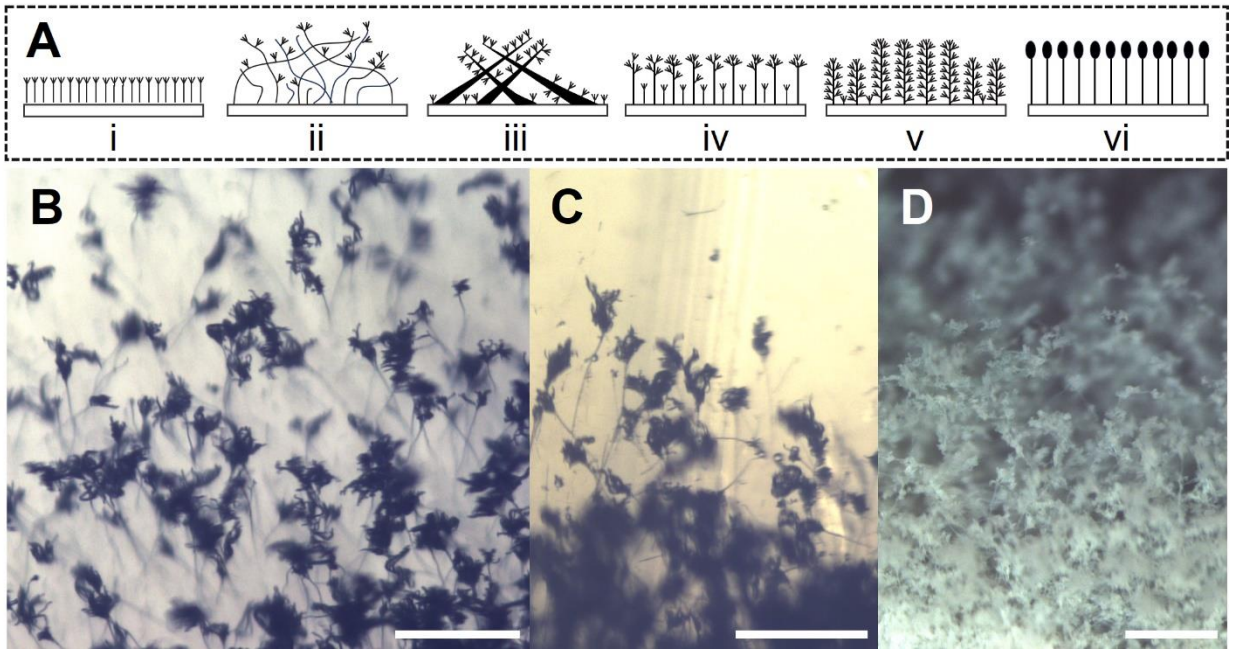

Figure 2.1.1 - How conidiophores contribute to colony texture. A. Overview of different colony textures found in *Penicillium sp*. **i.** Velutinous **ii.** Lanose **iii.** Funiculose **iv – vi.** Fasciculate **B.** CHEM 5317 grown on CYA agar for 14 days at 25ºC. Scale bar = 25 µm. **C.** CHEM 5317 on CYA grown for 14 days at 25ºC. Scale bar = 25 µm. **D.** CHEM 5317 grown on CYA for 14 days at 25ºC. Scale bar = 75 µm.

2.1.3 *Penicillium sp.* Micromorphology

The micromorphological characteristics included in taxonomic analyses of *Penicillium* species focus on substructures of the strain's conidiophore. This stalk structure in *Penicillium* micromorphology is the portion of the fungus that undergoes asexual reproduction, producing conidia, the reproductive spores, at the apex[88] (**Figure 2.1.2**). As shown in **Figure 2.1.2**, the phialides are flask-shaped structures from which the conidia are expelled and reside between the metulae and the conidia. Conidia are produced in long chains in *Penicillium sp.*, and their exact shape varies between species. Conidia may be globose, ellipsoidal, cylindrical, or fusiform in

shape, green in colour and possess either smooth or rough walls. The characteristics of the *Penicillium* conidiophore typically described in *Penicillium sp.* taxonomy include the dimension, shape, and texture of the stipe, metulae, and conidia; the number of branching points between the stipe and phialides; the number of vesicles; the shape and size of the phialides; presence of cleistothecia, and aspects of asci and ascospores in sexually reproducing species.[17,57]

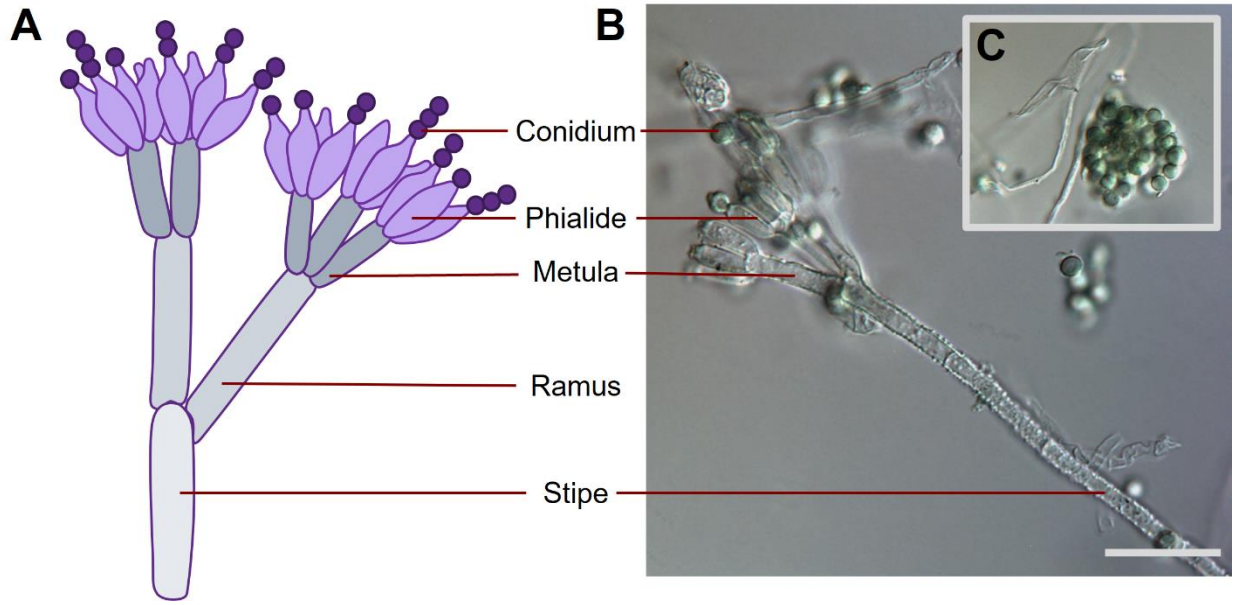

Figure 2.1.2 - Structure of a *Penicillium* conidiophore. A. Diagram depicting structure of a *Penicillium* conidiophore. Includes relevant substructures such as the stipe, rami, metulae, phialides, and conidia. **B.** CHEM 5317 grown on CYA, growth day 14. Scale bar = 5 µm. **C.** Close-up of a clump of conidia from CHEM 5317 on CYA, growth day 14. Scale bar in **B**.

As briefly discussed above, different levels of branch pattern complexity exist in different *Penicillium sp.,* and the number of branch points between the stipe at the bottom of the conidiophore and the phialides, the flask-shaped cells where conidia emerge at the apex of the conidiophore, are useful for differentiating between species.[87] As shown in **Figure 2.1.3**, single conidiophores are monoverticillate (**Figure 2.1.3 B**); conidiophores exhibiting a simple to complex branching pattern with multiple branches are divaricate (**Figure 2.1.3 C**); one-stage level

branching is biverticillate (**Figure 2.1.3 D, E**); two-stage level branching is terverticillate (**Figure 2.1.3 F**); and three-stage level branching is quaterverticillate (**Figure 2.1.3 G**).

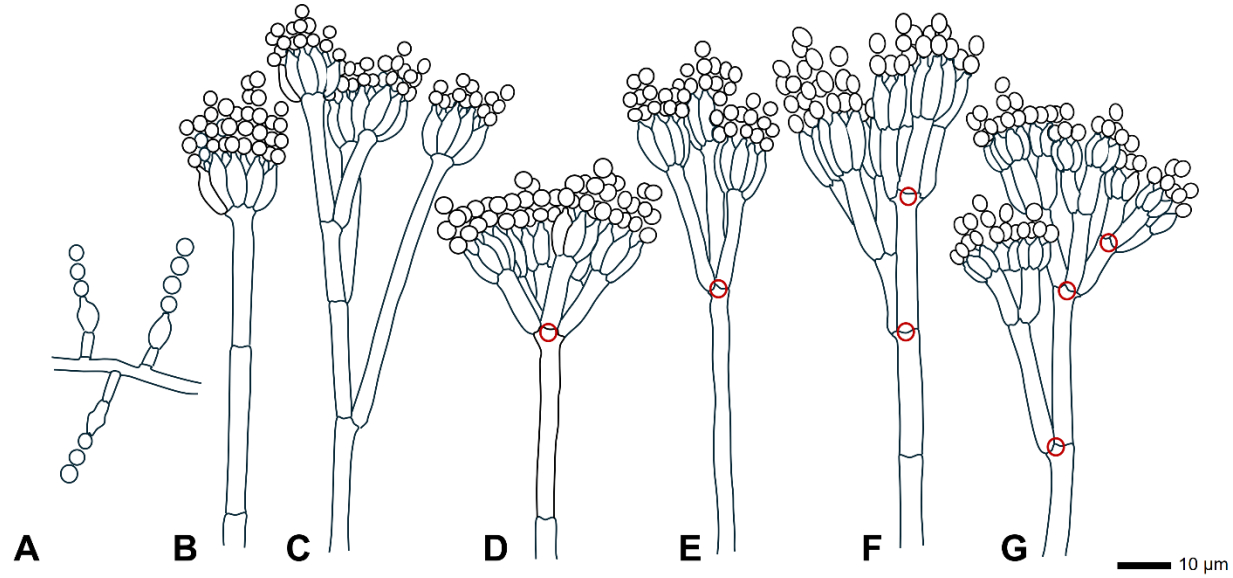

Figure 2.1.3 - Conidiophore branching patterns in *Penicilllium sp.* Adapted from Visagie *et al*. (2014).[17] Scale bar = 10 µm. Branching points are indicated with a red circle. **A.** Conidiophores with solitary phialides. **B.** Monoverticillate. **C.** Divaricate. **D, E.** Biverticillate. **F.** Terverticillate. **G.** Quaterverticillate.

2.1.4 *Penicillium thymicola* Morphology

The official species description of *Penicillium thymicola* by Frisvad and Samson states that the species exhibits a velutinous colony texture due to conidiophores born from subsurface hyphae and on a micromorphological level, terverticillate conidiophores.[14] Other specific micromorphological characteristics of *P. thymicola* from this species description are outlined in **Table 2.1.1**. In addition to these micromorphological traits, *P. thymicola* was also stated to produce yellow exudate when grown on Czapek Yeast Agar (CYA).[14]

Table 2.1.1 – *Penicillium thymicola* official species description. Official species description of micromorphological characteristics of *P. thymicola* adapted from Frisvad and Samson (2004).[14]

Conidiophore Substructure	*P. thymicola* Description	Size (µm)
Conidia	Green; rough-walled; globose to sub-globose in form	2.6 – 3.2
Phialides	Cylindrical, tapering	7-9 x 2.5-3.0
Metulae	Cylindrical	8-14 x 3.2-4.4
Rami	Cylindrical	10-20 x 3.5-4.5
Stipe	Rough-walled	200-500 x 3.5-4.2

2.1.5 Chapter 2 Overview

In this chapter, the macro- and micromorphology of the newly isolated strain of *P. thymicola,* CHEM 5317, was compared against the previously characterised strain, DAOMC 180753, and the official species description of *P. thymicola* IBT 5891. The *P. thymicola* strains were grown on six different media types, two containing the antifungal nystatin, to investigate how changes in growth medium affected the macro- and micromorphological characteristics exhibited by both fungal strains. These observations were utilised to establish major phenotypic differences between the CHEM 5317 and DAOMC 180753 strains.

2.2 Materials and Methods

2.2.1 Phenotypic Characterization

CHEM 5317 was isolated as a *Streptomyces sp.* culture contaminant in the laboratory, originally from International Streptomyces Project 2 (ISP2) agar. The *P. thymicola* DAOMC 180753 strain was obtained on solid media, curtesy of the Canadian Collection of Fungal Cultures

(CCFC). A small amount of fungal mycelium was scraped from the solid media and spores were diluted in MiliQ (MQ) water to inoculate new solid media. Serial dilutions were performed in order to obtain single spore colonies. To three-point inoculate the six solid media used in these experiments, spores were suspended in semi-solid agar and plates were inoculated using a needle. CHEM 5317 and DAOMC 180753 were inoculated on the following six solid media, in hexicate: Czapek Yeast Agar (CYA), Yeast Extract Sucrose (YES), Oatmeal Agar (OMA), Dichloran Glycerol (DG18), CYA with nystatin (CYANY), and YES with nystatin (YESNY). Exact media formulations can be found in **Appendix 2A**. Cultures were grown for 14 days at 25ºC in the dark. Colony growth was measured after 14 days of growth by measuring the diameter of the widest portion of a colony and general macromorphological characteristics were recorded after the standard 14-day growth period.

2.2.2 Micromorphological Characterization

Micromorphological characterization was performed from 7-day old colonies grown on CYA media. Conidiophore micromorphology was assessed using a BX50 compound microscope (Olympus, Tokyo) coupled with an Infinity X USB microscope camera and Infinity Capture software (Lumenera, Ottawa). Spores were mounted on glass slides using 60 % lactic acid. Colony surface architecture (i.e. the colony texture on micromorphological level) was analyzed using an Olympus SZX12 dissecting microscope.

2.3 Results and Discussion

2.3.1 Macromorphological Analysis of CHEM 5317 and DAOMC 180753

The growth of CHEM 5317 and DAOMC 180753 was recorded by measuring each individual colony's diameter on each media and averaging these values for each media type. The average colony diameters for CHEM 5317 and DAOMC 180753 for each media type and their standard deviations are found in **Table 2.3.1**.

Table 2.3.1 - Average colony diameters of CHEM 5317 and DAOMC 180753 on growth day 14. Colony diameters were measured on day 14 of growth across the widest part of the colony. Diameters were recorded for each colony on the three-point inoculated plate and averaged for each plate, then averaged across all six replicates of the media type.

Media	CHEM5317 (cm)		DAOMC180753 (cm)	
	Colony diameter (cm)	StDev (cm)	Colony diameter (cm)	StDev (cm)
CYA	2.79	0.0838	3.82	0.210
YES	2.42	0.404	3.15	0.458
DG18	1.91	0.654	0.942	0.112
OMA	1.23	0.0305	3.84	0.111
CYANY	1.27	0.0598	3.40	0.144
YESNY	1.52	0.102	3.70	0.300

CHEM 5317

The observed phenotype of the CHEM 5317 colonies differed noticeably across the six different media employed in this experiment, which was anticipated due to the differences in carbon sources in each media composition. Three of the six media types, CYA, OMA, and CYANY exhibited colonies consistent with the general phenotype of *Penicillium* fungal species (**Figure 2.3.1**). More specifically, these colonies possessed a blue-green mycelium with a white 'halo' surrounding the outer circumference of the colony. Exudate was also present on these three media, ranging from clear on OMA to a more vibrant yellow on CYA and CYANY. The phenotype

of CHEM 5317 was consistent with the official species description of *P. thymicola* on CYA, as it exhibited the anticipated velutinous colony texture, green mycelium, and yellow exudate.

The colony macromorphology shifted more drastically on the low water activity media, DG18, YES, and YESNY (**Figure 2.3.1**). This media appeared to have suppressed growth and sporulation in contrast with the other three media, as evidenced by their lack of sporulation by day 7 of growth on these media. On DG18, the CHEM 5317 colony texture appeared smoother, with a beige centre surrounded by a deep green ring, and white halo. On DG18, the CHEM 5317 colonies were also more appressed to the agar and lacked exudate. The colonies on DG18 were smaller in diameter than the colonies on all other media types and the average colony diameter on this media was 1.91 $\pm$ 0.654 cm, in comparison to CHEM 5317 on CYA which had an average colony diameter of 2.79 $\pm$ 0.0838 cm. On YES and YESNY media, CHEM 5317 was sulcate in appearance, possessing deep grooves on the colony surface, with abundant aerial hyphae. These colonies did not reach sporulation, which was indicated by a lack of colour change from white to green during the 14-day growth period, instead exhibiting a cream and pink hue in their mycelia. Interestingly, the colonies on the nystatin-containing medium YESNY produced copious amounts of bright orange exudate (**Figure 2.3.2**), in contrast to the colonies on YES agar alone, which produced no exudate across the six replicates (**Figure 2.3.1**).

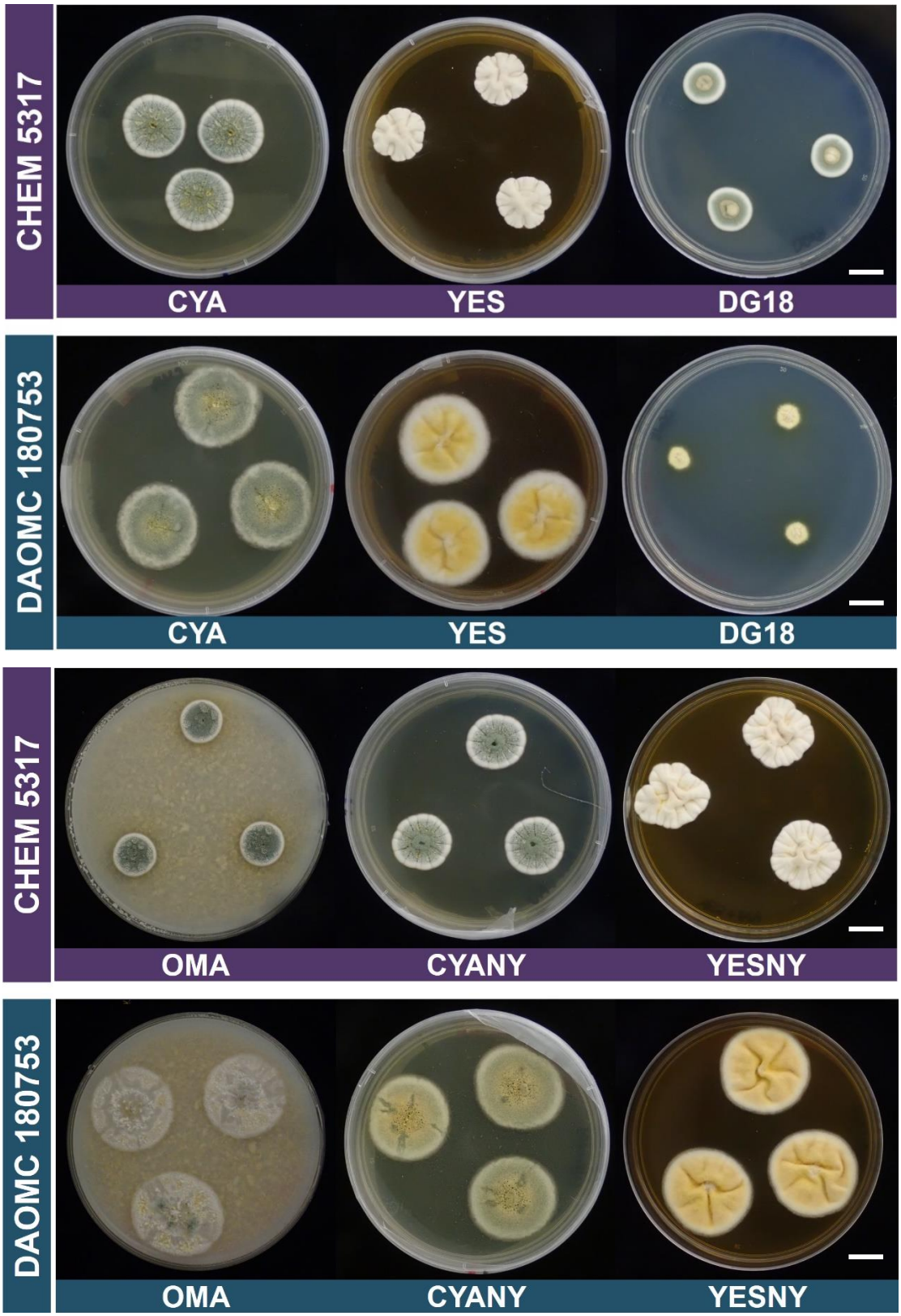
CHEM 5317
CYA
YES
DG18
DAOMC 180753
CYA
YES
DG18
CHEM 5317
OMA
CYANY
YESNY
DAOMC 180753
OMA
CYANY
YESNY

Figure 2.3.1 – CHEM 5317 and DAOMC 180753 colonies on six media types. CHEM 5317 and DAOMC 180753 7-day old cultures, grown at 25ºC in darkness. First row: CHEM 5317 CYA, YES, and DG18. Second row: DAOMC 180753 CYA, YES, and DG18. Third row: CHEM 5317 OMA, CYANY, and YESNY. Fourth row: DAOMC 180753 OMA, CYANY, and YESNY. Error bars in each row = 1 cm.

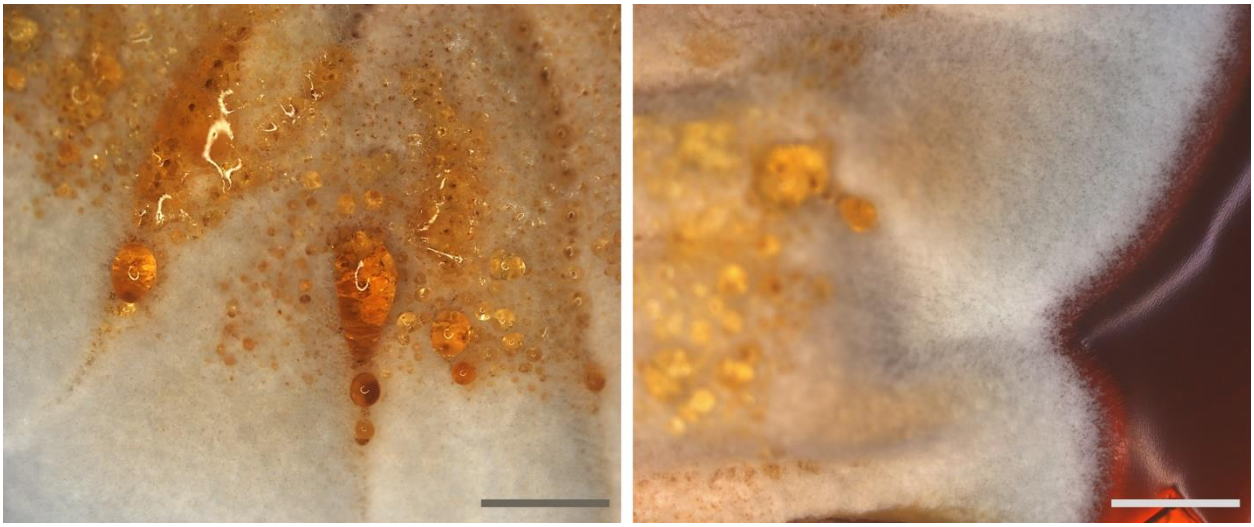

Figure 2.3.2 - Exudate droplets from CHEM 5317 on YESNY agar, growth day 7. CHEM 5317 grown on YESNY agar for 14 days at 25ºC in the dark. Exudates observed as bright orange droplets on colony surfaces. Scale bars = 500 µm.

DAOMC 180753

The macromorphology of DAOMC 180753 appeared to be more heavily impacted than that of CHEM 5317 by the varying nutrient composition of the six media types used in this experiment, as shown in **Figure 2.3.1**. On CYA and CYANY, DAOMC 180753 exhibited an olive-green toned mycelium with a cream-coloured outer halo, consistent with the general appearance of *Penicillium* colonies. The texture between the CYA media with and without nystatin differed slightly, as the colonies on CYA exhibited a much more lanose texture, whereas on CYANY DAOMC 180753 produced fewer aerial hyphae, thus diminishing this trait. The DAOMC 180753 phenotype on CYA was only somewhat consistent with the official *P. thymicola* species description, as this strain exhibited a lanose colony texture instead of the anticipated velutinous

texture and did not possess a strictly green mycelium, expressing a more yellow mycelium toward the center of the colony.

The colonies grown on the low-water activity media, particularly DG18, displayed the most incongruence with the other five media. On DG18 media, the DAOMC 180753 strain struggled to grow and reach sporulation, growing to a meager average colony diameter of 0.942 $\pm$ 0.112 cm retaining a small yellow-green appressed appearance on the surface of the agar. On YES and YESNY, DAOMC 180753 grew with the same lanose texture as observed on CYA and CYANY, but also did not reach sporulation, as was observed on DG18. Instead, the colonies on YES and YESNY exhibited a yellow mycelium and the colonies on YES and YESNY never turned green by growth day 14, indicating that sporulation never occurred for DAOMC 180753 on this medium. Unlike CHEM 5317, the DAOMC 180753 strain underwent a qualitatively significant change in morphology on OMA compared to CYA. On OMA, DAOMC 180753 grew to be white and yellow, scabrous, and granular on the surface of the oat agar. Initially, DAOMC 180753 did not produce exudate on this medium by growth day 7, but at the end of the growth period (day 14), clear exudate had been produced by the majority of the colonies. Similar to CHEM 5317, the DAOMC 180753 strain produced exudate on all media types except for YES without nystatin and DG18.

The absence of exudate production on the DG18 and YES media for both CHEM 5317 and DAOMC 180753 strains is consistent with *Penicillium* growth on low water activity media. As outlined by the media formulations in **Appendix 2A**, DG18 agar contains 220 g of glycerol/L and YES contains 150 g of sucrose/L of media, which impacts the osmotic pressure of fungi growing on this substrate. Certain fungi have been shown to tolerate specific solutes in low water activity media (e.g., sucrose), better than others.[89] Since exudate is water-based, the logic follows that a

lower water activity medium would limit its ability to expel secondary metabolites through water-based droplets. That said, both strains produced exudate on YESNY, which has the same media formulation as YES, but contains the antifungal nystatin. The presence of the antifungal in the media appeared to have an unelucidated relation to the triggering of the production of exudate in both strains, but the phenomenon has not been previously reported and could not be determined to be causative.

An additional concern pertaining to the macromorphology of the DAOMC 180753 strain was the apparent drastic shift in phenotype of this fungal strain compared to what was initially observed and reported by Nguyen *et al.* in 2016.[60] As shown in **Figure 2.3.3**, the DAOMC 180753 strain in 2016 more closely resembled the official species description of *P. thymicola.* While the exact colony texture could not be accurately described based on the photo from 2016, the colony texture of DAOMC 180753 in 2023 appeared much more lanose and roughened in comparison. It also appeared that the previously white outer ring of the 2016 colonies had faded to a cream-brown colour in the 2023 sample. While the media used in **Figure 2.3.3 A** was undisclosed, it is assumed that it was 2% Blakeslee's malt extract agar (MEA), based on the experimental procedure outlined by Nguyen *et al.*[60]

The morphological differences observed by the DAOMC 180753 strains grown eight years apart (**Figure 2.3.3**) demonstrates how unreliable morphology-based taxonomy *Penicillium* species can be using a morphological approach alone. The apparent changes in mycelial traits, including the shift in colony colour and potential change in colony texture may indicate strain degeneration in the DAOMC 180753 culture. Briefly, strain degeneration is described as the phenotypic instability of a microorganism caused by an inability to reproduce desired morphological or chemical traits across generations.[90] The exact causes of fungal strain

degeneration currently remain unelucidated. Strain degeneration occurs frequently to filamentous fungi in the laboratory environment[91] and is likely to occur for strains in long-term freezer storage[92], as was the case for the DAOMC 180753 strain presented in this thesis. Alternatively, it is possible that the DAOMC 180753 colonies exhibited drastically different traits between 2016 and 2023 because the strains being compared were not members of the same *Penicillium* species of fungi. Explicitly, it is entirely plausible that an error occurred in long-term storage, wherein a storage vesicle was labeled incorrectly, leading to a different species of *Penicillium* being labeled as DAOMC 180753. While this hypothesis could not be confirmed via morphology alone, it would provide an explanation as to why the DAOMC 180753 strain analysed in 2023 for this thesis research did not share many of the characteristics of *P. thymicola* based on the species description.

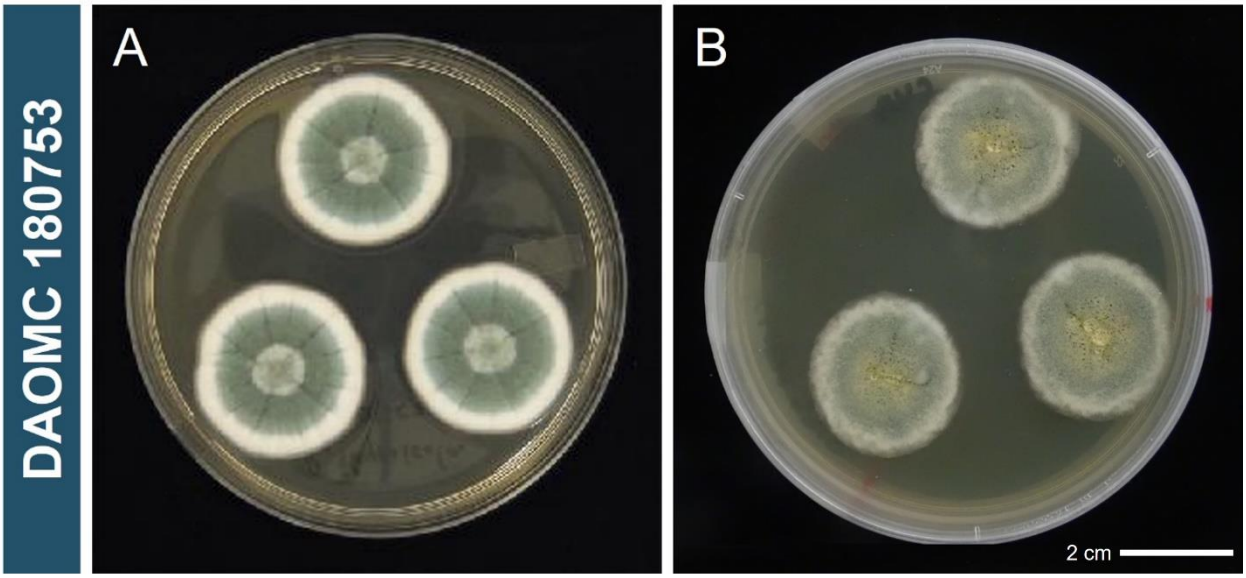

Figure 2.3.3 - *P. thymicola* DAOMC 180753 in 2016 vs 2023. A. *P. thymicola* DAOMC 180753 on undisclosed media, taken in 2016. Image originally from JGI website (mycocosm.jgi.doe.gov/Penth1). **B.** *P. thymicola* DAOMC 180753 grown for 7 days at 25ºC in darkness on CYA, taken in 2023.

2.3.2 Micromorphological Analysis of CHEM 5317 and DAOMC 180753

CHEM 5317

The micromorphology of CHEM 5317 was examined by suspending spores from CYA colonies in lactic acid and analyzing the substructures of the conidiophore via compound microscope. Based on the microscope images assembled in **Figure 2.3.4**, it was determined that CHEM 5317 exhibited a terverticillate branching pattern (**Figure 2.3.4 B, D**), with each conidiophore comprising two or three metulae per whorl. The conidia of CHEM 5317 were green on CYA, smooth-walled to slightly roughened and relatively uniform and globose in shape and appeared in chains when attached to the phialides (**Figure 2.3.4 B, C, D**). The metulae were cylindrical in shape, with small bulbous vesicles where the metulae connect to the phialides (**Figure 2.3.4 B**). The surface architecture of the stipe is noticeably granular (**Figure 2.3.4 D**), with coarse incrustations evident along the structure. The micromorphology of CHEM 5317 was consistent with the species description by Frisvad and Samson[14], except for the presence of rami, which were not observed in the CHEM 5317 micromorphological images shown due to the orientation of the conidiophore in the lactic acid suspension.

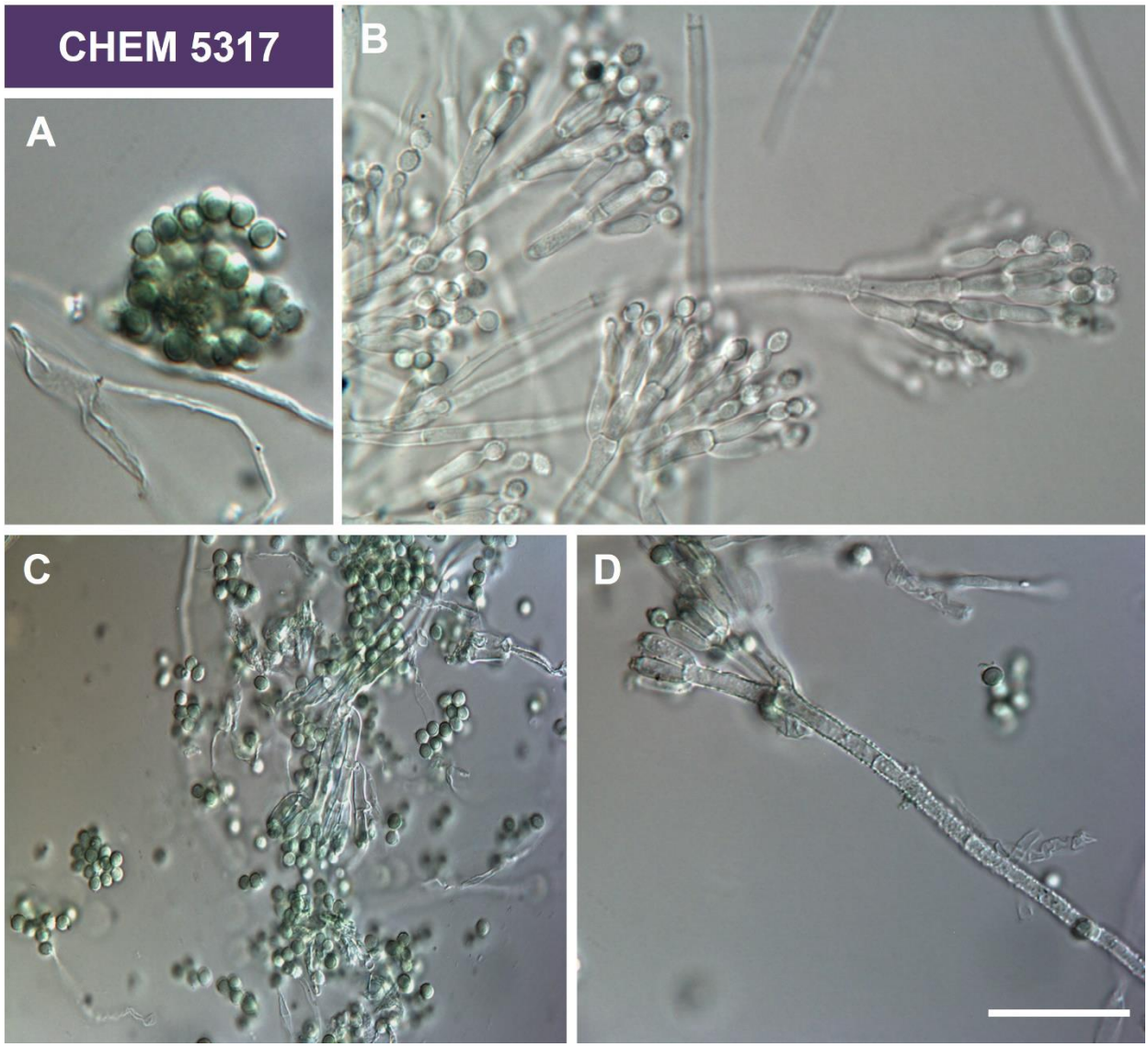

Figure 2.3.4 - CHEM 5317 Micromorphology. A. A bundle of CHEM 5317 conidia on CYA growth day 14. Grown at 25ºC in darkness. **B.** CHEM 5317 conidiophores grown on CYA for 14 days at 25ºC. **C.** CHEM 5317 conidiophores on CYA agar grown for 14 days at 25ºC. **D.** CHEM 5317 on CYA agar grown for 14 days at 25ºC in darkness. Scale bar = 5 µm.

DAOMC 180753

The micromorphology of DAOMC 180753 was analyzed using the same method as used for CHEM 5317. Based on the microscopic observations, as shown in **Figure 2.3.5**, it was ascertained that the DAOMC 180753 conidiophores exhibited a terverticillate branching pattern,

with observable rami in all three images. Many of the DAOMC 180753 conidia were green in hue, but the majority were gray in colour and smooth to slightly roughened in appearance. The conidia not attached to the phialides were globose in shape, with conidia still attached to the conidiophore exhibiting more of a sub-globose shape (**Figure 2.3.5 A**). There were very few conidia both on the conidiophore and adhering together in the mounting fluid in the DAOMC 180753 samples. The metulae and rami were both cylindrical in shape and did not exhibit noticeable tapering on either end of their structure. The surface architecture of the stipe was smooth to roughened in appearance and not overly granular in appearance.

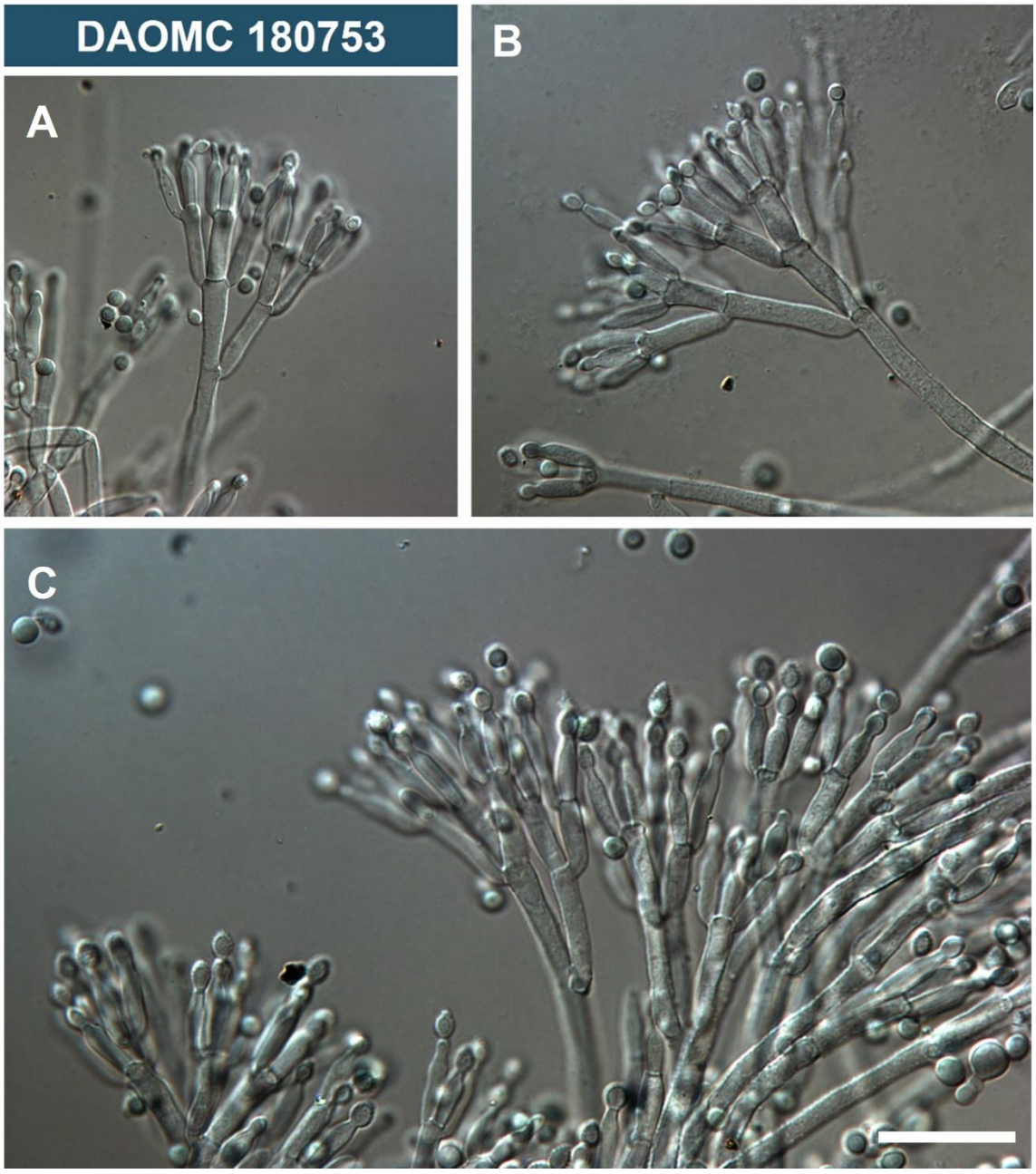

Figure 2.3.5 - DAOMC 180753 Micromorphology. A. DAOMC 180753 grown on CYA for 14 days at 25ºC. **B.** DAOMC 180753 grown on CYA for 14 days at 25ºC. **C.** DAOMC 180753 grown on CYA for 14 days at 25ºC. Scale bar = 5 µm.

2.4 Chapter 2 Summary

In this thesis chapter, the macro- and micromorphological features of the *P. thymicola* strains CHEM 5317 and DAOMC 180753 were compared against each other and the official species description by Frisvad and Samson[14] of the type strain, *P. thymicola* IBT 5891. The major macro- and microscopic features analyzed in this morphological approach to taxonomy are highlighted in **Table 2.4.1.** While CHEM 5317 exhibited the majority of the anticipated macro-morphological characteristics of *P. thymicola* based on the official species description, the DAOMC 180753 phenotype strayed greatly from expectations.

Table 2.4.1 - Species description of micromorphology of *P. thymicola* type strain (IBT 5891) contrasted with experimental observations of CHEM 5317 and DAOMC 180753. Experimental observations of CHEM 5317 and DAOMC 180753 micromorphology performed on day 14 of growth on CYA. Both strains grown at 25ºC in the dark.

Feature	IBT 5891	CHEM 5317	DAOMC 180753
Branching pattern	Terverticillate	Terverticillate	Terverticillate
Colony texture	Velutinous	Velutinous	Lanose
Conidia	Rough-walled; globose to sub-globose; green on CYA	Smooth to roughened; globose to sub-globose; green on CYA	Smooth to roughened; globose; green/gray on CYA
Phialides	Cylindrical; tapering	Cylindrical; tapering	Cylindrical; tapering
Metulae	Cylindrical	Cylindrical	Cylindrical
Rami	Cylindrical	N/A	Cylindrical
Stipe	Rough-walled	Rough-walled to granular	Slightly roughened
Exudate on CYA	None or yellow	Clear to yellow	Clear to yellow

The first and most notable macro-morphological difference between the two strains was their diverging colony textures. CHEM 5317 exhibited the anticipated velutinous colony texture characteristic of *P. thymicola*, whereas the DAOMC colonies were strictly lanose in texture. As shown in **Figure 2.4.1**, CHEM 5317 displayed a mycelium that was soft and plush in appearance

(**Figure 2.4.1 B, C**). In contrast, the lanose texture of DAOMC 180753 was observed as longer hyphal filaments interwoven as aerial mycelium (**Figure 2.4.1 F**). As discussed, colony texture is the result of how the conidiophores of a fungal colony are emerging from the growth substrate. A velutinous colony texture is the result of conidiophores growing erect from the substrate, whereas a lanose texture is due to interwoven aerial hyphae.[87] As such, the difference in colony texture is indicative of a divergence in the growth of the conidiophores in the CHEM 5317 and DAOMC 180753.

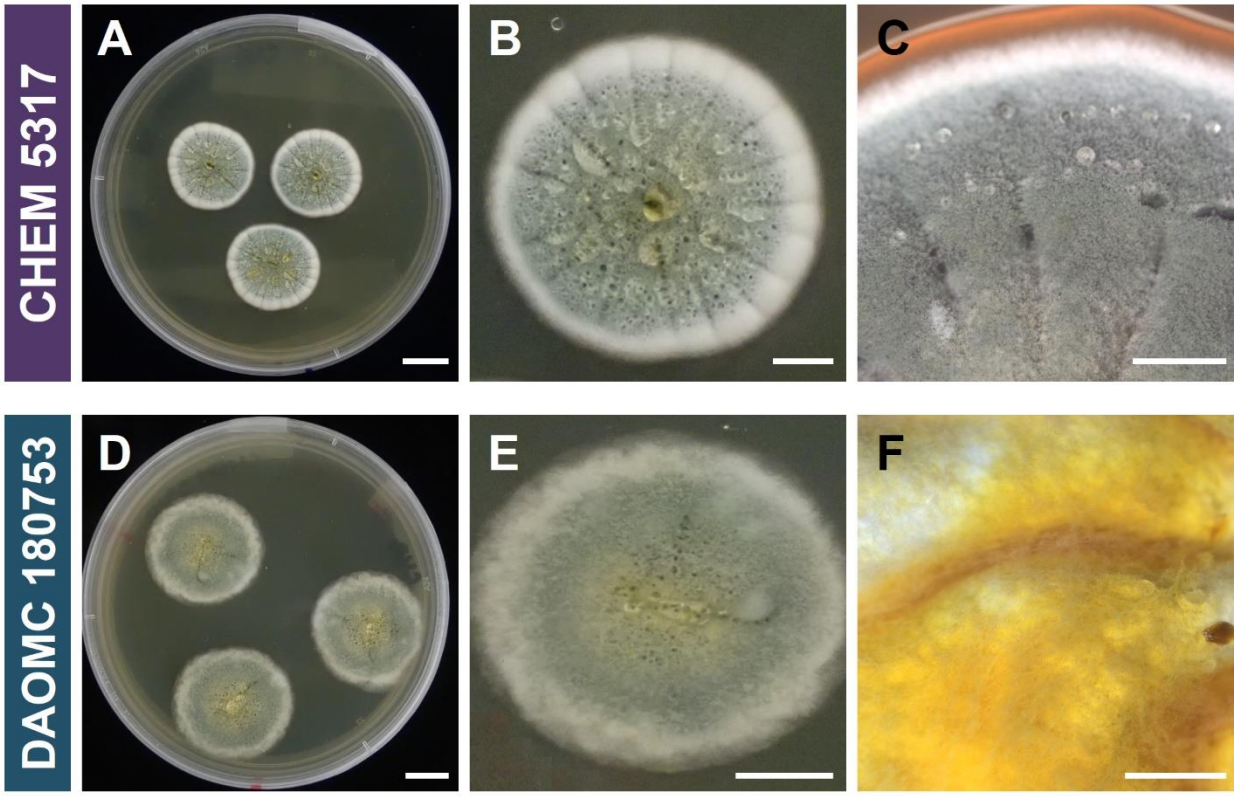

Figure 2.4.13- CHEM 5317 and DAOMC 180753 colony textures on CYA media. A. CHEM 5317 on CYA. Growth day 7. Scale bar = 1 cm. **B.** CHEM 5317 on CYA, growth day 7, taken from A. Scale bar = 0.5 cm. **C.** CHEM 5317 grown on CYANY for 14 days at 25°C. Scale bar = 500 µm. **D.** DAOMC 180753 on CYA. Growth day 7. Scale bar = 1 cm. **E.** DAOMC 180753 on CYA, taken from D. Scale bar = 1 cm. **F.** DAOMC 180753 on YES for 14 days at 25°C. Scale bar = 500 µm.

2.6 Appendix 2.0

Appendix 2A: Media Formulations

Czapek Yeast Agar (CYA) (1 L):
3.00 g $NaNO_3$
1.00 g KH_2PO_4
500 mg $MgSO_4 \cdot 7H_2O$
10.0 mg $FeSO_4 \cdot 7H_2O$
5.00 g Yeast Extract
30.0 g Sucrose
20.0 g Agar
1.00 L MQ H_2O
1.00 mL Trace Element Solution
1 g $ZnSO_4 \cdot 7H_2O$
0.5 g $CuSO_4 \cdot 5H_2O$
100 mL MilliQ H_2O

Yeast Extract Sucrose (YES) (1 L):
20.0 g Yeast Extract
150 g Sucrose
500 mg $MgSO_4 \cdot 7H_2O$
20.0 g Agar
1.00 L MQ H_2O

DG18 (1L):
5.00 g Peptone
10.0 g Glucose
1.00 g KH_2PO_4
0.500 g $MgSO_4 \cdot 7H_2O$
1.00 mL Dichloran (0.2 % in EtOH)
220 g Glycerol
0.100 g Chloramphenicol
15.0 g Agar
1.00 L MQ H_2O

Oatmeal Agar (OMA) (1 L):
60.0 g Oatmeal
12.5 g Agar
1.00 L MQ H_2O

Czapek Yeast Agar + Nystatin (CYANY) (1 L):
3.00g $NaNO_3$
1.00 g KH_2PO_4
500 mg $MgSO_4 \cdot 7H_2O$
10.0 mg $FeSO_4 \cdot 7H_2O$
5.00 g Yeast Extract
30.0 g Sucrose
20.0 g Agar
1.00 L MQ H_2O
1.00 mL Trace Element Solution
227 mg Nystatin

Yeast Extract Sucrose + Nystatin (YESNY) (1 L):
20.0 g Yeast Extract
150 g Sucrose
500 mg $MgSO_4 \cdot 7H_2O$
20.0 g Agar
1.00 L MQ H_2O
227 mg Nystatin

Appendix 2B: Macromorphology of all CHEM 5317 and DAOMC 180753 Replicates

CHEM 5317

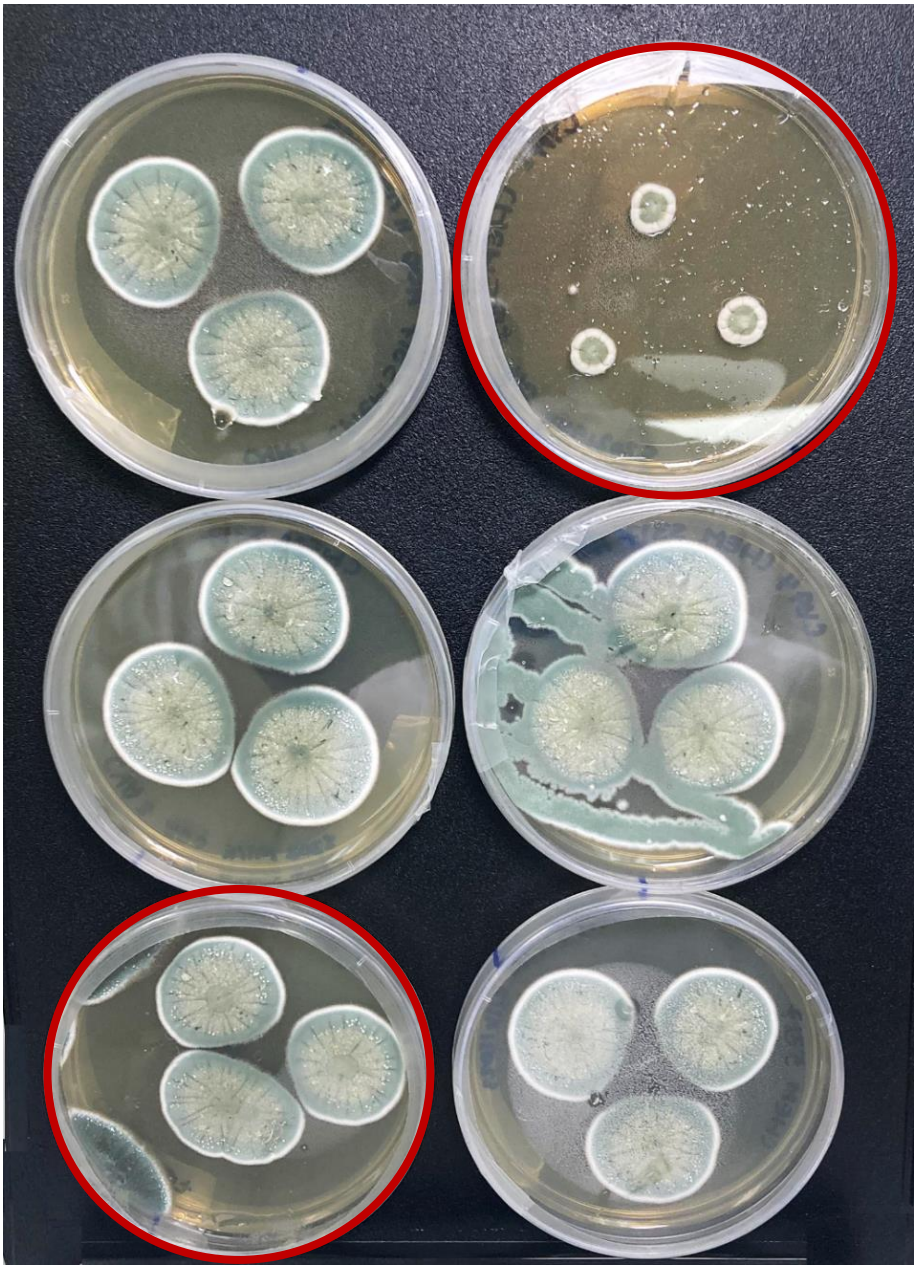

Figure 2B.1 - CHEM 5317 Replicates on CYA. CHEM 5317 on growth day 14 on CYA media. Grown at 25°C in the dark. Plate containing macromorphological outliers highlighted in red.

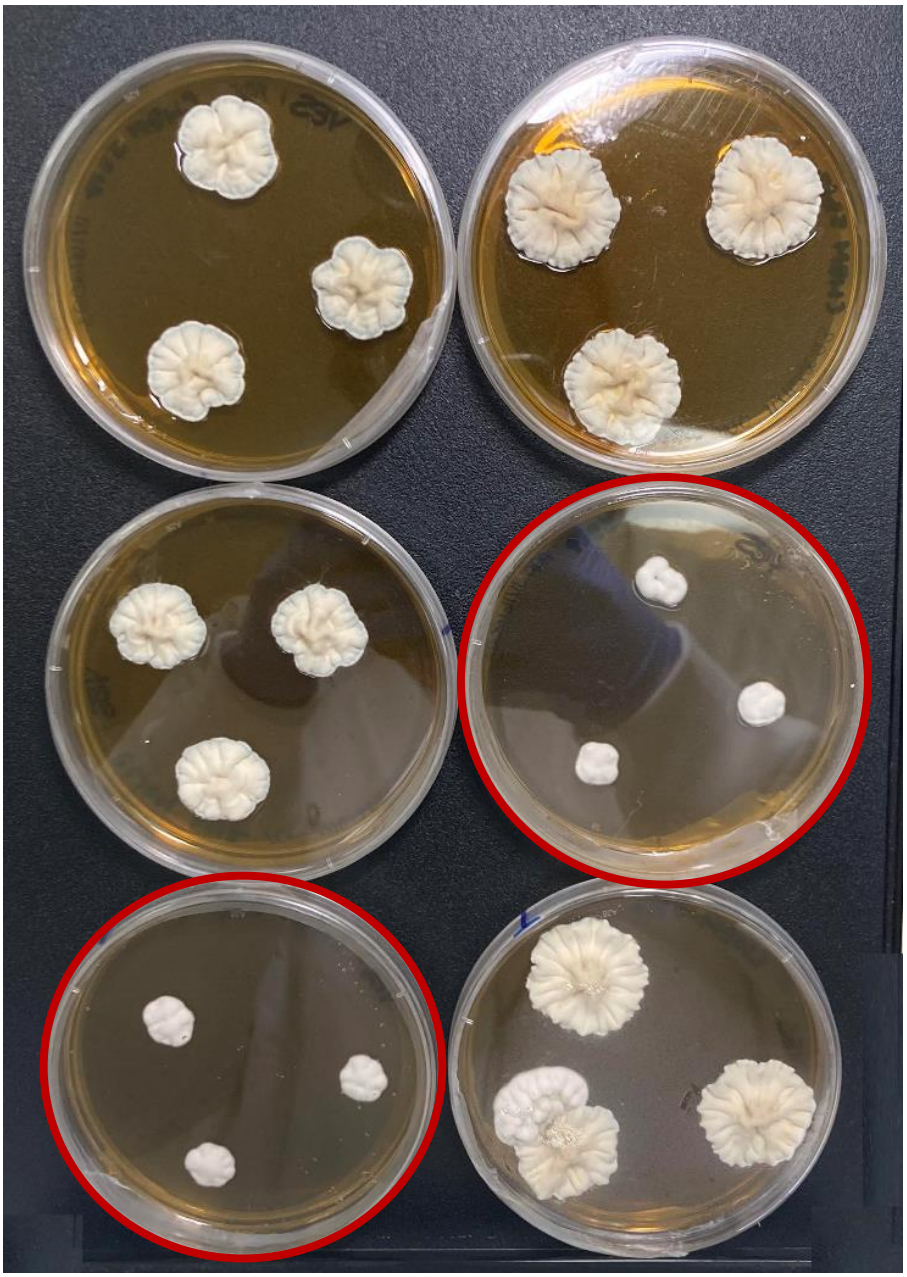

Figure 2B.2 - CHEM 5317 Replicates on YES. CHEM 5317 on YES media growth day 14. Grown at 25ºC in the dark. Plates containing macromorphological outliers highlighted in red.

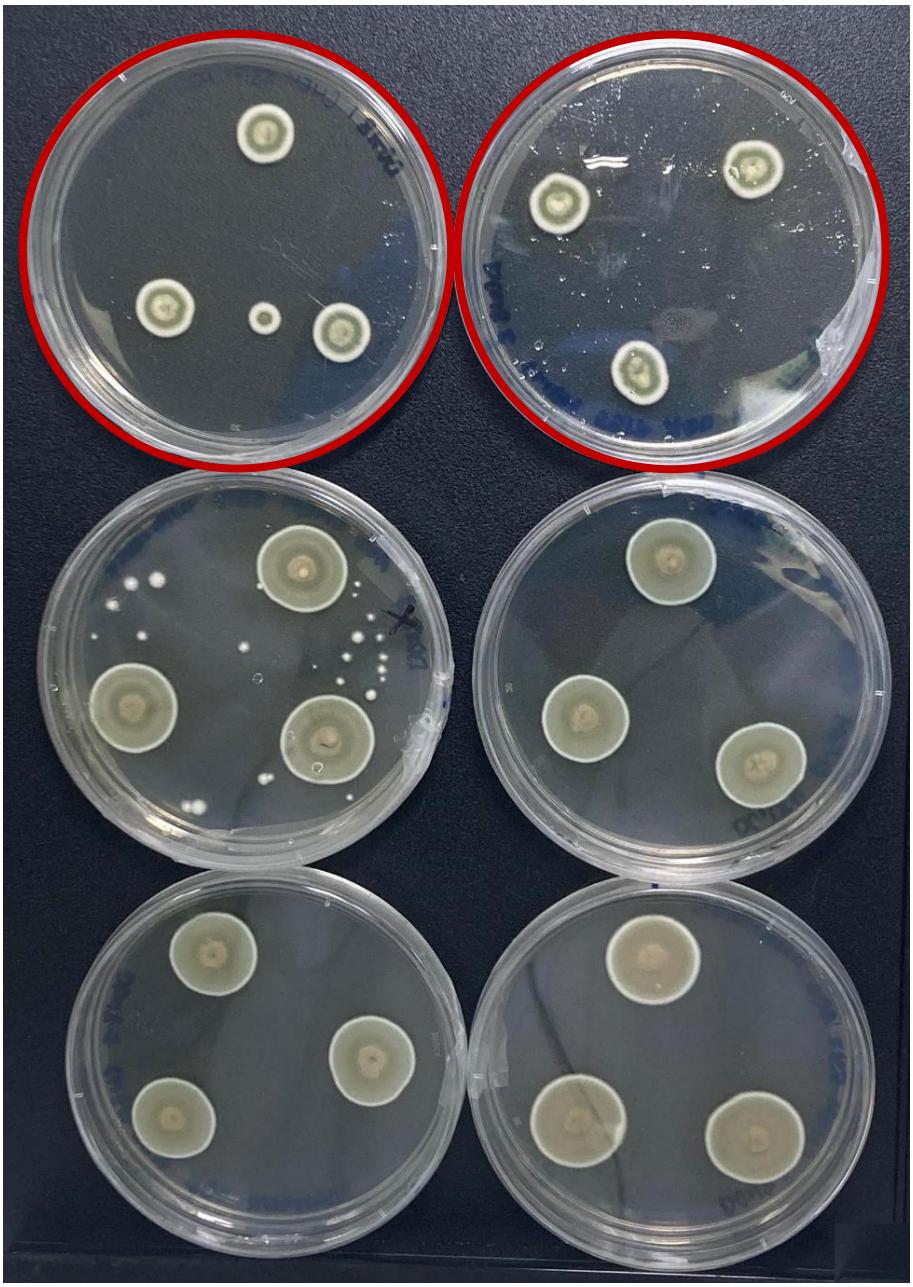

Figure 2B.3 - CHEM 5317 Replicates on DG18. CHEM 5317 on DG18 media, growth day 14. Grown at 25°C in the dark. Plates containing macromorphological outliers highlighted in red.

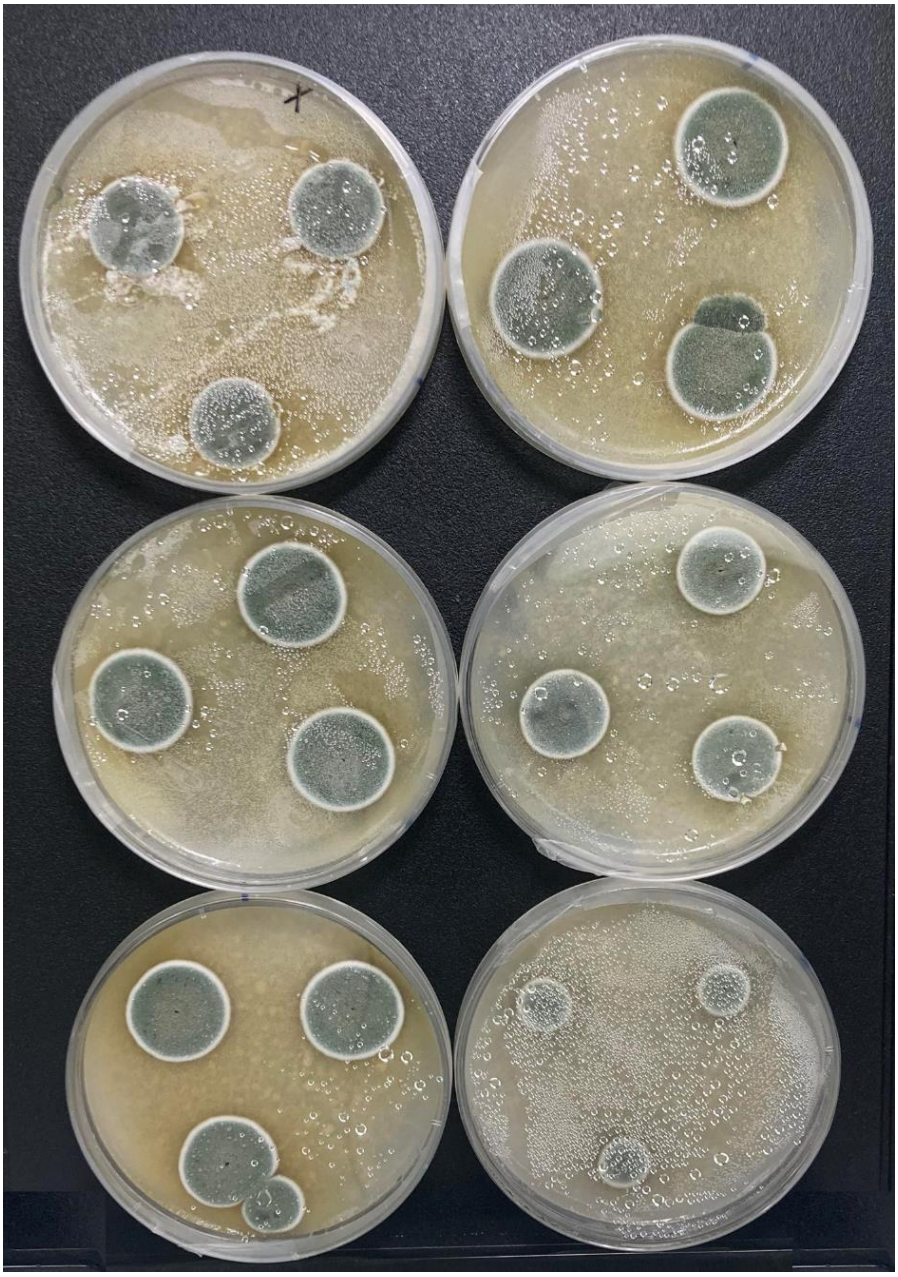

Figure 2B.4 - CHEM 5317 Replicates on OMA. CHEM 5317 on OMA media, growth day 14. Grown at 25ºC in the dark.

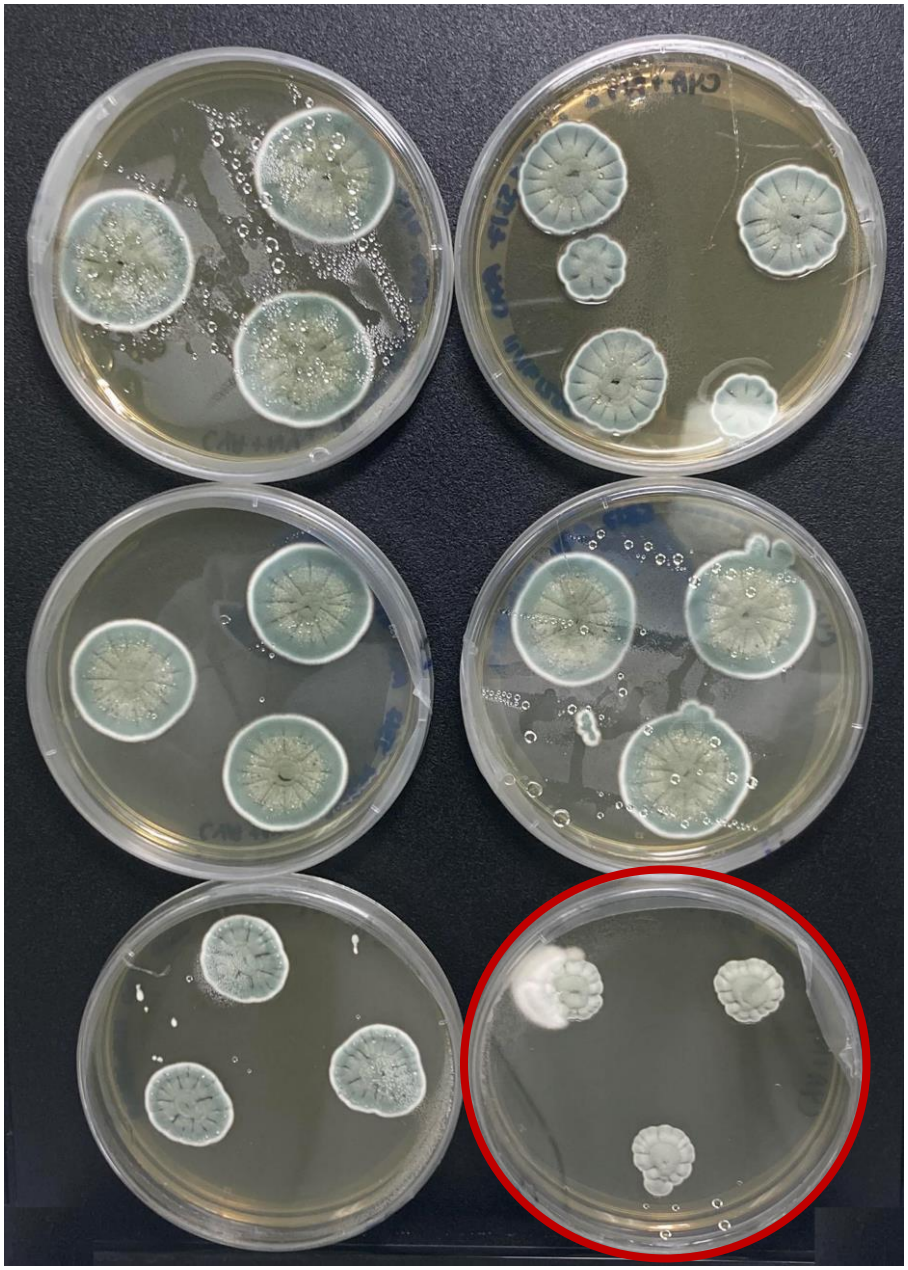

Figure 2B.5 - CHEM 5317 Replicates on CYANY. CHEM 5317 on CYANY media, growth day 14. Grown at 25ºC in the dark. Plate containing macromorphological outliers highlighted in red.

Figure 2B.6 - CHEM 5317 Replicates on YESNY. CHEM 5317 on YESNY media, growth day 14. Grown at 25ºC in the dark. Contaminated colony highlighted in red.

DAOMC 180753

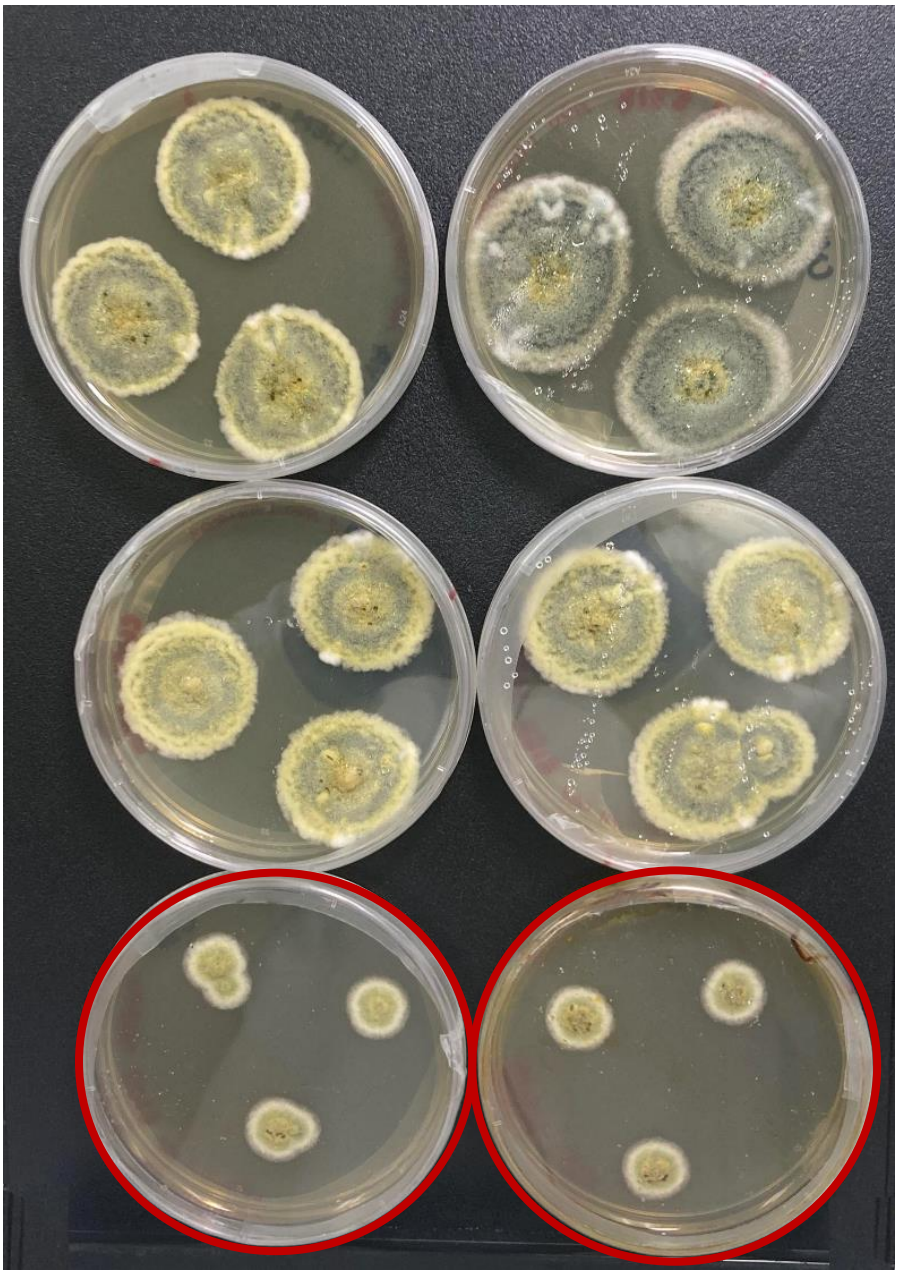

Figure 2B.7 - DAOMC 180753 Replicates on CYA. DAOMC 180753 on CYA media, growth day 14. Grown at 25ºC in the dark. Plates containing macromorphological outliers highlighted in red.

Figure 2B.8 - DAOMC 180753 Replicates on YES. DAOMC 180753 on YES media, growth day 14. Grown at 25ºC in the dark.

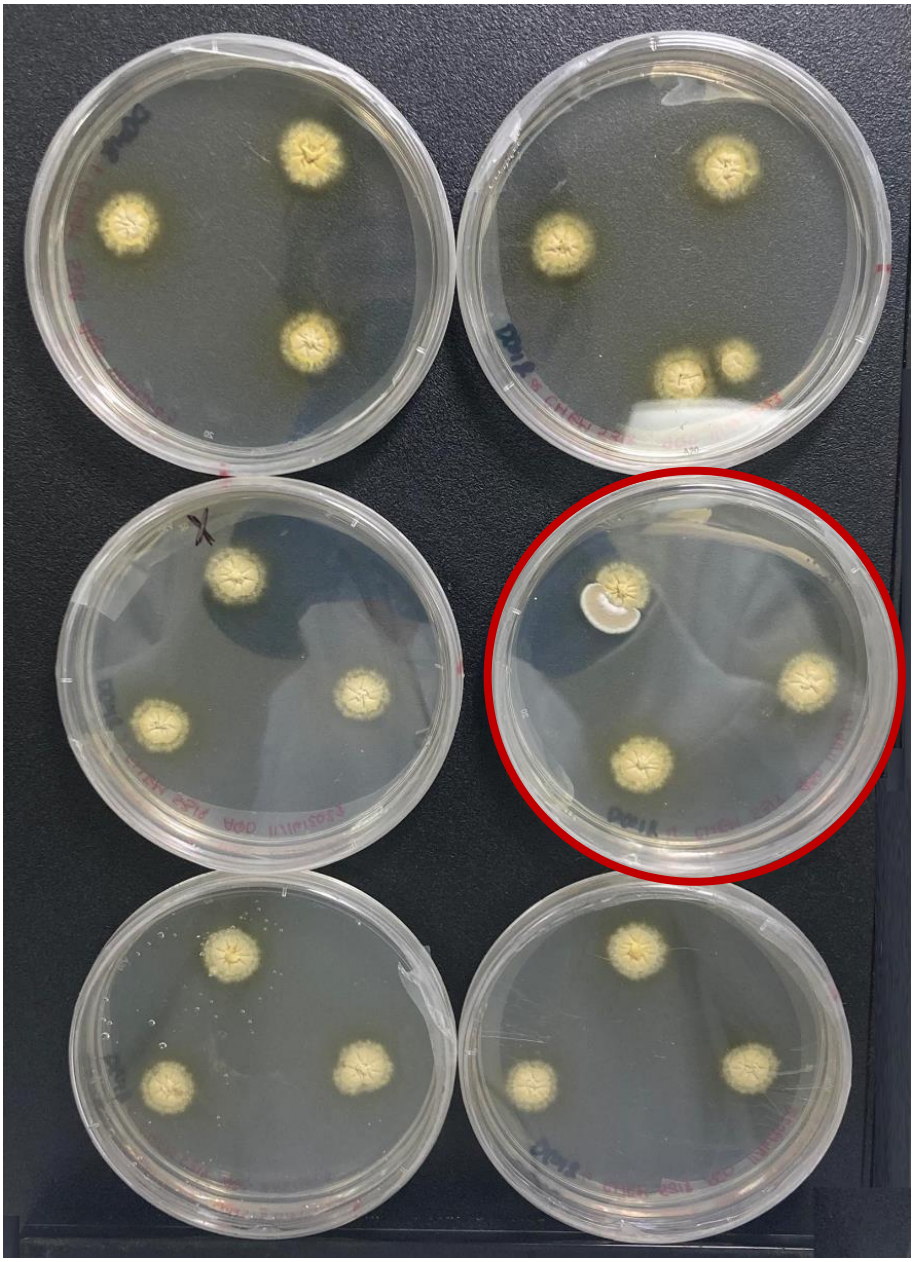

Figure 2B.9 - DAOMC 180753 Replicates on DG18. DAOMC 180753 on DG18 media, growth day 14. Grown at 25ºC in the dark. Plate containing contaminated colony highlighted in red.

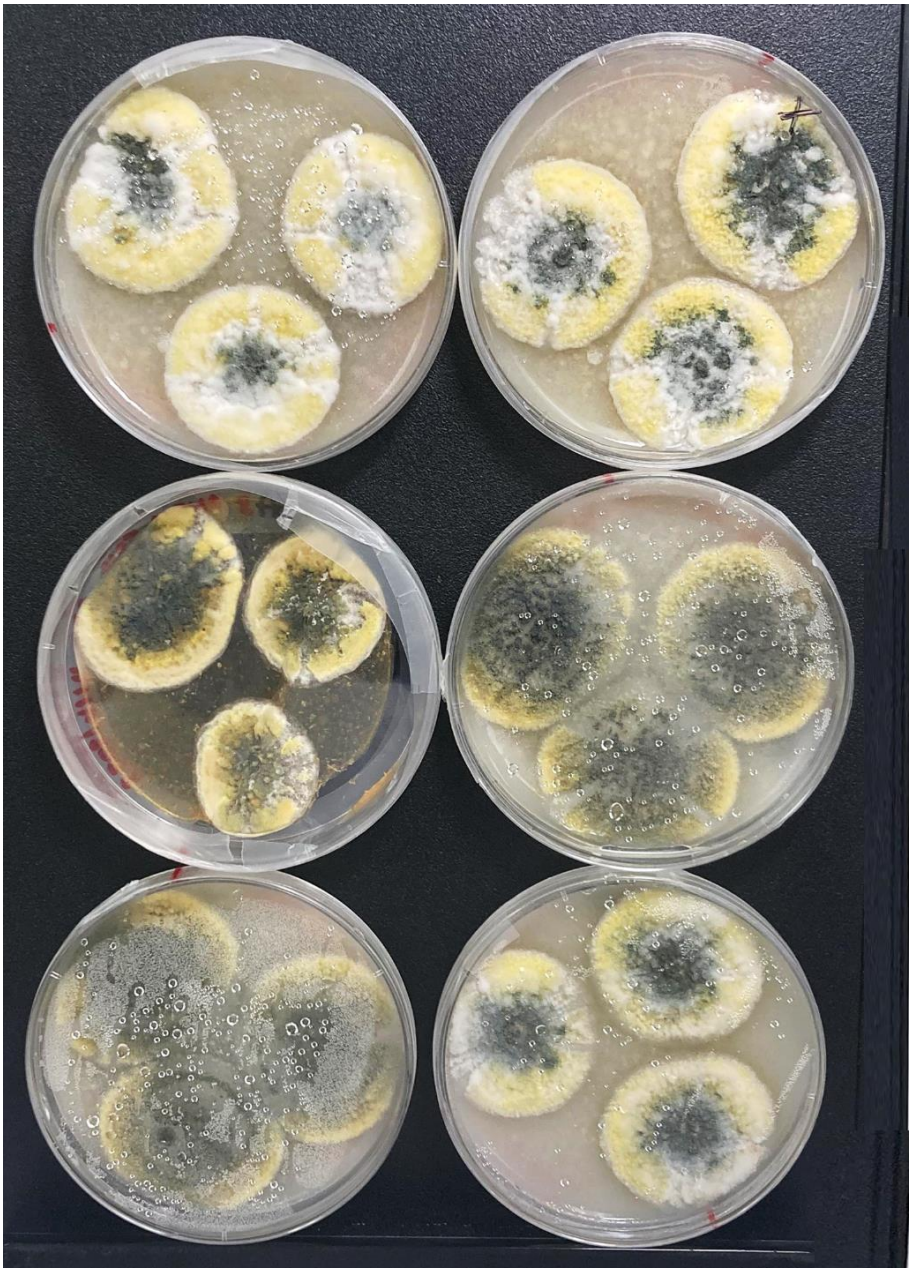

Figure 2B.10 - DAOMC 180753 Replicates on OMA. DAOMC 180753 on OMA media, growth day 14. Grown at 25ºC in the dark.

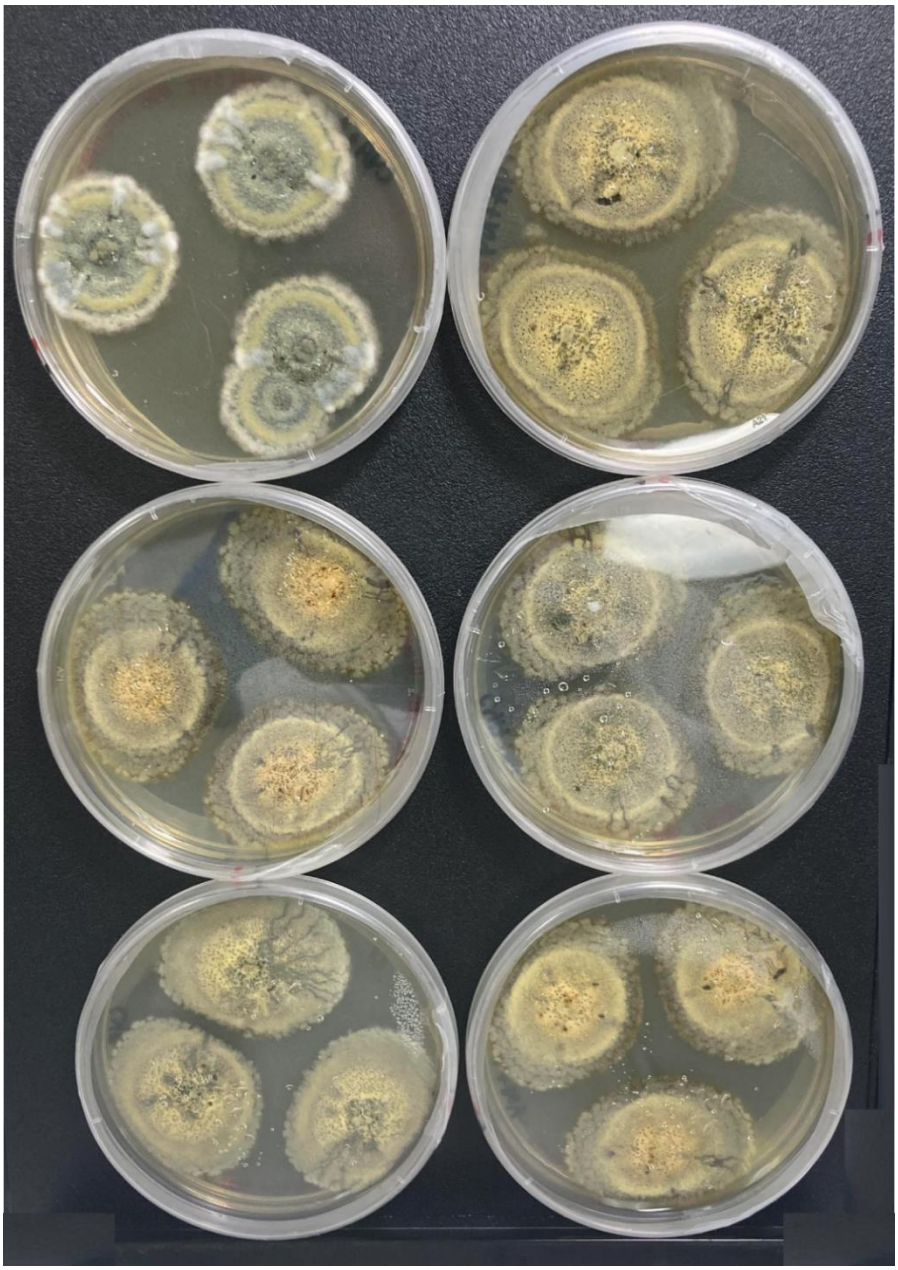

Figure 2B.11 - DAOMC 180753 Replicates on CYANY. DAOMC 180753 on CYANY media, growth day 14. Grown at 25ºC in the dark.

Figure 2B.12 - DAOMC 180753 Replicates on YESNY. DAOMC 180753 on YESNY media, growth day 14. Grown at 25ºC in darkness.

Chapter 3: Phylogenetic Analysis of CHEM 5317 and DAOMC 180753 Barcode Gene Sequences

3.1 Introduction

3.1.1 Phylogeny as an Approach to Fungal Taxonomy

The modern use of the tree structure to classify and visualize genetically related biological organisms stems from Charles Darwin's original concept of a tree of life that connects species to one unique common ancestor.[93] Historically, phylogenetic tree diagrams were used to visualize relationships between species in taxonomic studies before the widespread use of DNA sequencing technologies in the late 20th century.[94] In our current era, molecular phylogenetics is commonly used to compare the genomes of related organisms, such as in the identification of genes and non-coding RNA sequences in newly sequenced genomes;[95,96] the analysis of evolutionary relationships based on transcriptomic data;[97,98] and in the taxonomic analysis of metagenomes.[99] From a taxonomy perspective, two strains are considered to be members of the same fungal species if they exhibit monophyly in a phylogenetic tree; or a group of closely-related organisms descended from a common ancestor.[100]

3.1.2 The Evolution of DNA Sequencing

Sanger sequencing, developed in 1977, remains the "gold standard" for DNA sequencing to this day, particularly for the sequencing of individual genes.[101,102] The modern Sanger sequencing reaction involves the addition of fluorescently labeled 2',3'-dideoxynucleotide triphosphates (ddNTPs), which can be incorporated into the growing DNA chain. The addition of a ddNTP into the DNA chain terminates its amplification due to the absence of the 3'-OH group

in the ddNTP.[103] In the end, the Sanger sequencing reaction produces single-stranded DNA (ssDNA) of various lengths, marked at the 3' end with a specific fluorophore that specifies its nucleotide.[104,105] The major limitations of Sanger sequencing include its ability to only work for short read lengths ranging from 700 to 1000 base pairs (bp), low throughput, and high cost for the user per DNA base sequenced compared to massively parallel sequencing technologies.[105,106] These challenges, coupled with a newfound hunger to sequence more complex genomes more rapidly (e.g., The Human Genome Project in 2003[107]) gave rise to the massively parallel next generation sequencing (NGS) methods between 2004 and 2008.

NGS methods offer high throughput parallel sequencing reactions from massive sequence libraries, thus allowing millions of individual sequencing reactions to occur in tandem.[108,109] One of these NGS methods is the Illumina HiSeq System, which utilizes a 'sequencing by synthesis' method, wherein a library of fixed adapters is ligated to randomly fragmented genomic DNA.[110] Illumina sequencing offers read lengths of up to 300 bp coupled with a throughput of up to 6000 Gb, in the case of NovaSeq.[111] Illumina is the most widely used sequencing platform for metagenomic and metatranscriptomic investigations.[111] Third generation long-read sequencing technology, such as that of the Oxford Nanopore platform, is often coupled with NGS methods for eukaryotic genome sequencing. The Nanopore sequencing method can attain read lengths of 2.4 megabases.[112] Nanopore's particularly high raw read error rate of 6-12%, necessitates post-sequencing error correction algorithms and makes this technology less appealing for single amplicon sequencing.[112,113] However, combining high throughput short-read and long-read strategies is ideal for the sequencing of eukaryotic genomes with repetitive DNA elements that pose a problem for short-read sequencing technologies on their own.[114]

3.1.3 Fungal barcode genes

The dawn of widespread DNA sequencing technologies and modern-day molecular biology techniques at the end of the 20th century has given taxonomists the ability to compare the sequences of highly conserved genes of different fungal species.[7,17] As discussed in Chapter 2 of this thesis, the Amsterdam Declaration marked a controversial turning point in the naming of fungal species. In addition to the naming convention, the Amsterdam declaration also made stipulations about the application of genetic markers in fungal taxonomy.[9] Therein, it was determined that any chosen genetic marker must include at a minimum the barcode standard for fungi, the Internal Transcribed Spacer (ITS) sequence. Published phylogenetic analysis used to demonstrate monophyly of fungal strains must use publicly availably DNA sequences and have at least 2 full length nucleotide sequences of the genomic regions. In addition, quality control measures must be undertaken, including the use of chimera checking software. The sequences must also be registered by a recognized open-access online database (e.g., National Center for Biotechnology Information (NCBI), MycoBank, Joint Genome Institute (JGI)).[9]

At present, there are four established barcode genes used to taxonomically identify *Penicillium* species isolates: the ITS of the rRNA gene cluster, the β-tubulin gene, the calmodulin (CMD) gene, and the RNA Polymerase II second largest subunit (RPB2) gene sequences.[15,17,115–117] These barcode genes have been chosen for fungi as they meet the standard ideal criteria for barcode gene sequences: relatively easy PCR amplification, low intra-species variability, consistent gene length, and the presence of only a single copy of the gene within a genome.[118] While typically the ITS region is the first-line method in taxonomy with barcode genes, the three additional genes described are often used in tandem to refine the precision of these results. The ITS region is known to be less accurate in the identification of *Penicillium sp.* in greater specificity

than genus, as many *Penicillium* species have similar or identical ITS DNA sequences.[119] In general, the use of multi-locus sequence typing, or the use of multiple barcode genes in one taxonomic study, increases the accuracy of results, and is preferred over using a single gene for taxonomy.[120,121]

The ITS region in eukaryotes refers to two non-protein coding RNA sequences between the 18S, 5.8S, and 28S ribosomal RNA (rRNA) genes transcribed by RNA polymerase I that are excised by posttranscriptional modifications.[58] The tubulin genes are protein-coding genes that are a major component of cellular microtubules, involved in cell division, ciliar and flagellar motility, and intracellular transport in eukaryotic organisms.[122] Although there are numerous types of tubulin genes in eukaryotes, the α-, β-, and γ-tubulin genes are ubiquitous in all eukaryotic organisms.[122] Despite all fungi possessing these three different tubulin genes, many fungal species only code for one copy of the α-, β-, and γ-tubulin genes[122], thus making them reliable indicators of taxonomy. That said, the use of the β-tubulin gene is not infallible, and intraspecies variations in its nucleotide sequence has been reported in *Penicillium* species.[123–128] When identifying a strain of fungi as a potential new species, care must be taken to not rely solely on differences between the β-tubulin sequences for this reason. Calmodulin, or 'calcium-modulating protein', is the most common and versatile calcium-binding protein found in all eukaryotes.[129] As its name implies, calmodulin acts as one of the intracellular targets of Ca^{2+}, whose signal is required for the activation of the calmodulin protein.[129] When in its active state, calmodulin participates in the calcium signal transduction pathway and can regulate a diverse range of target proteins, such as cyclic nucleotide phosphodiesterase for the cyclic nucleotide metabolism and NAD^{+} kinase involved in energy metabolism.[129] The RPB2 gene codes for the second largest protein subunit in

the RNA polymerase II holoenzyme, which comprises approximately ten to twelve protein subunits that are scattered throughout the eukaryotic genome.[130–133]

3.1.4 Chapter Overview

In this chapter, the phylogenetic relationships between the two strains of *P. thymicola*, CHEM 5317 and DAOMC 180753, are analyzed in conjunction with closely related *Penicillium* species of *Penicillium* section *Fasciculata,* including the *P. thymicola* type strain, IBT 5891. The phylogenetic analysis was performed using the concatenated sequences of three previously established barcode genes for fungi: the Internal Transcribed Spacer (ITS), β-tubulin, and calmodulin (CMD). The results of the whole genome sequencing of CHEM 5317 using a combination of Illumina short-read sequencing and Oxford Nanopore long-reads are also reported.

3.2 Materials and Methods

3.2.1 DNA Extraction

CHEM 5317 and DAOMC 180753 were inoculated and grown in CYA liquid cultures for 5 days at room temperature (RT) and fungal mycelium was harvested via vacuum filtration. The harvested mycelium was then frozen overnight at -80ºC prior to DNA extraction. The DNA extraction protocol used was adapted from originally Möller and colleagues[134], with modifications outlined by Dettman and Eggerston.[135] The following modifications were made from the protocol of Dettman and Eggerston. In step 1, a mortar and pestle were used to grind the frozen fungal mycelium, rather than zirconium beads. Instead of using ammonium acetate as indicated in step 20 in the protocol, 80 µL of 3 M sodium acetate was added to the supernatant samples before incubating on ice for 30 min. Samples were then centrifuged at max speed for 10 min at 4ºC, as

indicated. Finally, dried DNA pellet was resuspended in 70 µL of 10 mM Tris, then incubated at 65°C for 10 min in a heat block. Extracted DNA was then quantified and stored in freezer at -20°C.

3.2.2 PCR Amplification of Barcode Genes

The previously established barcode genes for *Penicillium sp.,* ITS, β-tubulin, CMD, and RPB2, were PCR amplified in 25 µL reactions. Universal primers were used to PCR amplify the genes of interest (GOIs) in both *P. thymicola* strains and are listed in **Appendix 3A**. The PCR protocols followed for barcode gene amplification are shown in **Table 3.2.1**.

ITS & β-tubulin:

To amplify the ITS and β-tubulin genes, a standard one-step PCR protocol was used with Taq DNA polymerase (New England Biolabs (NEB)). Each reaction contained 1 µL of extracted fungal gDNA. The exact PCR protocols used to amplify the ITS and β-tubulin genes are outlined in **Table 3.2.1**.

CMD:

To amplify the calmodulin gene, a standard PCR protocol was used with Titanium Taq DNA polymerase (NEB). Each reaction contained 1 µL of extracted gDNA and 0.2 µL of 50X Titanium Taq polymerase. The exact CMD PCR amplification protocol can be found in **Table 3.2.1**.

RPB2:

In the attempt to successfully amplify the RPB2 gene, multiple PCR protocols were utilised; a standard one-step PCR protocol and touch-up PCR with different temperature intervals were used with Titanium Taq DNA polymerase (NEB). Both sets of primers listed in **Appendix**

3A were used. Touch-up PCR with 48-50-52 attempted first, then the same protocol with 50-53-55, as outlined in **Table 3.2.1**.

Table 3.2.1 - *Penicillium* barcode gene PCR protocols. PCR protocols adapted from Visage *et al.* (2014).[17]

Gene	Protocol Type	Denaturing	# Cycles	Denaturing	Annealing	Elongation	Final Elongation	Hold
ITS	Standard	94ºC, 5 min	35	94ºC, 45s	57ºC, 45s	72ºC, 60s	72ºC, 7 min	10ºC, ∞
β-tub	Standard	94ºC, 5 min	35	94ºC, 45s	60ºC, 45s	72ºC, 60s	72ºC, 7 min	10ºC, ∞
CMD	Standard	95ºC, 5 min	40	95ºC, 50s	58ºC, 50s	72ºC, 60s	72ºC, 7 min	10ºC, ∞
RPB2	Touch-up	94ºC, 5 min	5	94ºC, 45s	50ºC, 45s	72ºC, 60s	72ºC, 7min	10ºC, ∞
			5	94ºC, 45s	52ºC, 45s	72ºC, 60s		
			25	94ºC, 45s	55ºC, 45s	72ºC, 60s		
RPB2	Touch-up	94ºC, 5 min	5	94ºC, 45s	48ºC, 45s	72ºC, 60s	72ºC, 7 min	10ºC, ∞
			5	94ºC, 45s	50ºC, 45s	72ºC, 60s		
			25	94ºC, 45s	52ºC, 45s	72ºC, 60s		

Confirmation of amplification of GOIs was performed using agarose gel electrophoresis. Sanger sequencing was then performed on the positive PCR reactions to confirm the DNA sequences for each gene in either *P. thymicola* strain. The resulting DNA sequences were assembled and trimmed in Geneious Prime. Pairwise sequence alignments to compare the GOIs in both strains were performed using NCBI Basic Local Alignment Search Tool (BLAST).

3.2.3 CHEM 5317 Genome Assembly

Genome assembly

Long-read sequencing of CHEM 5317 genome was performed using the Oxford Nanopore platform at Agriculture and Agri-Food Canada. Assembly of the long-read sequences was performed using CANU v. 1.8[136] using default settings, with an estimated genome size of 34 Mb (genome size =34m). Correction of the CANU assembly was done using Nanopolish v. 0.11.1, then a round of Pilon v. 1.23[137] correction using Illumina sequencing-generated short reads from the same strain.

Gene model prediction

The completed genome assembly was repeat-masked using tantan and *de novo* gene-prediction using the Funannotate pipeline v. 1.8.14[138], with default parameters. Augustus pre-trained models for *Aspergillus nidulans* were used to assist in training.

3.2.4 Phylogenetic Analysis

Phylogenetic tree was constructed using Geneious Prime (Dotmatics). Barcode gene DNA sequences for *Penicillium* sp. in clade *Fasciculata* and outgroup (*Penicillium coralligerum*) were obtained from the NCBI database. Sequences were aligned using Clustal Omega and trimmed down to the same length in Geneious Prime. Concatenation of the sequence alignments and phylogenetic tree were also performed in Geneious Prime. The Jukes-Cantor genetic distance model and neighbour-joining tree build method were used to construct the phylogenetic tree. The robustness of the tree was evaluated with the bootstrap resampling method at 100 replications. The completed phylogenetic tree was exported to Fig Tree and rooted with outgroup *Penicillium coralligerum* CBS 123.65.

3.3 Results and Discussion

3.3.1 Barcode Gene Amplification and Sanger Sequencing

Genomic DNA extractions from fungal mycelium of both *P. thymicola* strains CHEM 5317 and DAOMC 180753 cultures provided templates for PCR amplification of the four barcode genes for *Penicillium* species to confirm that CHEM 5317 was a strain of *P. thymicola*. Three of the four barcode genes were successfully PCR amplified (refer to **Appendix 3B** for gel figures). Sanger sequencing of the amplicon products confirmed them to be the ITS, β-tubulin, and CMD barcode genes for *P. thymicola*. Unfortunately, the RPB2 gene could not be amplified in sufficient quantities for sequencing due to low specificity of amplification and only achieving low levels of PCR amplification (data not shown). This was not unexpected, as the RPB2 gene is notoriously difficult to PCR amplify, even with the optimised touch-up PCR protocols and there is no published RPB2 DNA sequence for the *P. thymicola* type strain.[17]

The DNA sequences obtained for the three barcoding genes for both strains were individually aligned with the *P. thymicola* type strain IBT 5891 to compare nucleotide sequences using the nucleotide sequence alignment NCBI BLASTN tool. The ITS gene of CHEM 5317 had a 99% query coverage and 100% percent identity with IBT 5891, whereas the DAOMC 180753 strain had a 98% query coverage and 100% percent identity when compared to the type strain. For the β -tubulin gene, CHEM 5317 had a query coverage of 97% and a percent identity of 98.26%. In contrast, DAOMC 180753 had a 100% query coverage and a percent identity of 98.26%. Lastly, the calmodulin gene of both CHEM 5317 and DAOMC 180753 had a query coverage of 100% and a percent identity of 99.78%. The barcode gene sequences of the two fungal strains were also compared to each other using NCBI BLAST. The ITS and calmodulin gene sequences had a 100%

identity between the two strains, with no nucleotide mismatches or gaps in the alignment. The β-tubulin gene had a 99.50% percent identity, with two nucleotide mismatches between the two sequences.

To compare the barcode gene sequences with all other available sequences, the nucleotide sequences were individually queried in the NCBI database using NCBI BLAST. Since the DNA sequences for the three barcode genes for both CHEM 5317 and DAOMC 180753 were identical, the database searches revealed the same results for both strains. The CHEM 5317 and DAOMC 180753 ITS sequences most closely matched with the *P. thymicola* ITS region from type material (IBT 5891) and *P. verrucosum* strain H09-121, both aligning with 100% identity. The β-tubulin gene of CHEM 5317 and DAOMC 180753 most closely matched β-tubulin genes from other *P. thymicola* strains with 99% identity. The CMD gene sequence most closely matched *P. thymicola* strain CBS 111225 calmodulin, with a 99.78% identity.

3.3.2 Phylogenetic Analysis using Barcode Gene Sequences

A phylogenetic analysis was performed using the three concatenated barcode loci for *Penicillium* sp. (ITS, β-tub, and CMD) to determine the relationship between CHEM 5317, DAOMC 180753, and closely related members of the *Penicillium* genus clade *Fasciculata*. The 21 species chosen for this analysis are all members of *Penicillium* section *Fasciculata*, series *Camemberti, Viridicata, Corymbifera,* and *Verrucosa*. The outgroup chosen was *P. coralligerum* CBS 123.65, a member of a clade very distantly related to *P. thymicola,* from clade *Canescentia.*[119] A complete list of the selected *Penicillium sp.* used in the phylogenetic analysis is provided in **Appendix 3C**.

Examination of the phylogenetic tree in **Figure 3.3.1** shows that CHEM 5317 and DAOMC 180753 cluster together with the *P. thymicola* type strain IBT 5891 with a bootstrap value of 100. The two closest relatives of *Penicillium thymicola*, *P. nordicum* and *P. verrucosum* are found on a branch from the node immediately adjacent of the two *P. thymicola* strains with a bootstrap value of 97. The phylogenetic grouping of CHEM 5317 and DAOMC 180753 together indicates that they are each other's closest relative of the *Penicillium* species included in the phylogenetic analysis. They share a common ancestor based on the three barcode genes used to genomically identify them. Additionally, these two strains clustered with the *P. thymicola* type strain IBT 5891 with a bootstrap value of 100, thus indicating that these three strains always group together with the resampling algorithm. Such bootstrap values indicate that their clustering does not arise from pure chance, but rather in all tree constructions by the bootstrapping algorithm, the *P. thymicola* strains exhibit monophyly. These results align well with current evolutionary theory, where all members of a single species must remain monophyletic during phylogenetic analysis.[139] Thus, the phylogenetic analysis of the three barcode gene sequences supports the initial hypothesis that CHEM 5317 and DAOMC 180753 are strains of the *P. thymicola* species of fungi.

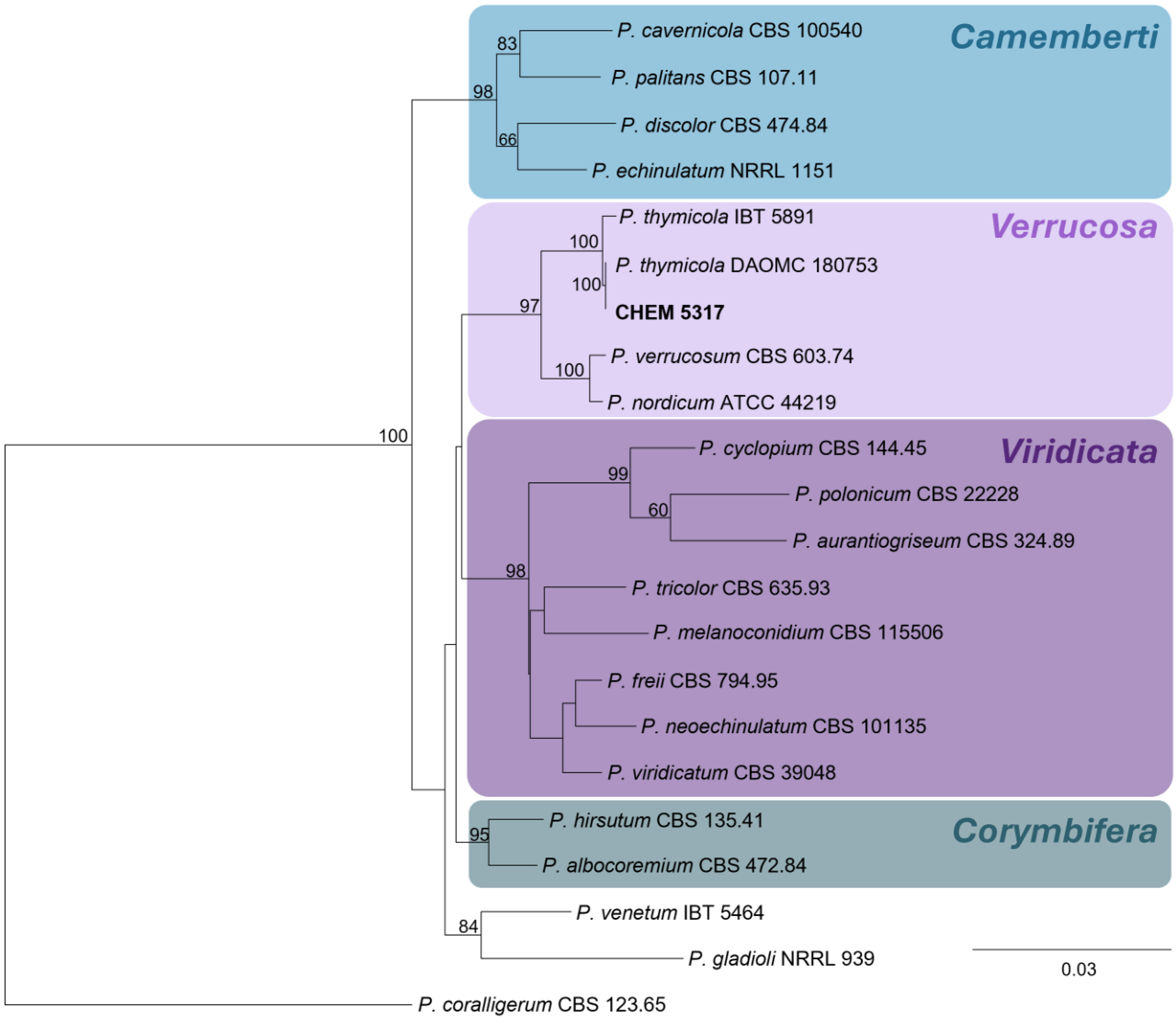

Figure 3.3.1 - Phylogenetic tree of *Penicillium sp.* of section *Fasciculata*. Phylogenetic cladogram of representative *Penicillium sp.* from section *Fasciculata*, comprising four series: *Camemberti, Viridicata, Corymbifera,* and *Verrucosa.* The cladogram was assembled from the concatenated nucleotide sequences of three fungal barcode genes (ITS, β-tubulin, CMD). The tree was rooted using *Penicillium coralligerum* CBS 123.65 as the outgroup. CHEM 5317, the strain isolated in this research project, is feature in bold text. Numbers at nodes represent the bootstrap values (n = 100). Tree computed using Geneious Prime (Dotmatics) with Neighbour-Joining analysis and formatted with FigTree.

3.3.3 Genome Sequencing Results

The *P. thymicola* strain CHEM 5317 was subjected to long-read sequencing using the Oxford nanopore platform. The resulting whole genome was a total of 33.6 Mb in length, produced from 816 312 reads that were assembled from 1019 scaffolds. The longest scaffold was 1 290 259 bp in length. The estimated total coverage was approximately 200X. The mean chromosome length was 6 726 140 bp with a standard deviation of 3.8 Mb. The GC content of the genome was 47.6%. The longest chromosome of the five was 13.2 Mb.

3.5 Chapter 3 Summary

In this thesis chapter, the ITS, β-tubulin, and CMD gene sequences were used to analyze the phylogenetic relationship of CHEM 5317 and DAOMC 180753 in comparison with the gene sequences of other *Penicillium sp.* of clade *Fasciculata*. Through this phylogenetic analysis, CHEM 5317 and DAOMC exhibited monophyly and formed a clade with the *P. thymicola* type strain, IBT 5891. These results corroborated the results of the multi-locus sequence alignment, which determined that the DNA sequences for the barcode genes between IBT 5891, CHEM 5317, and DAOMC 180753 were all identical, or nearly so. Additionally, the three *P. thymicola* strains formed a clade with their closest relatives in series *Verrucosa*, *P. nordicum* and *P. verrucosum*, supporting the evidence that these three species of fungi are very closely related. Globally, these results support the initial hypothesis that CHEM 5317 and DAOMC 180753 are both strains of *P. thymicola.*

Appendix 3.0

Appendix 3A: Barcode Gene Primers

Table 3A.1 - Barcode Gene Primer Sequences

Gene	Primer Name	Direction	Primer Sequence (5' – 3')	Source
ITS	ITS1	Forward	TCC GTA GGT GAA CCT GCG G	White *et al.* 1990[140]
	ITS4	Reverse	TCC TCC GCT TAT TGA TAT GC	White *et al* 1990[140]
β-tubulin	Bt_2a	Forward	GGT AAC CAA ATC GGT GCT GCT TTC	Glass & Donaldson 1995[141]
	Bt_2b	Reverse	ACC CTC AGT GTA GTG ACC CTT GGC	Glass & Donaldson 1995[141]
CMD	CMD5	Forward	CCG AGT ACA AGG ARG CCT TC	Hong *et al* 2006[142]
	CMD6	Reverse	CCG ATR GAG GTC ATR ACG TGG	Hong *et al* 2006[142]
	CF1	Forward	GCC GAC TCT TTG ACY GAR GAR	Peterson *et al.* 2005[143]
	CF4	Reverse	TTT YTG CAT RAG YTG GAC	Peterson *et al.* 2005[143]
RPB2	5F	Forward	GAY GAY MGW GAT CAY TTY GG	Liu *et al.* 1999[144]
	7CR	Reverse	CCC ATR GCT TGY TTR CCC AT	Liu *et al.* 1999[144]
	5Feur	Forward	GAY GAY CGK GAY CAY TTC GG	Houbraken *et al.* 2012[145]
	7CReur	Reverse	CCC ATR GCY TGY TTR CCC AT	Houbraken *et al.* 2012[145]

Appendix 3B: PCR Amplification of Barcode Genes

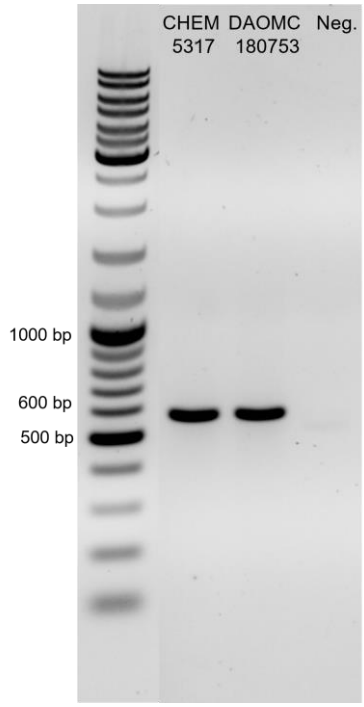

Figure 3B.1 - PCR Amplification of ITS Region of CHEM 5317 and DAOMC 180753. ITS region band visible at ~ 590 bp. Sample type from left to right: lane 1 CHEM 5317, lane 2 DAOMC 180753, and lane 3 negative control.

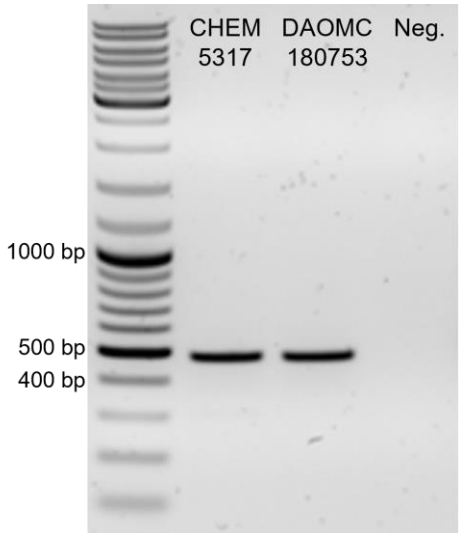

Figure 3B.2 - PCR Amplification of β-tubulin gene in CHEM 5317 and DAOMC 180753. β-tubulin band at ~ 480 bp. Gel Lane 1 is CHEM 5317, lane 2 is DAOMC 180753, and lane 3 is negative control.

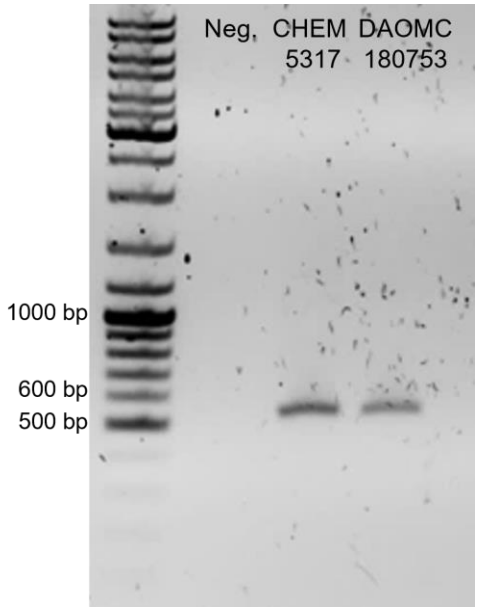

Figure 3B.3 - PCR Amplification of Calmodulin gene in CHEM 5317 and DAOMC 180753. Calmodulin band at ~ 550 bp. Gel lanes from left to right: lane 1 negative control, lane 2 CHEM 5317, and lane 3 DAOMC 180753.

Appendix 3C: *Penicillium sp.* Included in Phylogenetic Analysis

Table 3C.1- *Penicillium species* included in phylogenetic analysis of CHEM 5317 and DAOMC 180753. Includes outgroup, *Penicillium coralligerum* CBS 123.65. CBS = culture collection of the CBS-KNAW Fungal Biodiversity Centre (Utrecht, Netherlands); IMI = CABI Genetic Resources Collection (Surrey, UK); IBT = Culture collection of Center for Microbial Biotechnology (CMB) at Department of Systems Biology, Technical University of Denmark; NRRL = ARC Culture Collection, US Department of Agriculture, Peoria, Illinois, USA; ATCC = American Type Culture Collection, Manassas, VA, USA

CBS #	Name	Other collections	Origin	GenBank accession or reference		
				ITS	β-tubulin	CMD
472.84	*Penicillium albocoremium*	FRR 2931 = IBT 10682 = IBT 21502	Salami, Denmark	AJ004819.1	AY674326.1	KU896819.1
324.89	*Penicillium aurantiogriseum*	NRRL 971 = CBS 249.89 = ATCC 48920 = FRR 971 = IBT 14016	N/A	AF033476.1	AY674296.1	KU896822.1
100540	*Penicillium cavernicola*	IBT 14499	Cave wall of Lechuiguilla Cave, New Mexico (USA)	NR_16384.1	KJ834439.1	KU896827.1
123.65	*Penicillium coralligerum*	ATCC 16968 = NRRL 3465	France	JN617667	KJ834444	KJ866994
144.45	*Penicillium cyclopium*	ATCC 8731 = IBT 5130 = NRRL 1888	Rotten fruit, Sweden	JN097811.1	AY674310.1	KU896832.1
474.84	*Penicillium discolor*	IBT 21523 = IBT 5738 = IBT 14440 = FRR 2933	New Zealand	AJ004816.1	AY674348.1	KU896834.1
317.48	*Penicillium echinulatum*	ATCC 10434 = NRRL	Petri dish contaminant, Ottawa, Canada	AF033473.1	AY674341.1	DQ911133.1

		1151 = IBT6294 = FRR 1151				
476.84 794.95	*Penicillium freii*	IBT 4137	Barley, Denmark	JN942696.1	AY674290.1	KU896836.1
332.48	*Penicillium gladioli*	ATCC 10448 = FRR 939 = IBT 14772 = NRRL 939	Corn of *Gladiolus* sp. from Netherlands imported to Columbia, USA	AF033480.1	FJ004412.1	KU896837.1
135.41	*Penicillium hirsutum*	ATCC 10429 = FRR 2032 = IBT 21531 = NRRL 2032	Aphid, Netherlands	NR_163544.1	AF003243.1	KU896840.1
115506	*Penicillium melanoconidium*	IBT 3444	Wheat, Denmark	AJ005483.1	AY674304.1	KU896843.1
101135	*Penicillium neoechinulatum*	CBS 169.87 = IBT 3493 = IBT 21537 + NRRL 13486	Cheek pouch of *Dipodomys spectabilis* 8 km east of Portal, Arizona	JN942722.1	AF003237.1	KU896844.1
N/A	*Penicillium nordicum*	ATCC 44219 = IBT 133007 DTO098-F7	Salami, Italy	KJ834513.1	KJ834476	KU896845.1
107.11	*Penicillium palitans*	ATCC 10477 = IBT 23034 = NRRL 2033	N/A	NR_171582.1	KJ834480.1	KU896847.1
222.28	*Penicillium polonicum*	IBT 12821 =NRRL 995 YC-IK12	Soil, Poland	AF033475.1	AY674305.1	MN124169.1
111225	*Penicillium thymicola*	IBT 5891	N/A	KJ834518	AY674321	FJ530990
635.93	*Penicillium tricolor*	IBT 12493 = DAOM 216240	*Triticum aestivum,* Saskatchewan, Canada	JN942704.1	AY674313.1	KU896852.1

20157	*Penicillium venetum*	ATCC 16025 = IBT 5464	*Armoracia rusticana,* Kgs. Lyngby, Denmark	AJ005485.1	AY674335.1	KU933407.1
603.74	*Penicillium verrucosum*	ATCC 48957 = FRR 965 = IBT 12809 = IBT 4733 = IMI 200310 = NRRL 965	N/A	NR_119495.1	MN969405.1	DQ911138.1
390.48	*Penicillium viridicatum*	ATCC 10515 = FRR 963 = IBT 23041 = NRRL 963	Air, Washington DC, USA	AY373939.1	AY674295.1	KU896856.1

Chapter 4: Metabolomic Analysis of CHEM 5317 and DAOMC 180753

4.1 Introduction

4.1.1 Metabolomics Overview

Secondary metabolite profiling as a technique in fungal taxonomy was first performed by Frisvad and Filtenborg (1983), who used an agar-plug-thin-layer-chromatography (TLC) technique to profile species in the genus *Penicillium*.[146] In the years since, the techniques used in metabolomic analyses have evolved from TLC silica plates to include more accurate instrumentation, such as high-resolution mass spectrometry (HRMS).[147] The modern field of metabolomics is comprised of two differing strategies for comparing metabolite production in biological systems: targeted and untargeted metabolomics. Targeted metabolomics focuses on a species' known metabolites, typically of a specific chemical class of molecules or compound of interest within a known metabolome.[148,149] Untargeted metabolomics provides a more comprehensive overview of an organism's metabolic profile: the number of compounds analyzed is much larger than in targeted metabolomics, as both known and unknown compounds in the dataset are analyzed.[150] One of the greatest advantages of using an untargeted metabolomics approach in metabolic profiling is the ability to collect vast amounts of data without pre-existing knowledge clouding analytical expectations. The workflow for an untargeted metabolomics study, as outlined in **Figure 4.1.1**, begins with raw data acquisition via High-Resolution Mass Spectrometry (HRMS) or High-Resolution Mass Spectrometry/Mass Spectrometry (HRMS/MS). Data acquisition is then followed by data preprocessing, mass feature detection, and application of

statistical and/or chemometric methods of mass feature screening, before mass feature characterisation is performed.[151]

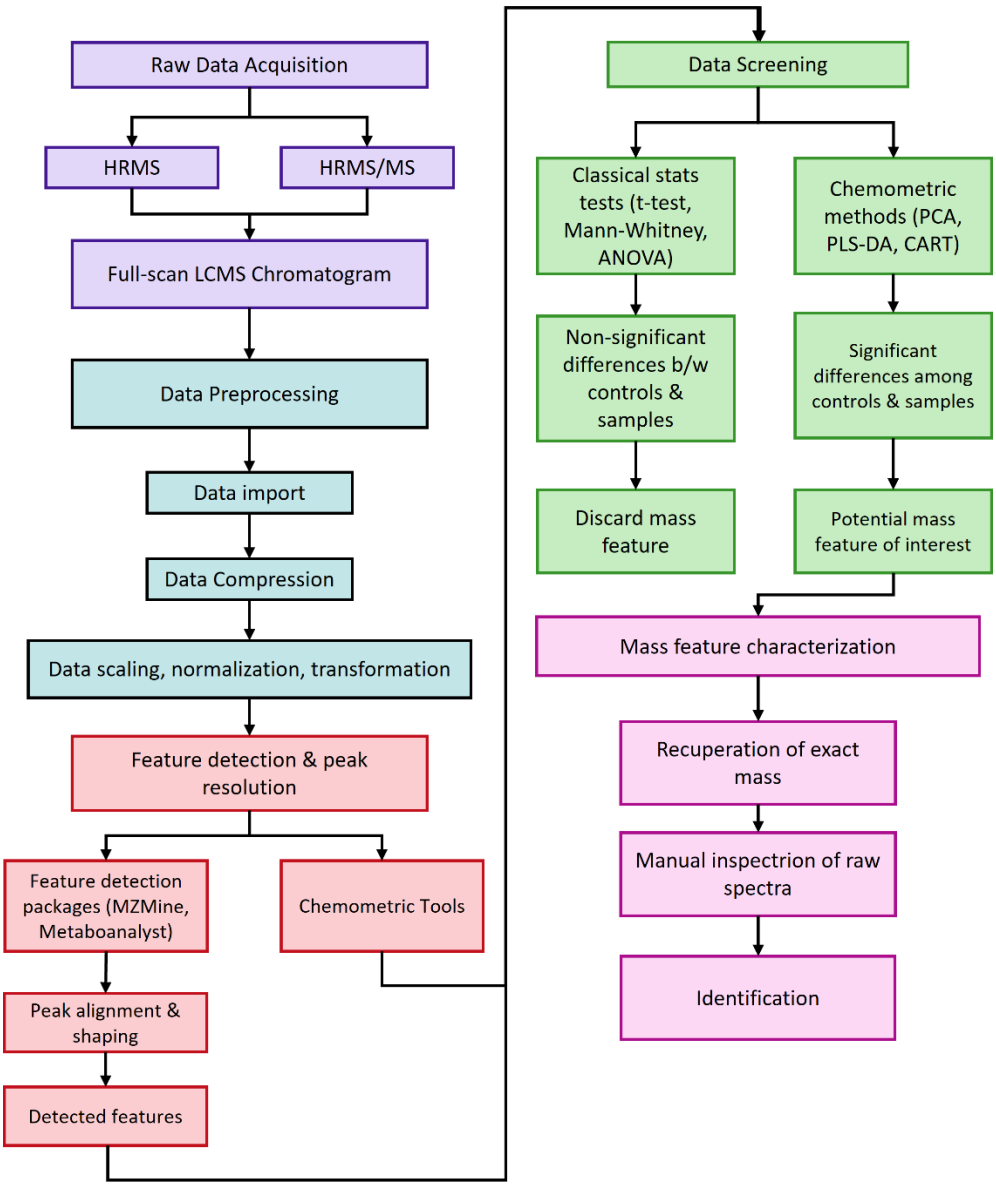

Figure 4.1.1 - Workflow of an Untargeted Metabolomics Study. Adapted from Gorrochategui *et al*.[151] Workflow for an untargeted metabolomic study begins with raw data acquisition, followed by data preprocessing, mass feature detection, data screening, and finally mass feature characterisation.

4.1.2 Multivariate Analysis – Principal Component Analysis

The natural challenge when analyzing the data collected from untargeted metabolomics experiments is the processing and interpretation of a massive volume of measurements that vary in dimension (retention time vs mass scan range vs scan amplitude). Thus, analytical chemists must navigate the delicate balance of reducing the number of dimensions in a data set, without excluding measurements that are vital to generate meaning.[148,152] As such, multivariate and statistical analyses are employed to visualize datasets, such that the patterns characteristic of a metabolic fingerprint may be revealed.[148] The overarching objective of multivariate analysis is the decomposition of a data set to model these "hidden phenomena". It is assumed that the explanation(s) for the maximum variance among the data set are directly correlated to these hidden phenomena. Among the various methods utilized in multivariate analysis, the most common first-pass mode of analysis is the Principal Component Analysis (PCA). Principal component analysis is an unsupervised data analysis method that separates a data matrix (X) into two pieces: a 'structure' part and a 'noise' part, as demonstrated by **Equation 4.1.1** below, where TP^T represents the 'structure' and E represents the 'noise' of the dataset.[153]

$$X = TP^T + E$$

Equation 4.1.1: Principal component model, where X = data matrix, T = score matrix, P^T = loading matrix (transposed), and E = residual matrix. TP^T represents the structure, whereas E represents the noise in the dataset.

Principal Component Analysis both transforms the dataset into a coordinate system for visualization, and reduces the dimensions of the data model, as only the first several Principal Components (PCs) are used in the data modeling. In the principal component data model, the dataset is broken down into principal components PCs that each explain successively smaller and

smaller portions of the variance observed in the dataset. This portion of the data model may be visualized using a Scree plot, which displays how each principal component contributes to the total dataset variation, as shown in **Figure 4.1.2**. The first principal component, PC1, always explains the largest portion of the total variance in a dataset. The following principal component, PC2, explains the second largest; and subsequent principal components follow an identical pattern. The plot most frequently used in multivariate data analysis is the score plot of PC1 vs PC2, which visualises samples in PC variable space, and its corresponding loading plot, which depicts the individual variables in this space. In the context of a metabolomics analysis, these variables represent mass features in PC variable space. These plots are vital to metabolomic data analysis as these two specific PCs explain the greatest portion of the total variance observed in the dataset. Thus, identifying the samples or variables exerting the highest impact on variance in a dataset is vital to interpreting a dataset, selecting outliers in a data model, and gives insight into the quality of features included in the data model.

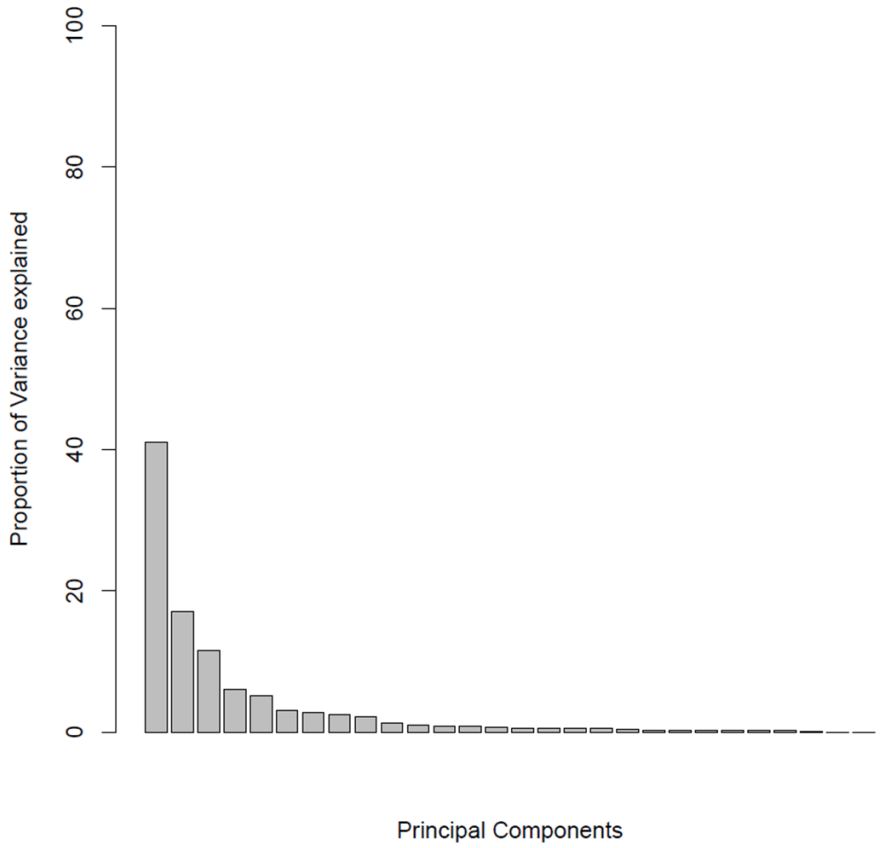

Figure 4.1.2 - Scree Plot Example. Scree plot associated with CHEM 5317 and DAOMC 180753 YES and YESNY agar and exudate principal component analysis shown in **Figure 4.3.2**. Principal component number is represented along x-axis and proportion of total dataset variation contributed by each principal component represented along y-axis.

4.1.3 Non-Ribosomal Peptide Synthetases

Fungal peptidyl alkaloids and other amino acid derivative natural products are synthesized primarily by Non-Ribosomal Peptide Synthetases (NRPSs). NRPSs are multi-modular mega-enzymes that catalyze the biosynthesis of peptides in an assembly-line fashion.[154] NRPS enzymes have the unique ability to select and incorporate non-proteinogenic amino acids as building blocks in peptide biosynthesis, such as ornithine and imino acids, which contributes to the high diversity of their biosynthetic products.[155,156]

Each module of an NRPS enzyme activates and couples an amino acid (or an amino acid derivative) to a growing peptide chain, passing the intermediary down the assembly line to eventually be cleaved.[154,157] NRPS modules are comprised of several protein domains that perform a specific task in peptide synthesis, as shown in **Figure 4.1.3**. The adenylation (A) domain selects, activates, and loads the amino acid onto the thiolation (T) domain (also referred to as the peptidyl carrier protein, or PCP, domain), which possesses a 4'-phosphopantetheine (Ppant) arm.[157] The tethered chain may then be shuttled through accessory protein domains in the NRPS module, including, but not limited to, epimerization (E), N-methylation (M), reductase (R), and heterocyclization (Cy) domains.[158] The tethered amino acid is then transferred to a condensation (C) domain, where the newly incorporated amino acid is coupled to the growing peptide chain upstream. The final domain, the thioesterase (TE) domain, cleaves the polypeptide from the NRPS enzyme, producing either a macrocyclization or a hydrolysis product.

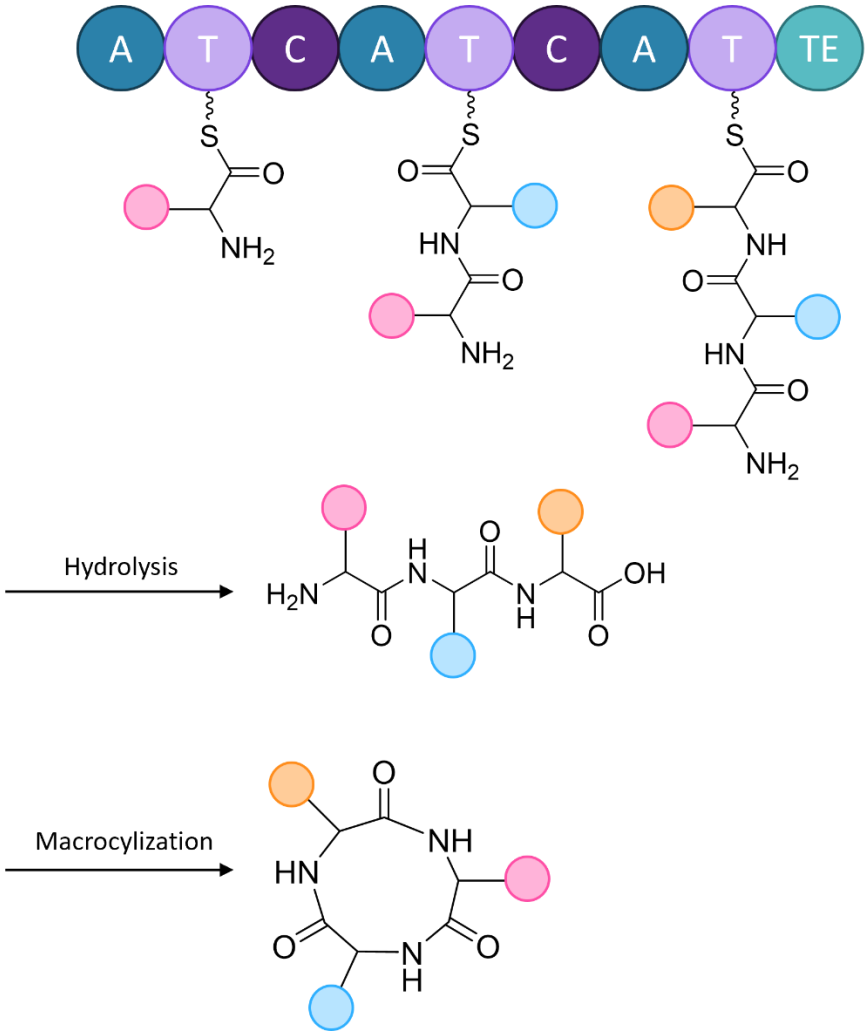

Figure 4.1.32 - NRPS Structural Overview. Schematic representation of the basic assembly line structure featured in NRPS enzymes. Necessary protein domains of NRPS enzymes shown: Adenylation (A), Thiolation (T, also referred to as PCP), Condensation (C), and Thioesterase (TE). Polypeptide chain may be released from the TE domain via hydrolysis to create a linear peptide chain, or via macrocyclization to form a ring. The circular 'functional groups' added to the growing peptide chain in the figure represent different amino acids added during NRPS synthesis.

4.1.3 The Quinazoline Family of Natural Products

The majority of the previously identified secondary metabolites produced by *P. thymicola* are peptidyl alkaloids made by NRPSs and are derived from anthranilic acid (Ant) building blocks. Anthranilic acid is a primary metabolite synthesized by organisms that can synthesize tryptophan, wherein a portion of the metabolic flux generally attributed to the production of chorismite is

redirected to phenylalanine and tryptophan biosynthesis.[159] As discussed in Chapter 1, *P. thymicola* produces four members of the quinazoline family of natural products, including fumiquinazolines F and T, alantrypinone, and serantrypinone. Fumiquinazolines are relatively new secondary metabolites that have emerged in the last two decades from terrestrial and marine fungi.[160] Metabolites belonging to the quinazoline family of secondary metabolites are identified by their pyrazino-[2,1-b]-quinazoline-3,6-dione core that is linked to a tryptophan indole moiety, as highlighted in **Figure 4.1.4**.[160,161] Tryptophan-derived alkaloids, such as fumiquinazolines, possess a high level of structural and bioactive diversity, with members of this class of natural products demonstrating antiepileptic[162], antimicrobial[163], and antimalarial[164] activities. Fumiquinazoline F, the simplest core structure of the quinazoline family, is biosynthesized by a trimodular NRPS with 3 A domains that incorporate Ant and two amino acids (L-tryptophan and L-alanine).[165–168] Postmodification of the fumiquinazoline F core structure is done by FAD-dependent monooxygenases and/or FAD-dependent pyrazinone oxidazes, generating the diversity of the fumiquinazoline family.[169]

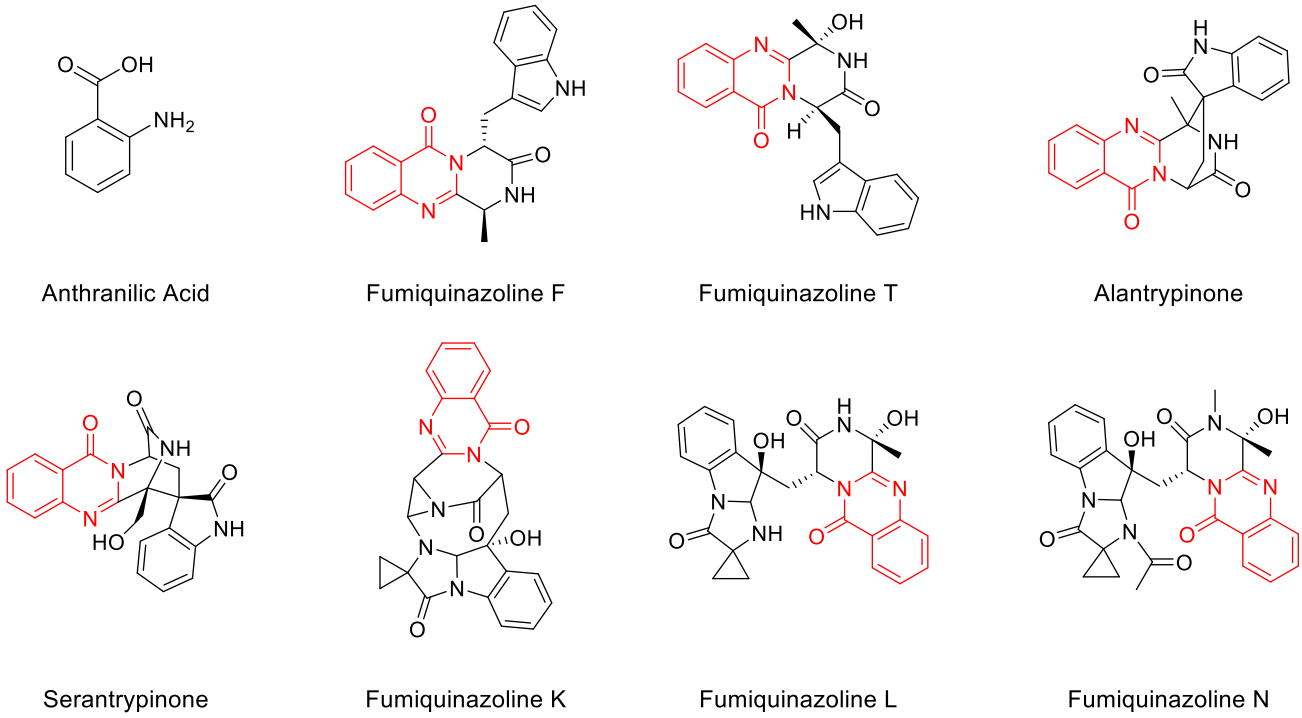

Figure 4.1.4 - Representative compounds of the quinazoline family of natural products. Biosynthesized with anthranilic acid building blocks, shown on top left. The pyrazino-[2,1-b]-quinazoline-3,6-dione core is highlighted in red. Fumiquinazolines F and T, alantrypinone, and serantrypinone have previously been isolated from *P. thymicola*. Fumiquinazolines K, L, and N demonstrate the chemical diversity of this natural product family compared to core structure, fumiquinazoline F.

4.1.5 Chapter 4 Overview

In this chapter, an untargeted high resolution mass spectrometry-based metabolomics approach was used to elucidate the secondary metabolite profiles of the two *P. thymicola* strains, CHEM 5317 and DAOMC 180753. Secondary metabolites were extracted from the agar of the six media types utilised and outlined in Chapter 2 for both fungal strains. The chemical profile of fungal exudate was also analysed, when present. Using Ultra-Performance Liquid Chromatography-High-Resolution Mass Spectrometry (UPLC-HRMS), the majority of the known metabolites of *P. thymicola* were identified from the strain CHEM 5317, while the chemical profile of DAOMC 180753 was more challenging to ascertain.

4.2 Materials and Methods

4.2.1 Culture Conditions

CHEM 5317 spore dilutions were performed using dH_2O and a toothpick to scrape mycelia from original isolate plates grown on ISP2 agar (formulations in **Appendix 2A**). 200 µL of the serial dilutions were plated on ½ Potato Dextrose Agar (PDA) + chloramphenicol plates and grown at 27ºC for four days in the dark. Single spore plates were made from spore dilution plates using a sterile needle and excising a fungal colony and placing directly into the centre of a new ½ PDB plate. Single spore plates were incubated at room temperature for 7 days in the dark. Plates for metabolomics analysis were three-point inoculated on chosen media, as recommended by Samson and Pitt[170] using semi-solid agar, in hexicate. expose the microorganism to multiple nitrogen sources, types of sugar, salt, and low water activity.

Six different types of solid media were used: CYA, YES, DG18, OMA, CYANY (CYA + Nystatin), and YESNY (YES + Nystatin); exact media formulations can be found in **Appendix 2A.** Plates were then grown at 25ºC in incubator for 14 days in the dark.

4.2.2 Metabolite Extraction from Fungal Mycelium and Agar

Metabolites were extracted from the fungal mycelium by taking 12 agar plugs of the fungal colonies per plate and transferring them to a sterile glass culture tube. Plugs were then frozen at -20ºC in the glass culture tubes prior to extraction. Metabolite extraction was conducted using ethyl acetate (EtOAc) as the solvent and agitated on rotary shaker for 90 minutes. Supernatant was transferred to a scintillation vial and dried via pin dryer. Dried extracts were resuspended in Optima LCMS-grade MeOH to a concentration of 1 mg/mL and 500 µL was transferred to an amber HPLC vial. Samples were stored at -20ºC prior to being run on UPLC-HRMS.

4.2.3 Exudate Collection

Fungal exudate was aspirated off the fungal colony surfaces after 14-day growth period using a 10 µL micropipette and transferred to a 1.5 mL microcentrifuge tube. Aspiration was performed with caution to not disturb fungal mycelium. Samples with noticeable mycelial contamination were syringe-filtered before being transferred to an amber HPLC vial. Samples stored at -20^{o}C until run on UPLC-HRMS.

4.2.4 UPLC-HRMS Data Collection

The agar and exudate samples were run separately on the UPLC-HRMS and the extract order was randomized. Samples were analyzed using a Thermo Ultimate 3000 ultra-high-performance liquid chromatography (UPLC) coupled with a Thermo LTQ Orbitrap XL high-resolution mass spectrometer (HRMS) and UltiMate Corona VeoRS charged aerosol detector (ThermoFisher Scientific Inc.). Chromatography was performed using a Phenomenex C_{18} Kinetex column (50 mm x 2.1 mm ID, 1.7 µm) with a flow rate of 0.35 mL/min. H_2O gradient used (+0.1% formic acid) and acetonitrile (ACN) (+0.1% formic acid) was as follows: starting at 5% ACN and increasing to 95% ACN over 4.5 min, holding at 95% ACN for 3.5 min and returning to 5% ACN for 0.5 min. 5% ACN was held for 5 min to allow column to equilibrate to return to starting conditions in preparation for the next sample. Mass spectrometer was operated in ESI^+ mode with a scanning range of 100 to 2000 m/z, with the following parameters: sheath gas (40), auxiliary gas (5), sweep gas (2), spray voltage (4.2 kV), capillary temperature (320^{o}C), capillary voltage (35 V), and tube lens (100 V).

4.2.5 Metabolomics Data Preprocessing Overview

Processing of the UPLC-HRMS raw data was completed in MZMine v. 2.53, wherein the raw data was transformed from a 3-dimensional matrix containing retention times, mass-to-charge ratios and relative intensities, into a 2-dimensional matrix that can be exported for statistical analysis. A comprehensive summary of the exact data parameters used for data preprocessing and dimension reduction of the data model contained herein is outlined in **Appendix 4B**. It is important to note that these data preprocessing parameters can and should be adjusted in conjunction with any dataset studied, and manual inspection of raw data files is key to preprocessing raw data to answer the research questions.[171]

An overview of the data preprocessing workflow in MZMine is shown in **Figure 4.2.1**. Upon importing the UPLC-HRMS raw data, mass peak detection is used to generate a list of ions (mass-to-charge ratios, m/z) that are above a user-specific noise threshold. Thus, any detected features below this noise threshold are eliminated from the mass list, which may contain peaks resulting from instrument noise, carryover between samples, and minor contaminants. Following peak detection, chromatograms are constructed, in this case using the ADAP Chromatogram Builder, which builds an extracted ion chromatogram (XIC) for each m/z value detected over a minimum number of consecutive scans. The resulting chromatograms are then separated into individual peaks via chromatogram deconvolution. The Join Aligner was then used to align mass features from different samples based on the mass and RT of each peak within a user-specific mass and RT tolerance range. Lastly, a gap filling step is performed using the Peak Finder (multithreaded) algorithm. This step ensures that no mass features were 'missed' during the previous steps that may be relevant to the data set. Some chromatographic features in an aligned feature list may not be detected in every sample for reasons such as a peak intensity below the

minimum abundance threshold, peaks being filtered out due to low peak intensity, misalignment as a result of m/z or RT shifts, inaccurate peak detection and deconvolution of co-eluting compounds. The Peak Finder algorithm works to reduce false missing values by re-integrating the peak area where the peak is expected in the original raw data. Before exporting the data matrix, a user may manually go through the final mass feature list and eliminate any noise peaks remaining in the data set. The final mass feature list is then exported to a .csv file for data processing and visualisation.

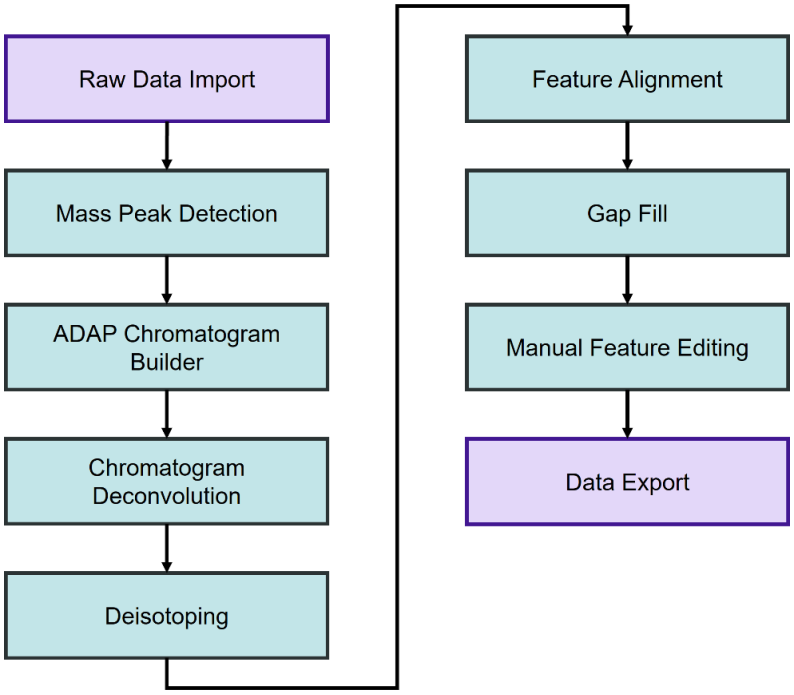

Figure 34.2.1 - Data preprocessing workflow in MZMine v. 2.53.

4.2.6 Metabolomics Data Processing and Multivariate Analysis

Data normalisation was performed in R Studio using a sum normalisation algorithm. In this type of data normalisation, column sums for all mass features are generated, then normalized

by dividing each mass feature by the overall sum of feature values for a sample. The sum of all feature values of a sample is divided by each mass feature by sum and repeated for each mass feature. Multivariate and univariate data analysis performed in R Studio using the Metabolomics Univariate and Multivariate Analysis (*MUMA*) package.

A comprehensive list of published metabolites produced by *P. thymicola* was compiled from the literature and their common ion adducts were calculated based on their monoisotopic masses (**Appendix 4A**).

4.2.7 Binary Heatmap

Replicate signal intensities that were exported from MZMine v. 2.53 were averaged for each media type in Excel. These values were then transformed into binary values using a threshold of 1E5, wherein values < 1E5 were represented as 0 and values > 1E5 were represented with as 1. This binary file was then imported into R to construct the basic binary heatmap using the *pheatmap* R package, using the clustering method 'ward.D2'.

4.3 Results and Discussion

4.3.1 Divergence of CHEM 5317 & DAOMC 180753 Metabolomic Profiles

The raw data files acquired using UPLC-HRMS were pre-processed using MZMine v. 2.53, wherein the metabolite extractions from both the mycelium and the fungal exudate were processed in a single batch. Data preprocessing in MZMine v. 2.53 reduced the number of identified mass features to approximately 500, which were exported as a 2-dimensional data matrix for data normalization and multivariate analysis in R.

As a first-line data visualization method, hierarchical clusters were created in R Studio to holistically compare the data content between the two strains in conjunction with the six different

media used. It was initially anticipated that the samples from the same media would cluster together, regardless of strain, as fungal strains of the same species are expected to produce similar chemistry in similar environments. Thus, the variance between each individual media type was expected to be larger than variance observed as a result of strain differences. Surprisingly, CHEM 5317 and DAOMC 180753 completely separated by strain in the hierarchical cluster, as shown in **Figure 4.3.1**. Within each strain group, the majority of samples grouped by media type, but never formed a media group with samples of the other strain. This preliminary hierarchical cluster analysis of the agar samples from both fungal strains revealed that the secondary metabolite profiles of CHEM 5317 and DAOMC 180753 contained potentially widespread disparities that required further statistical analysis.

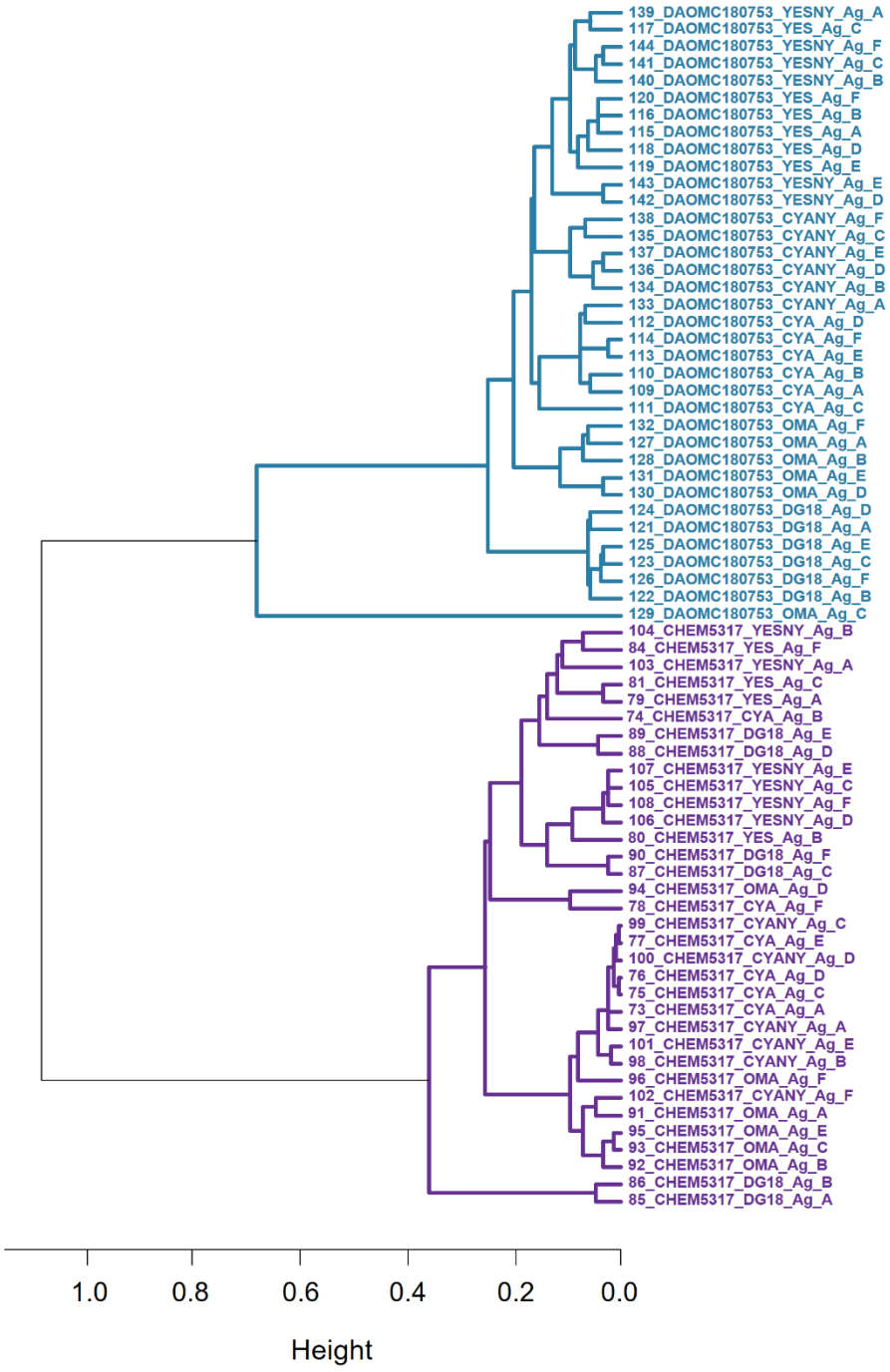

Figure 4.35 - Hierarchical Cluster Analysis of CHEM 5317 and DAOMC 180753 Agar Samples. Agar for both strains present in the analysis, wherein CHEM 5317 is shown in purple and DAOMC 180753 is shown in blue.

4.3.2 CHEM 5317 vs DAOMC 180753 Differences on YES and YESNY Media

To probe further into the differences between the CHEM 5317 and DAOMC 180753 metabolic profiles, the YES and YESNY agar and exudate samples were compared using PCA. As demonstrated by the score plot in **Figure 4.3.2 B**, the cumulative proportion of the variance explained by PC1 and PC2 was 58%. PC1, the largest principal component, represented the variance between the CHEM 5317 and DAOMC 180753 strains, contributing 41% of the total variance. The second principal component, representing the separation between the agar and exudate samples, accounted for 17% of the total 58% variance. The separation of the CHEM 5317 and DAOMC 180753 samples along PC1 supported initial observation from the hierarchical cluster (**Figure 4.3.1**) that the largest portion of the variance in the dataset was the result of differences in the metabolic profile between the two strains. Further, the variance between the YES and YESNY agar samples was minimal, indicating that the presence of nystatin in the solid media had a minimal effect on the metabolic profile of the mycelium, as demonstrated by both strains' agar samples grouping closely together along both PCs in the score plot. Conversely, the addition of nystatin in the YESNY media was associated with the production of exudate in both fungal strains, as no exudate was produced on the YES agar alone. This is demonstrated by the YESNY exudate samples grouping by strain and separating along PC2 in **Figure 4.3.2 B**.

As is evident by the PCA Loading plot shown in **Figure 4.3.2A**, the separation between the CHEM 5317 and DAOMC 180753 strains was not the result of sample outliers, but rather the entirety of the datapoints in the system contributing to the strain variance. Thus, it was postulated that several mass features were being produced by one strain and not the other. However, the sheer volume of mass features in each concentrated portion of the loading plot made it impossible to

identify specific mass features in each swarm that were potentially contributing heavily to this separation.

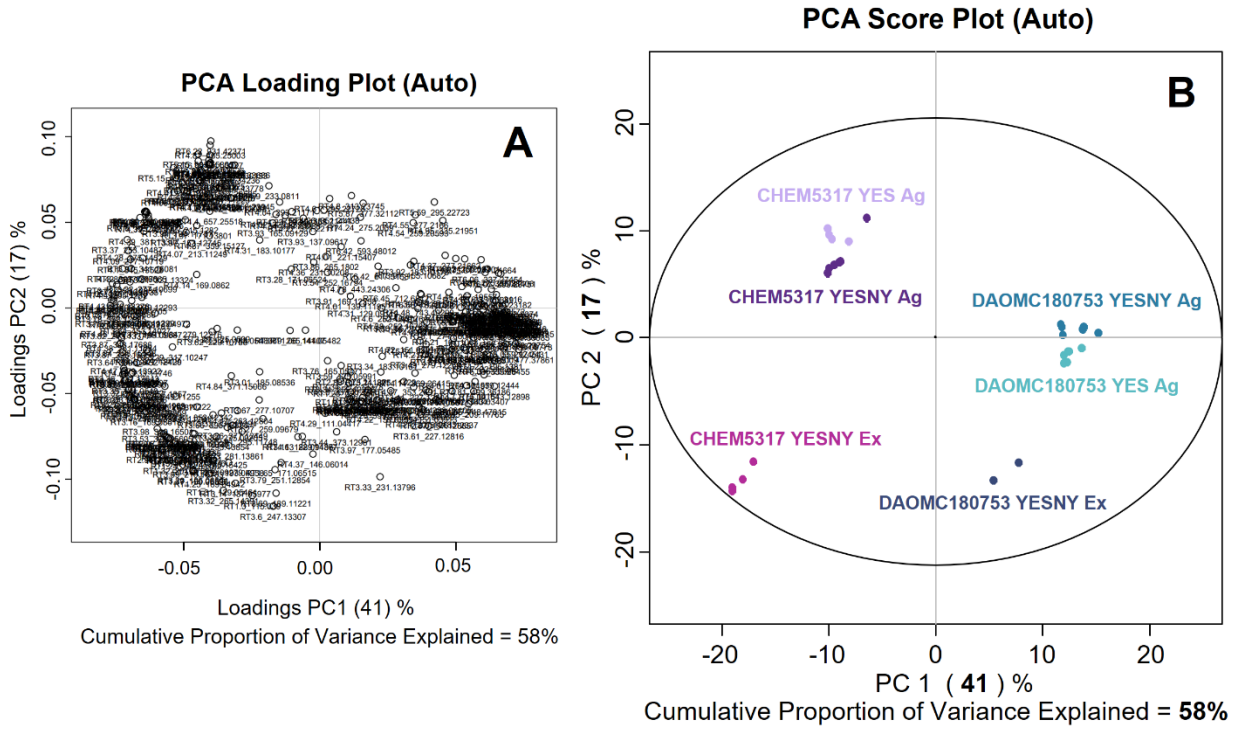

Figure 4.36 - Principal Component Analysis of CHEM 5317 and DAOMC 180753 on YES and YESNY Agar and Exudate. A. PCA loading plot. **B.** PCA score plot, autoscaled. Strain separation along PC1 explaining 41% of the total 58% variance. Agar and exudate samples separating along PC2, explaining 17% of the total variance.

4.3.3 CHEM 5317 Strain Profiling Based on *P. thymicola* known Metabolites

The secondary metabolites produced by *P. thymicola* were collated from the literature with the aim of investigating their abundance in CHEM 5317 and DAOMC 180753 using UPLC-HRMS. Using the exact masses of the published metabolites, common ion adducts for MS ESI$^+$ mode were calculated, as outlined in **Appendix 4A**. An outline of the *P. thymicola* known metabolites in comparison with our experimental observations are displayed in **Table 4.3.1**. The majority of the *P. thymicola* metabolites published in the literature are associated with the type

strain, IBT 5891, but the metabolites associated with DAOMC 180753, according to Nguyen *et al.*[60] have also been outlined.

Table 4.3.1 - Overview of *P. thymicola* Metabolites Observed in CHEM 5317 and DAOMC 180753. Metabolites produced by *P. thymicola* IBT 5891 and DAOMC 180753 according to literature review are shown on the left. An outline of the experimental observations of metabolite production by CHEM 5317 and DAOMC 180753 are listed on the right.

Metabolite	Literature		Experimental			
	IBT 5891	DAOMC 180753	CHEM 5317		DAOMC 180753	
			Agar	Exudate	Agar	Exudate
Alantrypinone[63]						
α-pyrone (PC-2)[14]						
Anacine[172]						
Daldinine D[64]						
Dipodazine[14]						
Fumiquinazoline F[14,173]						
Fumiquinazoline T[65]						
2-methylisoborneol[64]						
Ochratoxin A[60]						
Ochratoxin B[60]						
Penigequinolone[14]						
Pestafolide A[65]						
Pyranonigrin A[174]						
Serantypinone[64]						
Thymipyrone A[65]						
Verrucolone[14]						

In conjunction with data preprocessing in MzMine v 2.53 and statistical analysis performed in R Studio, the UPLC-HRMS .RAW data files were manually inspected using QualBrowser (XCalibur). Manual inspection performed on the chromatograms and mass spectra were to confirm the presence of the adducts of *P. thymicola* known metabolites in the data samples, as outlined in **Appendix 4A**.

Alantrypinone

The exact mass of alantrypinone (372.12 Da) was utilised to identify the common ion adducts of this natural product in the agar and exudate of CHEM 5317 and DAOMC 180753 via manual inspection in QualBrowser. No ion adducts associated with alantrypinone were found in the DAOMC 180753 agar or exudate samples. In CHEM 5317, the $[M + H]^+$ of alantrypinone was found in the MS data at *m/z* 373.1300 at RT 3.78 **(Figure 4.3.3 A).** At the same RT, the $[M+Na]^+$ and $[2M+H]^+$ signals were found at *m/z* 395.1120 and *m/z* 745.2531, respectively (**Figure 4.3.3A** and **C**). A box and whisker plot of the peak heights for the [M+H]+ of alantrypinone for CHEM 5317 and DAOMC 180753 YES and YESNY agar and exudate samples is found in **Figure 4.3.3 D**. The boxplot demonstrates the stark difference in peak heights for the [M+H]+ adduct of alantrypinone at RT 3.78 between the six samples shown, wherein the DAOMC 180753 samples demonstrated no evident peaks at this *m/z*, its samples remaining at the baseline peak height (**Figure 4.3.3 D**). Based on the boxplot, CHEM 5317 exhibited the highest signal intensity for the [M+H]+ adduct of alantrypinone compared to the other CHEM 5317 samples.

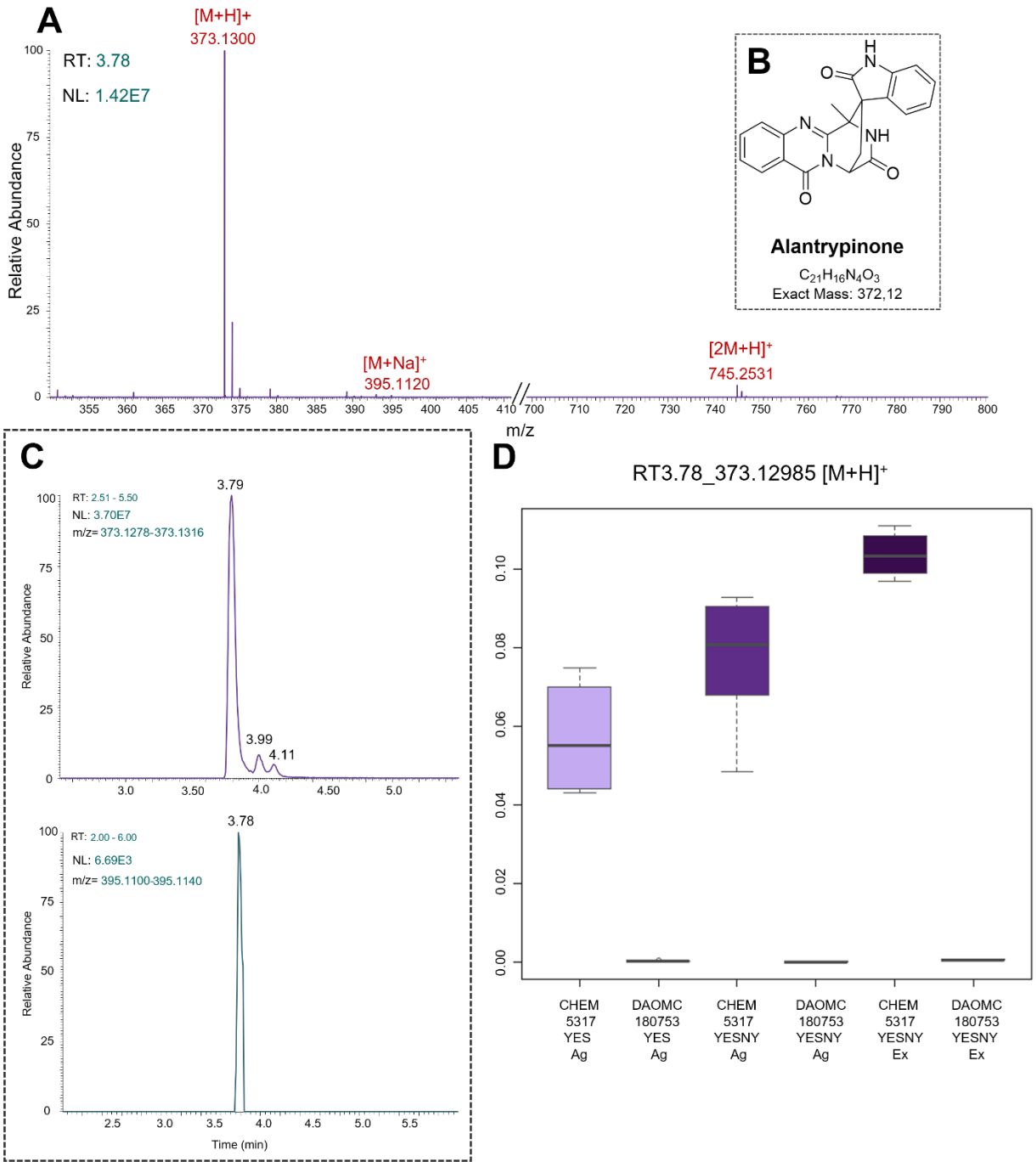

Figure 4.3.37 - Alantrypinone in CHEM 5317 YES Media. A: Alantrypinone mass spectrum of CHEM 5317 YES agar sample at RT 3.78. Alantrypinone $[M+H]^+$ at m/z 373.1300, $[M+Na]^+$ at m/z 395.1120, and $[2M+H]^+$ at m/z 745.2531. **B:** Alantrypinone chemical structure and exact mass at 372.12 Da. **C:** Alantrypinone $[M+H]^+$ XIC at RT 3.79 (purple) and [M+Na]+ at 3.78 (teal, below). **D.** Box and whisker plot for m/z 373.12985 representing alantrypinone $[M+H]^+$ at RT 3.78 of CHEM 5317 YES Ag, DAOMC 180753 YES Ag, CHEM 5317 YESNY Ag, DAOMC 180753 YESNY Ag, and CHEM 5317 YESNY Ex.

Fumiquinazoline F/G

The exact mass of fumiquinazoline F/G (358.14 Da) was utilised to identify the common ion adducts of this natural product in the agar and exudate of CHEM 5317 via manual inspection in QualBrowser. No ion adducts associated with fumiquinazoline F/G were found in the DAOMC 180753 MS data. In CHEM 5317, the $[M+H]^+$ of fumiquinazoline F/G was found in the MS data at *m/z* 359.1505 (**Figure 4.3.4A**) at RT 4.39. At the same RT, the $[M+Na]^+$ and $[M+K]^+$ signals were found at *m/z* 381.1323 and *m/z* 397.1064, respectively. The XICs for the $[M+H]^+$ and $[M+Na]^+$ peaks are shown in **Figure 4.3.4C**, at RT 4.39 and 4.38, respectively. A box and whisker plot of the peak heights for both CHEM 5317 and DAOMC 180753 YES and YESNY agar and exudate samples at *m/z* 359.15112, corresponding to the $[M+H]^+$ peak at RT 4.39 is found in **Figure 4.3.4D**. A similar boxplot is shown in **Figure 4.3.4E** for *m/z* 381.13307 at RT 4.39, corresponding to the $[M+Na]^+$ ion adduct. Based on the univariate data analysis shown in the box and whisker plots, only the DAOMC 180753 YESNY Ex samples showed any peak heights above the baseline, but altogether the DAOMC 180753 samples showed no presence of fumiquinazoline F/G. With regards to the CHEM 5317 data, CHEM 5317 YESNY Ag exhibited the highest signal intensity for the $[M+H]^+$ adduct of fumiquinazoline F/G.

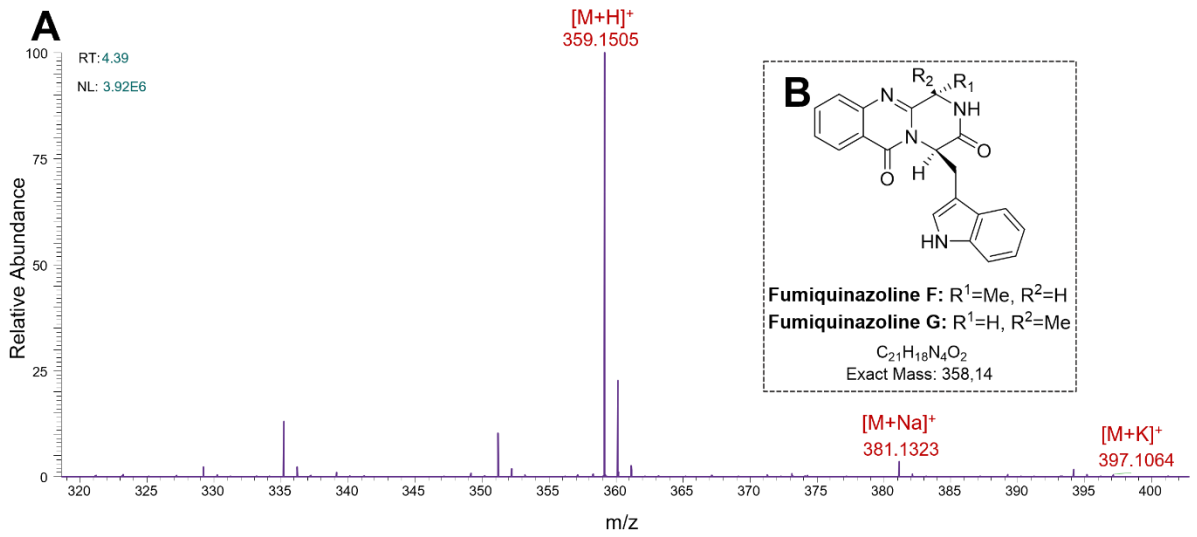
A
[M+H]+
359.1505
RT: 4.39
NL: 3.92E6
Relative Abundance
m/z
[M+Na]+
381.1323
[M+K]+
397.1064
B
Fumiquinazoline F: R1=Me, R2=H
Fumiquinazoline G: R1=H, R2=Me
C21H18N4O2
Exact Mass: 358,14

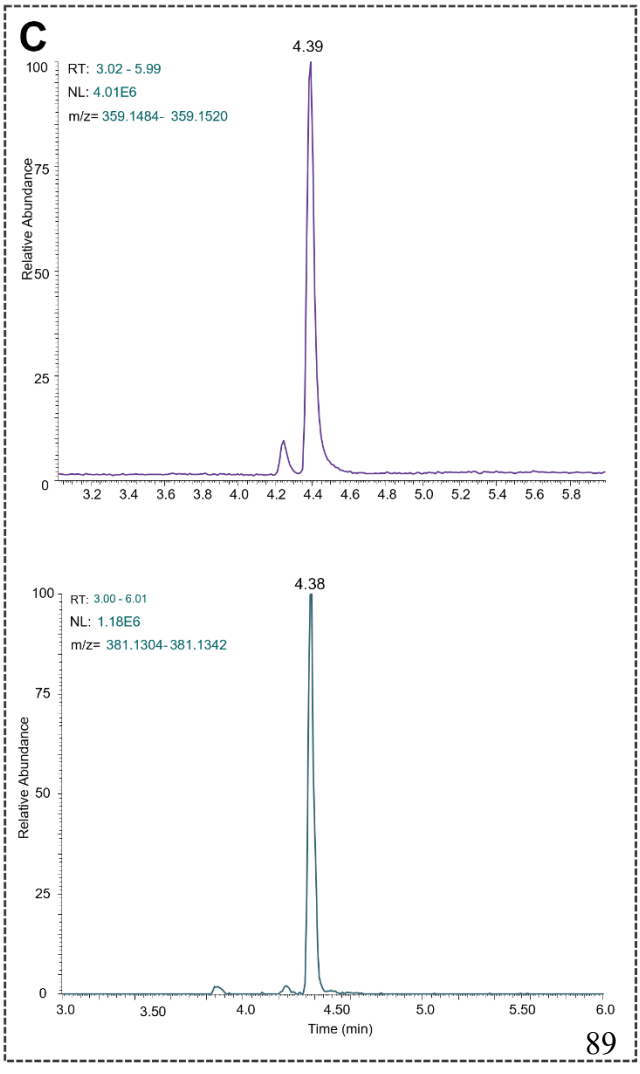
C
4.39
RT: 3.02 - 5.99
NL: 4.01E6
m/z= 359.1484- 359.1520
Relative Abundance
4.38
RT: 3.00 - 6.01
NL: 1.18E6
m/z= 381.1304-381.1342
Time (min)

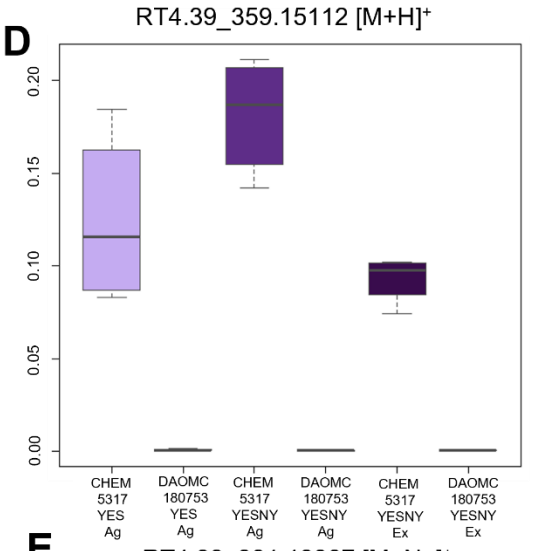
D
RT4.39_359.15112 [M+H]+
CHEM 5317 YES Ag
DAOMC 180753 YES Ag
CHEM 5317 YESNY Ag
DAOMC 180753 YESNY Ag
CHEM 5317 YESNY Ex
DAOMC 180753 YESNY Ex

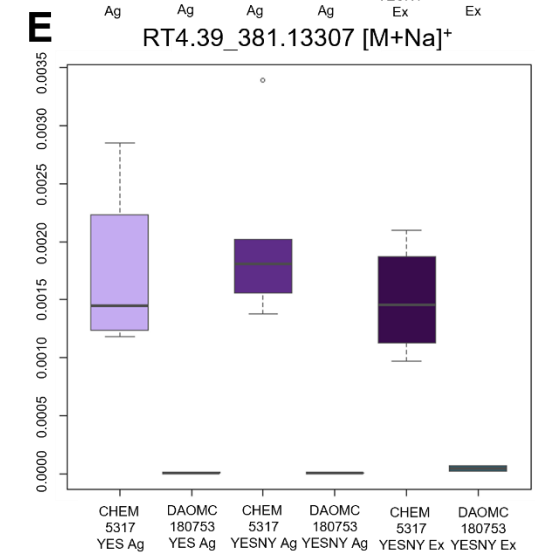
E
RT4.39_381.13307 [M+Na]+
CHEM 5317 YES Ag
DAOMC 180753 YES Ag
CHEM 5317 YESNY Ag
DAOMC 180753 YESNY Ag
CHEM 5317 YESNY Ex
DAOMC 180753 YESNY Ex

Figure 4.38- Fumiquinazoline F/G in CHEM 5317 YES Media. A: Fumiquinazoline F/G mass spectrum of CHEM 5317 sample at RT 4.39. Fumiquinazoline F/G $[M+H]^+$ at m/z 359.1505, $[M+Na]^+$ at m/z 381.1323, and $[M+K]^+$ at m/z 397.1064. **B:** Fumiquinazolines F and G chemical structures. **C:** Fumiquinazoline F/G XIC of $[M+H]^+$ at 4.39 (purple) and $[M+Na]^+$ at RT 4.38 (teal). **D:** Box and whisker plot for m/z 359.15112 at RT 4.39, corresponding to fumiquinazoline F/G $[M+H]^+$. CHEM 5317 YES Ag, DAOMC 180753 YES Ag, CHEM 5317 YESNY Ag, DAOMC 180753 YESNY Ag, and CHEM 5317 YESNY Ex. **E:** Box and whisker plot for m/z 381.13307 at RT 4.39, corresponding to fumiquinazoline F/G $[M+Na]^+$. Samples plotted are CHEM 5317 YES Ag, DAOMC 180753 YES Ag, CHEM 5317 YESNY Ag, DAOMC 180753 YESNY Ag, and CHEM 5317 YESNY Ex.

Fumiquinazoline T

The exact mass of fumiquinazoline T (374.14 Da) was utilised to identify the common ion adducts of this natural product in the agar and exudate of CHEM 5317 via manual inspection in QualBrowser. No chemical signals associated with fumiquinazoline T could be found in the DAOMC 180753 samples. In CHEM 5317, the $[M+H]^+$ of fumiquinazoline T was found in the MS data at *m/z* 375.1458 (**Figure 4.3.5A**) at RT 4.02. At the same RT, the $[M+Na]^+$ was identified at *m/z* 397.1279, the $[M+H-H_2O]$ at *m/z* 357.1356, and $[M+H-2H_2O]$ at *m/z* 339.1445. The XICs for the $[M+H]^+$ and $[M+Na]^+$ peaks are shown in **Figure 4.3.5C**, at RT 4.02. A box and whisker plot of the peak heights for both CHEM 5317 and DAOMC 180753 YES and YESNY agar and exudate samples at *m/z* 375.14419, corresponding to the $[M+H]^+$ peak at RT 4.02 is found in **Figure 4.3.5D**. Based on the results of the boxplot, it was evident that there was a considerable difference in relative abundance of the [M+H]+ ion adducts between the two strains. The DAOMC 180753 samples did not demonstrate any detectable peaks for m/z 375.1442 at RT 4.02, as these samples remained at baseline in the boxplot.

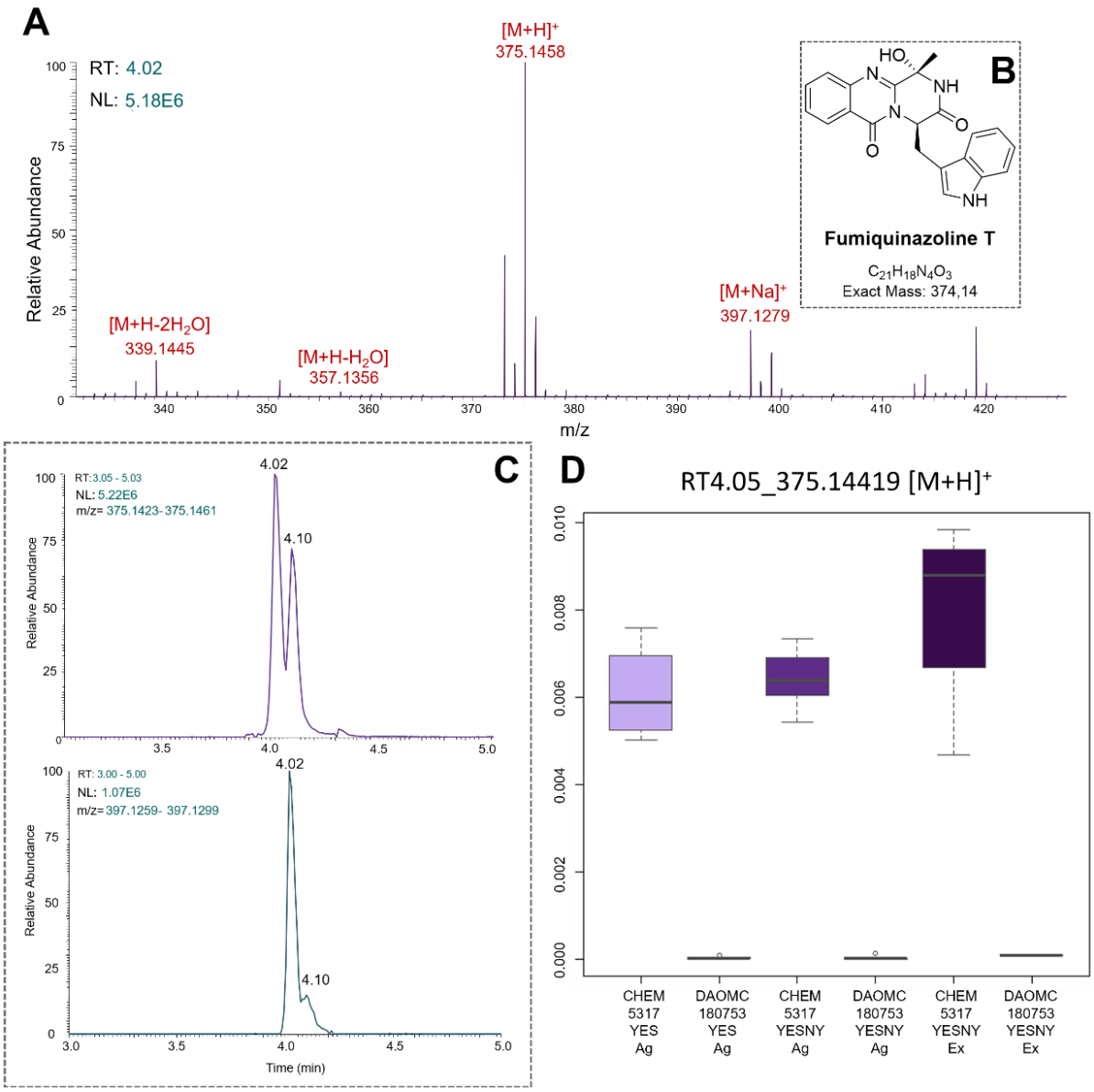

Figure 4.39 - Fumiquinazoline T in CHEM 5317 in YES Media. A: Fumiquinazoline T mass spectrum of CHEM 5317 at RT 4.02. Fumiquinazoline T $[M+H]^+$ at *m/z* 375.1458, $[M+Na]^+$ at *m/z* 397.1279, $[M+H-H_2O]$ at *m/z* 357.1356, and $[M+H-2H_2O]$ at *m/z* 339.1445. **B:** Fumiquinazoline T chemical structure. **C.** Fumiquinazoline T XIC at RT 4.02. **D:** Box and whisker plot for *m/z* 375.14419 at RT 4.05, corresponding with the $[M+H]^+$ of fumiquinazoline T. Shows samples CHEM 5317 YES Ag, DAOMC 180753 YES Ag, CHEM 5317 YESNY Ag, DAOMC 180753 YESNY Ag, and CHEM 5317 YESNY Ex.

Serantrypinone

The exact mass of serantrypinone (368.12 Da) was utilised to identify the common ion adducts of this natural product in the agar and exudate of CHEM 5317 via manual inspection of the raw data in QualBrowser. No chemical signals associated with serantrypinone were found in the DAOMC 180753 raw data. In CHEM 5317, the $[M+H]^+$ of serantrypinone was found in the MS data at *m/z* 389.1252 (**Figure 4.3.6A**) at RT 3.63. At the same RT, the $[M+Na]^+$ was identified at *m/z* 411.1072. The XIC for the $[M+H]^+$ peak is shown in **Figure 4.3.6C**, at RT 3.63. A box and whisker plot of the peak heights for both CHEM 5317 and DAOMC 180753 YES and YESNY agar and exudate samples at *m/z* 389.12452, corresponding to the $[M+H]^+$ peak at RT 3.64 is found in **Figure 4.3.6D**. Based on the results of the boxplot, it was evident that there was a considerable difference in relative abundance of the [M+H]+ ion adducts between the two strains. The DAOMC 180753 samples did not demonstrate any detectable peaks for m/z 389.1245 at RT 4.02, as these samples remained at baseline in the boxplot. The CHEM 5317 YESNY Ex samples exhibited the highest signal intensity of the six samples analysed via box and whisker plot.

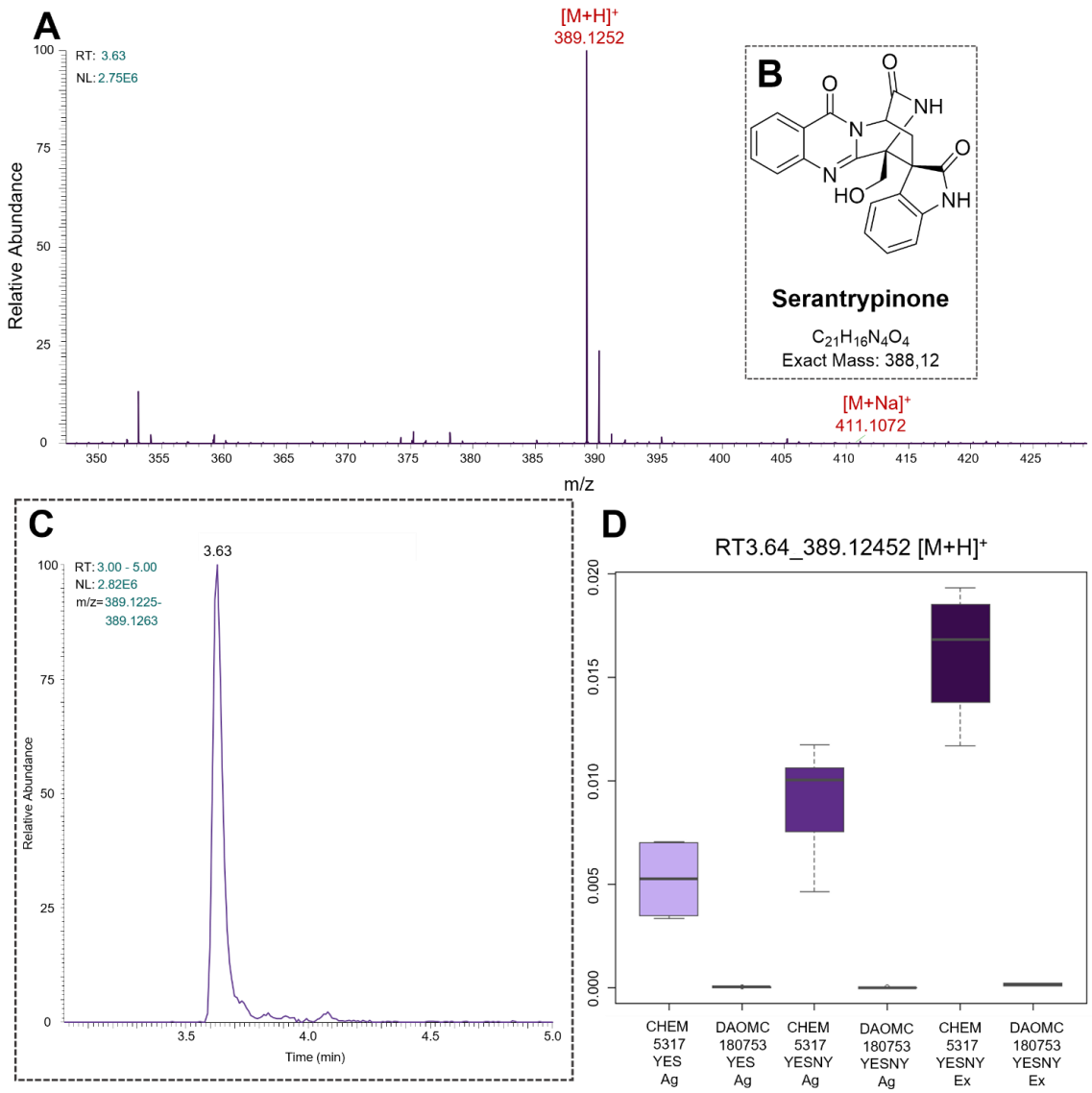

Figure 40- Serantrypinone in CHEM 5317 YES Media. A: Serantrypinone mass spectrum of CHEM 5317 at RT 3.63. Serantrypinone $[M+H]^+$ at *m/z* 389.1252 and $[M+Na]^+$ at *m/z* 411.1072. **B:** Serantrypinone chemical structure. **C:** Serantrypinone XIC at RT 3.63. **D:** Box and whisker plot for *m/z* 389.12452 at RT 3.64, corresponding with the $[M+H]^+$ of serantrypinone. Sample groups include CHEM 5317 YES Ag, DAOMC 180753 YES Ag, CHEM 5317 YESNY Ag, DAOMC 180753 YESNY Ag, CHEM 5317 YESNY Ex, and DAOMC 180753 YESNY Ex.

Anacine

The exact mass of anacine (342.17 Da) was utilised to identify the common ion adducts of this natural product in the agar and exudate of CHEM 5317 via manual inspection in QualBrowser. No evidence of anacine ion adducts were found in the DAOMC 180753 raw data. In CHEM 5317, the $[M+H]^+$ of anacine was found in the MS data at *m/z* 343.1769 (**Figure 4.3.7A**) at RT 3.86. At the same RT, the $[M+Na]^+$ was identified at *m/z* 365.1591. The XICs for the $[M+H]^+$ and $[M+Na]^+$ peaks are shown in **Figure 4.3.7C**, at RT 3.86. A box and whisker plot of the peak heights for both CHEM 5317 and DAOMC 180753 YES and YESNY agar and exudate samples at *m/z* 343.17686, corresponding to the $[M+H]^+$ peak at RT 3.87 is found in **Figure 4.3.7D**. Based on the results of the boxplot, it was evident that there was a considerable difference in relative abundance of the [M+H]+ ion adducts between the two strains. The DAOMC 180753 samples did not demonstrate any detectable peaks for m/z 343.1769 at RT 4.02, as these samples remained at baseline in the boxplot, whereas the CHEM 5317 YESNY Ex samples exhibited the highest signal intensity of the samples analysed in this plot.

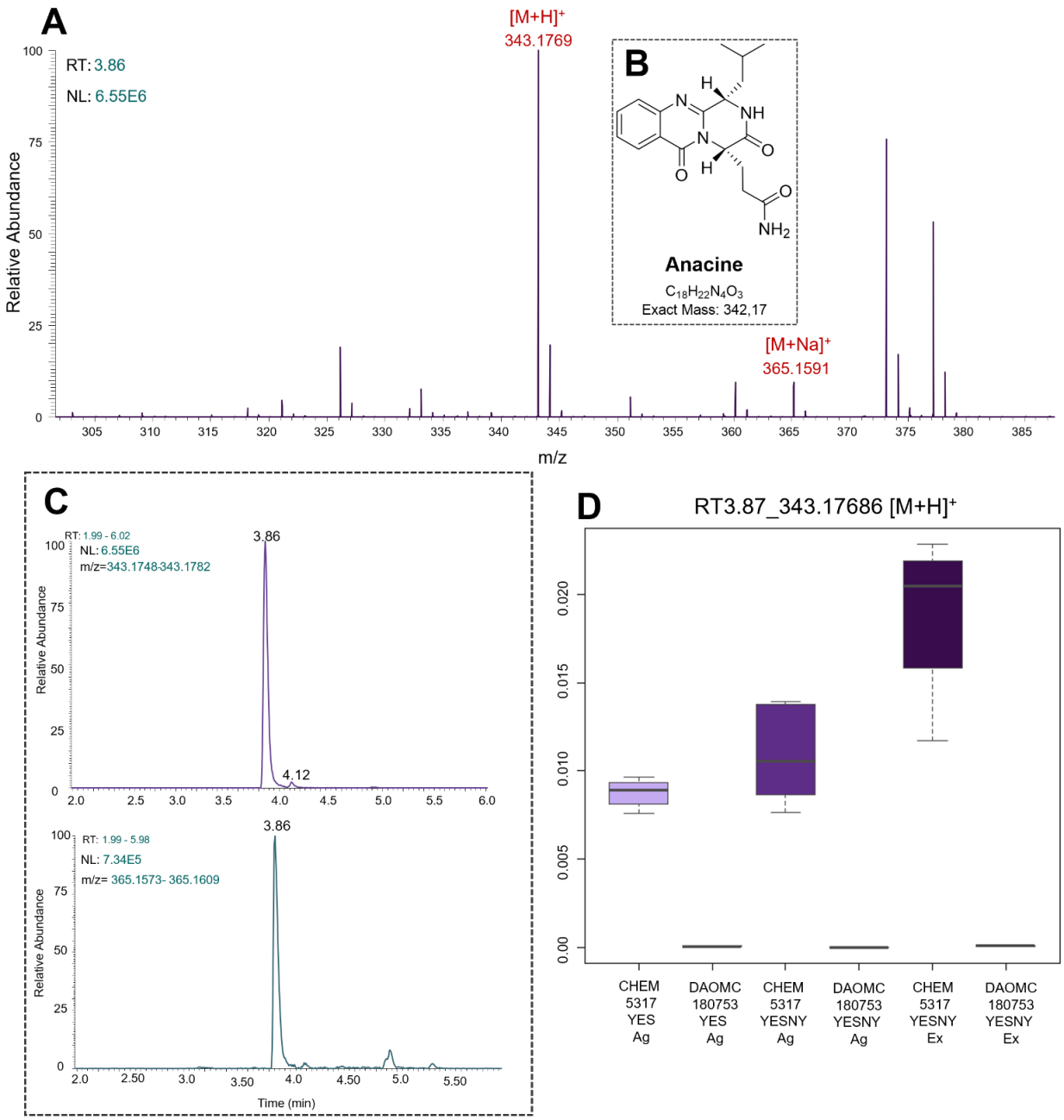

Figure 41 - Anacine in CHEM 5317 YES Media. A: Anacine mass spectrum of CHEM 5317 YES agar sample at RT 3.86. Anacine $[M+H]^+$ at *m/z* 343.1769 and $[M+Na]^+$ at *m/z* 365.1591. **B:** Anacine chemical structure. **C:** Anacine XIC of $[M+H]^+$ (purple) and $[M+Na]^+$ (teal) at RT 3.86. **D.** Box and whisker plot for *m/z* 343.17686 at RT 3.87 corresponding to anacine $[M+H]^+$ of CHEM 5317 YES Ag, DAOMC 180753 YES Ag, CHEM 5317 YESNY Ag, DAOMC 180753 YESNY Ag, and CHEM 5317 YESNY Ex.

Daldinin D

The exact mass of daldinin D (436.14 Da) was utilised to identify the common ion adducts of this natural product in the agar and exudate of CHEM 5317 via manual inspection in QualBrowser. No chemical signals associated with daldinin D were present in the DAOMC 180753 samples. In CHEM 5317, the $[M+H]^+$ of daldinin D was found in the MS data at *m/z* 437.1453 (**Figure 4.3.8A**) at RT 4.88. At the same RT, the $[M+Na]^+$ was identified at *m/z* 459.1267, the $[M+K]^+$ at *m/z* 475.1006, and the $[M+H-H_2O]$ at *m/z* 419.1348. The XICs for the $[M+H]^+$ and $[M+Na]^+$ peaks are shown in **Figure 4.3.8C**, at RT 4.88 and 4.89, respectively. A box and whisker plot of the peak heights for both CHEM 5317 and DAOMC 180753 YES and YESNY agar and exudate samples at *m/z* 343.17686, corresponding to the $[M+H]^+$ peak at RT 3.87 is found in **Figure 4.3.8D**. Based on the results of the boxplot, it was evident that there was a considerable difference in relative abundance of the $[M+H]^+$ and $[M+Na]^+$ ion adducts between the two strains. The DAOMC 180753 samples did not demonstrate any detectable peaks for m/z 437.1445 and m/z 459.1263 at RT 4.88, as these samples remained at baseline in the boxplot, whereas the CHEM 5317 YES Ag samples demonstrated the highest signal intensity of the samples analysed in the plot.

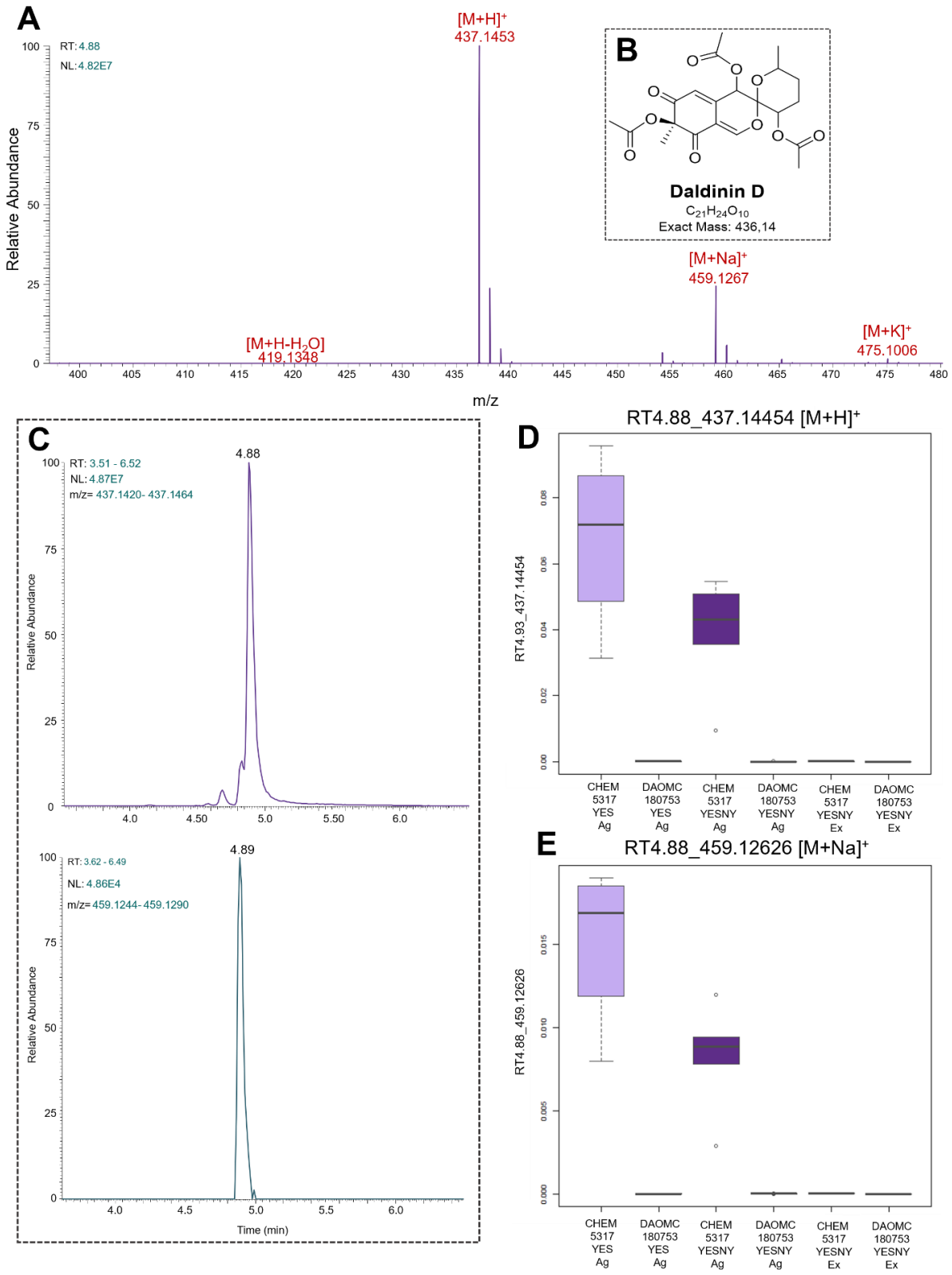
A
RT: 4.88
NL: 4.82E7
[M+H]+
437.1453
[M+Na]+
459.1267
[M+K]+
475.1006
[M+H-H2O]
419.1348
Relative Abundance
m/z
B
Daldinin D
C21H24O10
Exact Mass: 436,14
C
RT: 3.51 - 6.52
NL: 4.87E7
m/z= 437.1420- 437.1464
4.88
RT: 3.62 - 6.49
NL: 4.86E4
m/z= 459.1244- 459.1290
4.89
Time (min)
D
RT4.88_437.14454 [M+H]+
RT4.93_437.14454
E
RT4.88_459.12626 [M+Na]+
RT4.88_459.12626
CHEM 5317 YES Ag
DAOMC 180753 YES Ag
CHEM 5317 YESNY Ag
DAOMC 180753 YESNY Ag
CHEM 5317 YESNY Ex
DAOMC 180753 YESNY Ex

Figure 42.8 - Daldinin D in CHEM 5317 YES Media. A: Daldinin D mass spectrum of CHEM 5317 sample at RT 4.88. Daldinin D $[M+H]^+$ at *m/z* 437.1453, $[M+Na]^+$ at *m/z* 459.1267, $[M+K]^+$ at *m/z* 475.1006, and $[M+H-H_2O]$ at *m/z* 419.1348. **B.** Daldinin D chemical structure. **C:** Daldinin D XIC of $[M+H]^+$ (purple) at RT 4.88 and $[M+Na]^+$ (teal) at RT 4.89. **D:** Box and whisker plot for *m/z* 437.14454 at RT 4.93 corresponding to daldinin D $[M+H]^+$. Samples shown are CHEM 5317 YES Ag, DAOMC 180753 YES Ag, CHEM 5317 YESNY Ag, DAOMC 180753 YESNY Ag, and CHEM 5317 YESNY Ex. **E:** Box and whisker plot for *m/z* 459.12626 at RT 4.88 corresponding to daldinin D $[M+Na]^+$. Samples shown are CHEM 5317 YES Ag, DAOMC 180753 YES Ag, CHEM 5317 YESNY Ag, DAOMC 180753 YESNY Ag, and CHEM 5317 YESNY Ex.

Based on the results obtained from the UPLC-HRMS raw data, it was evident that CHEM 5317 was a prolific producer of the literature metabolites associated with the species *P. thymicola*. Interestingly, the DAOMC 180753 strain produced only one of the five previously established metabolites for this strain, the α-pyrone PC-2 (ochratoxins A and B, alantrypinone, and fumiquinazoline F were not found in this strain in our research). Additionally, the signals for pestafolide A and verrucolone were found in the DAOMC 180753 agar and thymipyrone A was found in the exudate (**Table 4.3.1**). While the ion adducts were found in the raw data for these four compounds, it is important to note that the signal intensities observed in the DAOMC 180753 samples were much smaller than those observed for CHEM 5317. When manually searching for the *P. thymicola* known metabolites in the DAOMC 180753 raw data, the majority of the $[M+H]^+$ ion adducts were lost in the noise (<1E4). This, in conjunction with the absence of signals observed in the univariate analysis (i.e. the box and whisker plots), it was determined that DAOMC 180753 did not produce the majority of the known metabolites for *P. thymicola.*

In contrast to the results observed for the DAOMC 180753 strain, the metabolomic profile of CHEM 5317 was consistent with the expected metabolomic fingerprint of *P. thymicola* based on the literature. Of the 16 known secondary metabolites produced by *P. thymicola*, CHEM 5317 produced 11. The 11 identified metabolites include all of the species-associated fumiquinazoline compounds: alantrypinone (**Figure 4.3.3**), fumiquinazoline F/G (**Figure 4.3.4**) fumiquinazoline T

(**Figure 4.3.5**) and serantrypinone (**Figure 4.3.6**). Among the non-fumiquinazoline metabolites, anacine (**Figure 4.3.7**) and daldinin D (**Figure 4.3.8**) were also observed. The ion adducts for PC-2 were also identified, but due to its small m/z, could not be extracted from other metabolites' chemical signals or the noise of the samples in general. A similar challenge was encountered when identifying the chemical signals for pestafolide A, pyranonigrin A, thymipyrone A, and verrucolone in the CHEM 5317 data. As such, while the m/z values were tentatively identified at the beginning of the metabolomic analysis, more definitive work is required in order to confirm the production of these metabolites by CHEM 5317.

4.3.6 CHEM 5317 & DAOMC 180753 Mass Feature Comparison

The two-dimensional data matrix exported from MZMine v. 2.53 was transformed into binary values after averaging the peak heights for the strain and media type replicates. The threshold was set to 1E5, wherein values <1E5 were converted to 0 and values >1E5 were converted to 1. The resulting binary heatmap, shown in **Figure 4.3.9**, demonstrated how few mass features were shared between CHEM 5317 and DAOMC 180753. In **Figure 4.3.9**, a blue line and bolded dendrogram section were used to highlight the location of the mass features that are associated with RT and *m/z* values consistent with the known metabolites of *P. thymicola*. These mass feature identifiers as the *P. thymicola* known metabolites was corroborated by the manual data inspection demonstrated in Section 4.3.5 of this thesis. The section of the heatmap displaying the *P. thymicola* known metabolites was largely blank for the agar and exudate of the DAOMC 180753 strain, whereas CHEM 5317 displayed larger signal intensities in this section. This data visualisation of all the mass features exported from MZMine further supported the observations of

the manual raw data inspection, where it was evident that the known metabolites for *P. thymicola* could not be found in DAOMC 180753 because they were completely absent from the dataset.

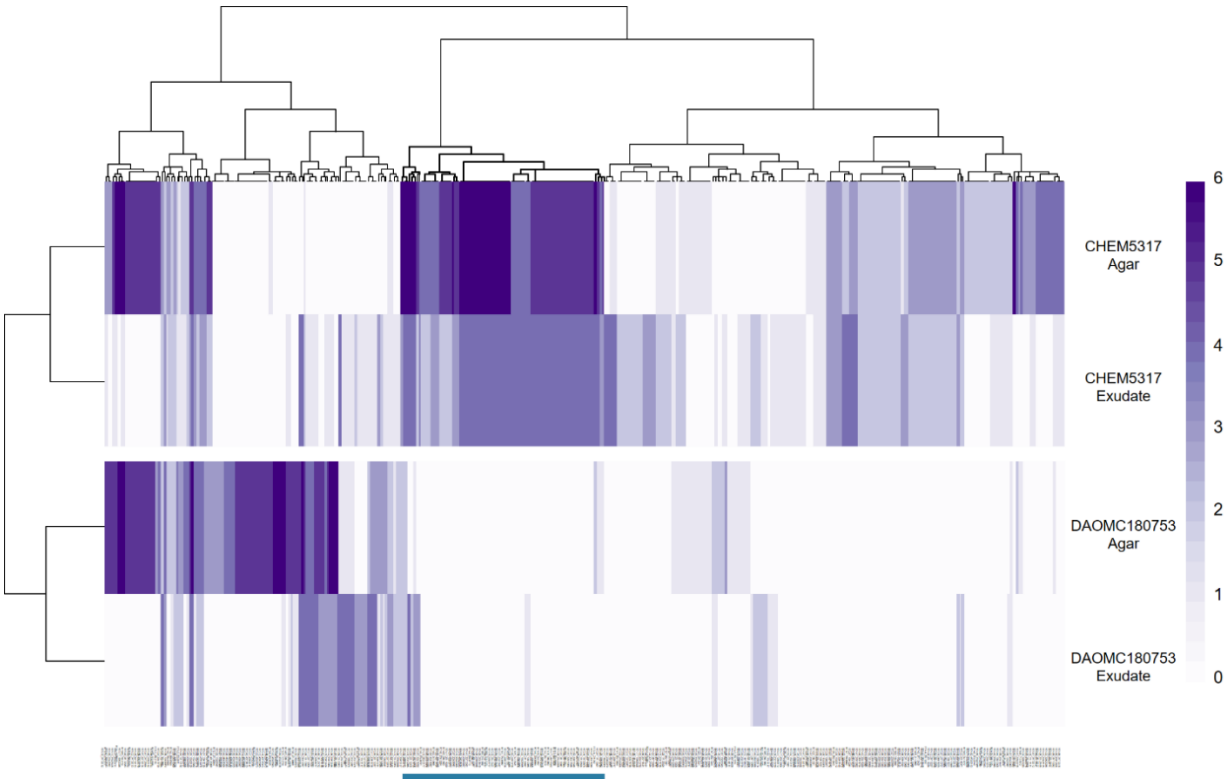

Figure 43.9 - *P. thymicola* CHEM 5317 and DAOMC 180753 Mass Feature Binary Heatmap. Dataset includes the 500 mass features derived from all six media types for both CHEM 5317 and DAOMC 180753, agar, and exudate samples, exported from MZMine v. 2.53. The blue line below the mass feature list indicates where the mass features associated with the *P. thymicola* known metabolites. As indicated by the colour intensity legend on the right, darker shades of purple indicate mass features present across different media for one strain. It is important to note that the highest intensity level for the exudate samples is 4 in contrast to 6 for the agar samples, as not all media produced exudate.

Despite the fact that the section of the heatmap containing the mass features associated with the *P. thymicola* known metabolites has negligible overlap between CHEM 5317 and DAOMC 180753, there is one section of overlap in both the agar and exudate samples on the far left of **Figure 4.3.9**. The overwhelming majority of these mass features have very small mass-to-charge ratios, with many of the *m/z* values falling below *m/z* 300. These mass features are also

associated with a RT of approximately 6 min and later, thus coming off the column toward the end of the 10-minute run. Compounds that elute very early (before 2 minutes) or at the end (after 7 minutes) of the MS run are more likely to be noise and may not represent real compounds that these two strains have in common.

4.4 Chapter 4 Summary

In this thesis chapter, the metabolite profiles of CHEM 5317 and DAOMC 180753 were analyzed via UPLC-HRMS and compared to the established metabolite profile of *P. thymicola* IBT 5891. It was determined based on this investigation that CHEM 5317 produced the majority of the expected metabolites of *P. thymicola*, while only PC-2, pestafolide A, and thymipyrone A were observed in the DAOMC 180753 dataset. A comparison of the presence of the mass features generated from MZMine v. 2.53 in both strains further supported the evidence that CHEM 5317 and DAOMC 180753 shared very few mass features in common, the majority of which were very small mass features with an *m/z* of less than 200. The lack of apparent secondary metabolite production in the DAOMC 180753 strain supports the hypothesis that the DAOMC strain may have begun to degenerate, which has been shown to decrease the number of secondary metabolites produced by a fungal strain and the titers of these compounds.[175]

Appendix 4.0

Appendix 4A: Known secondary metabolites produced by *P. thymicola* and common adducts.

Table 4A.1 - Known secondary metabolites produced by P. thymicola and common adducts.

Metabolite	*P. thymicola* Strain	Chemical Formula	Exact Mass (Da)	$[M+H]^+$ (*m/z*)	$[M+Na]^+$ (*m/z*)	$[2M+H]^+$ (*m/z*)	$[M-H_2O]$ (*m/z*)
Alantrypinone	IBT 5891	$C_{21}H_{16}N_4O_3$	372.1222	373.1297	395.1115	745.251756	354.1222
α-pyrone (PC-2)	DAOMC 180753	$C_{11}H_{17}O_4$	213.1127	213.1122	236.1019	427.232646	195.1127
Anacine	IBT 5891	$C_{18}H_{22}N_4O_3$	342.1692	343.1765	365.1584	685.345656	324.1619
Daldinin D	IBT 5891	$C_{21}H_{24}O_{10}$	436.1369	437.1442	459.1262	873.28114	418.1369
Dipodazine	IBT 5891	$C_{13}H_{11}N_3O_2$	241.0851	242.0924	264.07435	483.17753	223.08513
Fumiquinazoline F/G	IBT 5891	$C_{21}H_{18}N_4O_2$	358.1430	359.1502	381.1322	717.293226	340.1430
Fumiquinazoline T	IBT 5891	$C_{21}H_{18}N_4O_3$	374.1379	375.1442	397.1271	749.283056	356.1379
Ochratoxin A	DAOMC 180753	$C_{20}H_{18}ClNO_6$	403.0823	404.0895	426.07148	807.171806	385.02265
Ochratoxin B	DAOMC 180753	$C_{20}H_{19}NO_6$	369.1212	370.1285	392.1105	739.24975	351.1212
Penigequinolone	IBT 5891	$C_{27}H_{33}NO_6$	467.2308	468.2381	490.2200	935.46885	449.2308
Pestafolide A	IBT 5891	$C_{15}H_{22}O_5$	282.1467	283.1540	305.1359	565.300726	264.1467
Pyranonigrin A	IBT 5891	$C_{10}H_9NO_5$	223.0481	224.05534	246.03729	447.10342	205.04807
Thymipyrone A	IBT 5891	$C_8H_{10}O_4$	170.0579	171.0659	193.04713	341.123096	152.05791
Serantrypinone	IBT 5891	$C_{21}H_{16}O_4N_4$	388.1172	389.1244	411.1064	777.241586	370.1172
Verrucolone	IBT 5891	$C_6H_{10}O_4$	146.0579	147.06518	169.05009	293.123092	128.05791

2-methylisoborneol	IBT 5891	$C_{11}H_{20}O$	168.1514	169.1587	191.1406	337.310106	150.1514

Appendix 4B: Data Preprocessing Methods

Data preprocessing of UPLC-HRMS raw data for both agar and exudate samples were processed in tandem using MZMine v. 2.53. The mass detector was set to exact mass and a noise level of 1E4, the noise level of the UPLC-HRMS instrument. Using the ADAP chromatogram builder, the minimum group size in number of scans was set to 5, the group intensity threshold 1E4, the minimum highest intensity 3E4 and the *m/z* tolerance to 5 ppm. Following chromatogram building, the chromatograms were smoothed with a filter width of 5. The chromatograms were subsequently deconvoluted using the baseline cutoff algorithm, the *m/z* center calculation set to median, the minimum peak height as 5E4, the peak duration range to 1-7 mins, and the baseline level to 1E4. Using the Join Aligner, mass tolerance was set to 5 ppm, the weight for *m/z* set to 20, the RT tolerance set to 0.5 absolute min and weight for RT at 10. The data was then gap filled using the multithreaded peak finder.

Chapter 5: Summary and Conclusions

5.1 Thesis Overview

What defines a species? This question has been highly debated across the numerous realms of biology for decades. When considering microorganisms, this question becomes especially relevant, as morphology and chemotype can vary drastically as a direct result of the growth environment. The polyphasic approach to fungal taxonomy, one which considers ecological traits, phenotypic characteristics (colony morphology, conidial ontogeny/micromorphology, and secondary metabolite expression), and phylogenetic classifications, as described by Frisvad and Samson,[14,15] provides the highest level of precision in fungal taxonomy. The importance of implementing a polyphasic approach to taxonomy to *Penicillium* species identification and classification was highlighted in this thesis through an analysis of colony macro- and micromorphological characteristics (Chapter 2), barcode DNA sequences and their phylogenetic classification (Chapter 3) and an untargeted metabolomic analysis of secondary metabolites (Chapter 4) of two strains of *P. thymicola*. In each of these analyses, the novel strain, CHEM 5317, obtained as a culture contaminant at the onset of this thesis research, was compared to a second strain of *P. thymicola* DAOMC 180753, obtained from the Canadian Collection of Fungal Cultures (CCFC). The DAOMC 180753 strain of *P. thymicola* was the initial 100% match in a preliminary BLAST search of the CHEM 5317 β-tubulin gene sequence. Through this initial search, it was hypothesized that the novel strain of fungus was a member of the *P. thymicola* species. However, the side-by-side comparison of these two *Penicillium* strains brought into question how much variability can really be explained by intraspecies variation with the *Penicillium* genus.

5.2 Similarities and Differences of CHEM 5317 and DAOMC 180753

The phylogenetic analysis using three barcode gene sequences (ITS, β-tubulin, and CMD) to elucidate the relationship between CHEM 5317, DAOMC 180753, and the *P. thymicola* type strain IBT 5891, was the only analysis that revealed more similarities between the strains than differences. Through this study, it was determined that CHEM 5317 and DAOMC 180753 had nearly 100% identical DNA sequences for the three barcode genes, with only a couple of nucleotide misalignments in the CMD sequence. As such, they demonstrated monophyly in the resulting cladogram, grouping with the *P. thymicola* IBT 5891 strain with a bootstrap value of 100. Diagnostic similarities were also observed in the micromorphology of both strains. Both possessed terverticillate conidiophore branching patterns, rough-walled stipes, and green conidia on CYA media. While these shared micromorphological traits are important, it is vital to note that many species of *Penicillium* fungi also possess these characteristics, thus they do not provide a diagnostic insight into species categorization.

The most marked differences between CHEM 5317 and DAOMC 180753 were observed in their colony morphology and metabolic profiles. The colony texture of CHEM 5317 appeared velutinous whereas DAOMC 180753 was lanose. The DAOMC 180753 strain was also noticeably more appressed than CHEM 5317, which grew abundant aerial hyphae on all media types except DG18. Lastly, significant differences were observed when comparing the strains' secondary metabolite profiles in the metabolomic analysis. This UPLC-HRMS analysis of fungal mycelia and exudates revealed CHEM 5317 produced the majority of expected secondary metabolites for *P. thymicola* presented in the literature such as many members of the fumiquinazoline family of metabolites. In contrast, the chemical profile for DAOMC 180753 revealed very little information

about the strain. This strain did not produce many of the expected secondary metabolites for *P. thymicola* such as ochratoxins A or B.[60] In addition, the four that were detected (thymipyrone A, verrucolone, pestafolide A, and PC-2) were produced in very low titers, according to the results obtained via UPLC-HRMS.

5.3 Integration of Genomic and Metabolomic Approaches

The genomics and metabolomics approaches to taxonomy are intimately related by virtue of how biological organisms operate. The metabolites that are found in metabolomics data must be encoded somewhere in the organism's genome. The delicate dance between these two approaches is complicated because secondary metabolites are often encoded in accessory regions of the eukaryotic genome rather than the conserved or 'core' genome. Accessory regions of the genome frequently vary substantially, even within a species. Furthermore, even when present, the genes encoding secondary metabolites may or may not be expressed. Thus, the encoded secondary metabolite may or may not be produced. While these two features complicate the relationship between genome and metabolome, any secondary metabolites detected in a metabolomics analysis must have the corresponding genes that encoding it, often called a biosynthetic gene cluster (BGC) present in the genome.

BGCs encoded in the CHEM 5317 and DAOMC 180753 genomes were detected using the antibiotics and Secondary Metabolite Analysis Shell (antiSMASH) v. 7.1.0. This is the most effective and comprehensive bioinformatic tool for identification of diverse fungal BGCs directly from sequencing data.[176,177] In addition to identifying BGCs, antiSMASH annotated the genes present in the cluster and can make predictions about the encoded secondary metabolite based on known BGCs. Interestingly, despite observing the presence of various quinazoline natural

products in the mycelium and exudate of CHEM 5317 during the metabolomics analysis, the antiSMASH automated analysis was unable to identify an assembled fumiquinazoline BGC. This highlights one of the challenges of interpreting antiSMASH analyses. Typically, accurate interpretation of the results takes significant manual and expert based analysis in addition to the automated rules-based cluster analysis by the software.

Manual inspection of the antiSMASH output for the CHEM 5317 genome enabled identification of potential fumiquinazoline BGCs. A fumiquinazoline is expected to be produced by a trimodular NRPS system[167], of which multiple examples were identified in the genome. Of these candidates, the amino acid sequence of an unidentified NRPS gene in chromosome 3 region 4 had a 99% query coverage and 54% identity with the NRPS amino acid sequence of the fumiquinazoline BGC from *Aspergillus fumigatus* Af293.[166] An additional candidate was an unidentified Arginine-Containing Cyclodipeptide Synthase (RCDPS), which in a BLASTP search came up with a 99% query cover and 93% identity with a *P. thymicola* gene called PthA, which has recently been characterised as encoding a diketopiperazine product, as is present in fumiquinazoline.[178] However, as fumiquinazoline is produced by an NRPS system in *A. fumigatus*, it would be highly unusual to identify a fundamentally different biosynthetic origin (RCDPS vs NRPS) for the same natural product in a different species. This would be an extraordinary example of convergent evolution. Further investigations into the unidentified BGCs of the CHEM 5317 genome in relation to the metabolomic output is required and represents an exciting avenue of future work involving the annotation of previously unpublished BGCs in the *Penicillium* genus.

5.4 Fungal Strain Degeneration in Filamentous Fungi

Reusser (1963) first described the concept of species degeneration, characterizing the phenomenon as a phenotypic instability due to a microorganism's inability to maintain specific morphological characteristics or secondary metabolite profile across subsequent generations.[90] This definition has since expanded to include the attenuation of virulence traits of a strain.[179] This regularly occurring phenomenon is spontaneous and is primarily observed when working with filamentous fungi in the laboratory environment,[91] particularly with *Aspergillus*[180–182], *Trichoderma*[183], and *Penicillium,* all of which are speciose genera.[184–188] Strain degeneration can be evident in colony features such as a loss of sporulation - primarily noticeable through colour changes, loss of virulence, and the loss of secondary metabolite production.[179,189] The changes that affect multiple elements of the strain's growth due to degeneration occur at a higher incidence than typically seen for other mutations in the laboratory.[189]

In contrast to the controlled environments in the laboratory, in nature fungal species and other microorganisms are forced to compete with one another for access to necessary resources for survival. As a result, fungi are forced to adopt mechanisms to overcome these adversities, such as increasing their growth rate, activating specific metabolic pathways to mitigate stress, and production of counter-inhibitors.[190,191] The absence of selective pressure from the laboratory environment and the long-term storage of fungal cultures have been found to increase the risk of culture degeneration.[92] Fungal degeneration has also been hypothesized to be associated with chromosomal instability and genetic point-mutations.[192–194] However, the exact cause of fungal strain degeneration remains heavily disputed among researchers, as no definitive causes of this has been elucidated. The phenomenon of fungal strain degeneration does however serve as a possible

explanation for the discrepancies observed between the morphologies and metabolomic profiles exhibited by DAOMC 18075 compared to the *P. thymicola* type strain and CHEM 5317.

5.5 Conclusions and Future Directions

The morphological, phylogenetic, and metabolomic comparisons of *P. thymicola* CHEM 5317 and DAOMC 180753 presented in this thesis highlight the phenotypic variation that exists between strains of the *Penicillium* genus. Due to the massive differences in the morphological and metabolomic analyses between CHEM 5317 and DAOMC 180753 shown in this thesis, we were unable to confirm with confidence that both of these two strains are strains of *P. thymicola.* The CHEM 5317 strain exhibited characteristics that were consistent with those officially described by Frisvad and Samson[14] for *P. thymicola* in each of the three taxonomic approaches used. Morphologically, CHEM 5317 exhibited the expected velutinous colony texture of *P. thymicola*, a terverticillate conidiophore branching pattern, and vivid green conidia on CYA substrate. In the phylogenetic analysis, CHEM 5317 exhibited monophyly with the *P. thymicola* type strain IBT 5891 with a bootstrap value of 100. Lastly, the secondary metabolite profile of CHEM 5317 was largely similar to the profile published in the literature, wherein UPLC-HRMS was used to determine that CHEM 5317 produced expected metabolites of the fumiquinazoline family of natural products and certain alkaloids all known to be produced by *P. thymicola.* That said, the DAOMC 180753 strain only exhibited similarity to *P. thymicola* through the phylogenetic analysis, grouping in the same clade as CHEM 5317 and *P. thymicola* IBT 5891. The morphological phenotype of DAOMC 180753 contrasted with what was expected based on the official *P. thymicola* species description. The DAOMC 180753 colonies displayed a lanose colony texture and a more yellow-green to brown conidia colour. However, DAOMC 180753 did display

a terverticillate branching pattern, which coincided with the micromorphology of *P. thymicola*. The secondary metabolite profile of DAOMC 180753 did not align with the metabolite profile of *P. thymicola* published in the literature and that of CHEM 5317 presented in this thesis. DAOMC 180753 also did not produce any detectable amount of ochratoxins A or B, which were previously reported to have been produced by this strain.[60]

The traits of DAOMC 180753 strain described in this thesis diverged from those reported in the literature for the *P. thymicola* species and thus could not be confirmed to be a strain of the species *P. thymicola*. Due to the prevalence of strain degeneration in filamentous fungi, it is possible that strain degeneration may explain these divergent traits. However, it is also possible that this fungal strain is another species in the *Penicillium* genus and was miscategorised either upon isolation or in long-term storage. Thus, the necessity of using a polyphasic approach to fungal taxonomy for precise categorisation of *Penicillium sp.* is underscored by the effects of strain degeneration and how we define the species concept in fungi.

Future investigations should include a more robust analysis of the taxonomy of *Penicillium thymicola* and all available strains of this species. This taxonomic analysis should include the *P. thymicola* type strain IBT 5891 and the other available isolates from other culture collections to compare their phenotypes with the official species description. Moreover, a genome-level analysis using the Benchmarking Universal Single-Copy Orthologue (BUSCO) tool to analyze the completed CHEM 5317 genome would provide additional quantitative measurements regarding the completeness and quality of the assembled genome and identification of core vs accessory genes.[195] The *P. thymicola* genomes should also be further probed for their predicted biosynthetic gene clusters and their secondary metabolite profiles should be analyzed to establish characteristic metabolites produced by this species. [60]

The work of this thesis also calls into question whether DAOMC 180753 is a degenerated strain of *P. thymicola*, a strain of another existing *Penicillium* species, or a new fungal species entirely, based on the discrepancies in morphology and metabolite profile observed. We were unable to confirm that DAOMC 180753 is able to produce ochratoxin in this work, as previously established by Nguyen *et al.* in 2016.[60] However, if DAOMC 180753 is really an ochratoxin producing strain of *P. thymicola*, it requires attention, as this strain was initially isolated from a cheddar cheese food product and is currently the only known strain of *P. thymicola* to produce ochratoxins A or B. Both Health Canada[196] and the European Union[197] have imposed maximum levels allowed in cereals and food products with regards to ochratoxin A due to its adverse health effects. In mammals, ochratoxin A targets the kidneys and has been classified as a Group 2B possible carcinogen by the International Agency for Research on Cancer (IARC)[198]. The large-scale and long-term health effects of consuming ochratoxin A through diet are unconfirmed in humans, but the health effects observed by other mammal studies demonstrated numerous adverse health effects, such as the health consequences mentioned above. If DAOMC 180753 is a new species of *Penicillium* fungi, it may pose a risk to the agriculture and agri-food industry and the individuals consuming their products, if it produces ochratoxins, thus presenting the absolute necessity to accurately characterise this strain of fungi.

References

(1) Lofgren, L. A.; LeBlanc, N. R.; Certano, A. K.; Nachtigall, J.; LaBine, K. M.; Riddle, J.; *et al*. *Fusarium Graminearum:* Pathogen or Endophyte of North American Grasses? *New Phytologist* **2018**, *217* (3), 1203–1212. Doi:10.1111/nph.14894.

(2) Costa, J. H.; Bazioli, J. M.; de Moraes Pontes, J. G.; Fill, T. P. Penicillium Digitatum Infection Mechanisms in Citrus: What Do We Know so Far? *Fungal Biol* **2019**, *123* (8), 584–593. Doi:10.1016/j.funbio.2019.05.004.

(3) Diggins, F. W. E. The True History of the Discovery of Penicillin, with Refutation of the Misinformation in the Literature. *British Journal of Biomedical Sciences* **1999**, *56* (2), 83–93.

(4) Scott, P. M. Toxins of Penicillium Species Used in Cheese Manufacture. *J Food Prot* **1981**, *44* (9), 702–710. doi: 10.4315/0362-028X-44.9.702.

(5) Coton, E.; Jany, J.-L.; Coton, M. Penicillium Roqueforti. In *Encyclopedia of Dairy Sciences*; Elsevier, 2022; pp 599–606. doi: 10.1016/B978-0-08-100596-5.01092-1.

(6) Linné, C. von. *Systema Naturae per Regna Tria Naturae, Secundum Classes, Ordines, Genera, Species, Cum Characteribus, Differentiis, Synonymis, Locis.* --; impensis L. Salvii: Holmiae, 1758.

(7) Money, N. P. Fungal Diversity. In *The Fungi*; Elsevier, 2016; pp 1–36. doi: 0.1016/B978-0-12-382034-1.00001-3.

(8) Frisvad, J. C. Physiological Criteria and Mycotoxin Production as Aids in Identification of Common Asymmetric Penicillia. *Appl Environ Microbiol* **1981**, *41* (3), 568–579. doi: 10.1128/aem.41.3.568-579.1981.

(9) Hawksworth, D. L.; Crous, P. W.; Redhead, S. A.; Reynolds, D. R.; Samson, R. A.; *et al*. The Amsterdam Declaration on Fungal Nomenclature. *IMA Fungus* **2011**, *2* (1), 105–111. doi: 10.5598/imafungus.2011.02.01.14.

(10) Braun, U. The Impacts of the Discontinuation of Dual Nomenclature of Pleomorphic Fungi: The Trivial Facts, Problems, and Strategies. *IMA Fungus* **2012**, *3* (1), 81–86. doi: 10.5598/imafungus.2012.03.01.08.

(11) Taylor, J. W. One Fungus = One Name: DNA and Fungal Nomenclature Twenty Years after PCR. *IMA Fungus* **2011**, *2* (2), 113–120. Doi: 10.5598/imafungus.2011.02.02.01.

(12) Kendrick, B. *The Whole Fungus: The Sexual-Asexual Synthesis*; National Museum of Natural Sciences, National Museums of Canada, and the Kananaskis Foundation: Ottawa, 1979.

(13) Frisvad, J. C. Rationale for a Polyphasic Approach in the Identification of Mycotoxigenic Fungi. In *Determining Mycotoxins and Mycotoxigenic Fungi in Food and Feed*; Elsevier, 2011; pp 279–297. doi: 10.1533/9780857090973.4.279.

(14) Frisvad, Jens. C.; Samson, Robert. A. Polyphasic Taxonomy of Penicillium Subgenus Penicillium A Guide to Identification of Food and Air-Borne Terverticillate Penicillia and Their Mycotoxins. *Stud Mycol* **2004**, *49*, 1–174.

(15) Samson, R. A.; Houbraken, J.; Varga, J.; Frisvad, J. C. Polyphasic Taxonomy of the Heat Resistant Ascomycete Genus Byssochlamys and Its Paecilomyces Anamorphs. *Persoonia - Molecular Phylogeny and Evolution of Fungi* **2009**, *22* (1), 14–27. doi: 10.3767/003158509X418925.

(16) Vandamme, P.; Pot, B.; Gillis, M.; de Vos, P.; Kersters, K.; Swings, J. Polyphasic Taxonomy, a Consensus Approach to Bacterial Systematics. *Microbiol Rev* **1996**, *60* (2), 407–438. doi: 10.1128/mr.60.2.407-438.1996.

(17) Visagie, C. M.; Houbraken, J.; Frisvad, J. C.; Hong, S.-B.; Klaassen, C. H. W.; Perrone, G.; Seifert, K. A.; Varga, J.; Yaguchi, T.; Samson, R. A. Identification and Nomenclature of the Genus *Penicillium*. *Stud Mycol* **2014**, *78* (1), 343–371. doi: 10.1016/j.simyco.2014.09.001.

(18) Liu, D. Classification of Medically Important Fungi. In *Molecular Medical Microbiology*; Elsevier, 2024; pp 2763–2777. doi: 10.1016/B978-0-12-818619-0.00034-4.

(19) Kirk, P. M.; Cannon, P. F.; Minter, D. W.; Stalpers, J. A. *Ainsworth and Bisby's Dictionary of the Fungi*, 10th ed.; CAB International: Wallingford (UK), 2008.

(20) Schoch, C. L.; Sung, G.-H.; López-Giráldez, F.; Townsend, J. P.; Miadlikowska, J.; *et al*. The Ascomycota Tree of Life: A Phylum-Wide Phylogeny Clarifies the Origin and Evolution of Fundamental Reproductive and Ecological Traits. *Syst Biol* **2009**, *58* (2), 224–239. doi: 10.1093/sysbio/syp020.

(21) Volk, T. J. Fungi. In *Encyclopedia of Biodiversity*; Elsevier, 2013; pp 624–640. doi: 10.1016/B978-0-12-384719-5.00062-9.

(22) Maharachchikumbura, S. S. N.; Chen, Y.; Ariyawansa, H. A.; Hyde, K. D.; Haelewaters, D.; *et al*. Integrative Approaches for Species Delimitation in Ascomycota. *Fungal Divers* **2021**, *109* (1), 155–179. doi: 10.1007/s13225-021-00486-6.

(23) Brand, A.; Gow, N. A. Mechanisms of Hypha Orientation of Fungi. *Curr Opin Microbiol* **2009**, *12* (4), 350–357. doi: 10.1016/j.mib.2009.05.007.

(24) Harold, F. M. In Pursuit of the Whole Hypha. *Fungal Genetics and Biology* **1999**, *27* (2–3), 128–133. doi: 10.1006/fgbi.1999.1124.

(25) Money, N. P. Spore Production, Discharge, and Dispersal. In *The Fungi*; Elsevier, 2016; pp 67–97. doi: 10.1016/B978-0-12-382034-1.00003-7.

(26) Calvo, A. M.; Wilson, R. A.; Bok, J. W.; Keller, N. P. Relationship between Secondary Metabolism and Fungal Development. *Microbiology and Molecular Biology Reviews* **2002**, *66* (3), 447–459. doi: 10.1128/MMBR.66.3.447-459.2002.

(27) Yarzábal, L. A.; Chica, E. J. Role of Rhizobacterial Secondary Metabolites in Crop Protection Against Agricultural Pests and Diseases. In *New and Future Developments in Microbial Biotechnology and Bioengineering*; Elsevier, 2019; pp 31–53. doi: 10.1016/B978-0-444-63504-4.00003-7.

(28) Fox, E. M.; Howlett, B. J. Secondary Metabolism: Regulation and Role in Fungal Biology. *Curr Opin Microbiol* **2008**, *11* (6), 481–487. doi: 10.1016/j.mib.2008.10.007.

(29) Keller, N. P. Fungal Secondary Metabolism: Regulation, Function and Drug Discovery. *Nat Rev Microbiol* **2019**, *17* (3), 167–180. doi: 10.1038/s41579-018-0121-1.

(30) Keller, N. P. Fungal Secondary Metabolism: Regulation, Function and Drug Discovery. *Nat Rev Microbiol* **2019**, *17* (3), 167–180. doi: 10.1038/s41579-018-0121-1.

(31) Luckner, M. *Secondary Metabolism in Microorganisms, Plants, and Animals*; Springer Science & Business Media, 2013.

(32) Lewis, K. Platforms for Antibiotic Discovery. *Nat Rev Drug Discov* **2013**, *12* (5), 371–387. doi: 10.1038/nrd3975.

(33) Bu'Lock, J. D. Intermediary Metabolism and Antibiotic Synthesis; 1961; pp 293–342. doi: 10.1016/S0065-2164(08)70514-8.

(34) Sekiguchi, J.; Gaucher, G. M. Conidiogenesis and Secondary Metabolism in Penicillium Urticae. *Appl Environ Microbiol* **1977**, *33* (1), 147–158. doi: 10.1128/aem.33.1.147-158.1977.

(35) Bergmann, S.; Funk, A. N.; Scherlach, K.; Schroeckh, V.; Shelest, E.; Horn, U.; Hertweck, C.; Brakhage, A. A. Activation of a Silent Fungal Polyketide Biosynthesis Pathway through Regulatory Cross Talk with a Cryptic Nonribosomal Peptide Synthetase Gene Cluster. *Appl Environ Microbiol* **2010**, *76* (24), 8143–8149. Doi: 10.1128/AEM.00683-10.

(36) Losada, L.; Ajayi, O.; Frisvad, J. C.; Yu, J.; Nierman, W. C. Effect of Competition on the Production and Activity of Secondary Metabolites in *Aspergillus* Species. *Med Mycol* **2009**, *47* (s1), S88–S96. doi: 10.1080/13693780802409542.

(37) Brakhage, A. A.; Thön, M.; Spröte, P.; Scharf, D. H.; Al-Abdallah, Q.; Wolke, S. M.; Hortschansky, P. Aspects on Evolution of Fungal β-Lactam Biosynthesis Gene Clusters and Recruitment of Trans-Acting Factors. *Phytochemistry* **2009**, *70* (15–16), 1801–1811. doi: 10.1016/j.phytochem.2009.09.011.

(38) Crits-Christoph, A.; Bhattacharya, N.; Olm, M. R.; Song, Y. S.; Banfield, J. F. Transporter Genes in Biosynthetic Gene Clusters Predict Metabolite Characteristics and Siderophore Activity. *Genome Res* **2021**, *31* (2), 239–250. doi: 10.1101/gr.268169.120.

(39) Brakhage, A. A. Regulation of Fungal Secondary Metabolism. *Nat Rev Microbiol* **2013**, *11* (1), 21–32. doi : 10.1038/nrmicro2916.

(40) Geisen, R. Molecular Monitoring of Environmental Conditions Influencing the Induction of Ochratoxin A Biosynthesis Genes in *Penicillium Nordicum*. *Mol Nutr Food Res* **2004**, *48* (7), 532–540. doi: 10.1002/mnfr.200400036.

(41) Schmidt-Heydt, M.; Geisen, R. A Microarray for Monitoring the Production of Mycotoxins in Food. *Int J Food Microbiol* **2007**, *117* (2), 131–140. doi: 10.1016/j.ijfoodmicro.2007.01.014.

(42) Schmidt-Heydt, M.; Magan, N.; Geisen, R. Stress Induction of Mycotoxin Biosynthesis Genes by Abiotic Factors. *FEMS Microbiol Lett* **2008**, *284* (2), 142–149. doi: 10.1111/j.1574-6968.2008.01182.x.

(43) Rabha, J.; Jha, D. K. Metabolic Diversity of Penicillium. In *New and Future Developments in Microbial Biotechnology and Bioengineering*; Elsevier, 2018; pp 217–234. doi: 10.1016/B978-0-444-63501-3.00012-0.

(44) McRae, C. F.; Hocking, A. D.; Seppelt, R. D. Penicillium Species from Terrestrial Habitats in the Windmill Islands, East Antarctica, Including a New Species, Penicillium Antarcticum. *Polar Biol* **1999**, *21* (2), 97–111. doi: 10.1007/s003000050340.

(45) Gonçalves, V. N.; Campos, L. S.; Melo, I. S.; Pellizari, V. H.; Rosa, C. A.; Rosa, L. H. Penicillium Solitum: A Mesophilic, Psychrotolerant Fungus Present in Marine Sediments from Antarctica. *Polar Biol* **2013**, *36* (12), 1823–1831. doi: 10.1007/s00300-013-1403-8.

(46) Li, Y.; Ye, D.; Chen, X.; Lu, X.; Shao, Z.; Zhang, H.; Che, Y. Breviane Spiroditerpenoids from an Extreme-Tolerant *Penicillium* Sp. Isolated from a Deep Sea Sediment Sample. *J Nat Prod* **2009**, *72* (5), 912–916. Doi: 10.1021/np900116m.

(47) Xu, X.; Chen, J.; Xu, H.; Li, D. Role of a Major Facilitator Superfamily Transporter in Adaptation Capacity of Penicillium Funiculosum under Extreme Acidic Stress. *Fungal Genetics and Biology* **2014**, *69*, 75–83. doi: 10.1016/j.fgb.2014.06.002.

(48) Horiike, T.; Yamashita, M. A New Fungal Isolate, Penidiella Sp. Strain T9, Accumulates the Rare Earth Element Dysprosium. *Appl Environ Microbiol* **2015**, *81* (9), 3062–3068. doi: 10.1128/AEM.00300-15.

(49) Pitt, J. I. Biology and Ecology of Toxigenic Penicillium Species; 2002; pp 29–41. doi: 10.1007/978-1-4615-0629-4_4.

(50) Marcet-Houben, M.; Ballester, A.-R.; de la Fuente, B.; Harries, E.; Marcos, J. F.; González-Candelas, L.; Gabaldón, T. Genome Sequence of the Necrotrophic Fungus Penicillium Digitatum, the Main Postharvest Pathogen of Citrus. *BMC Genomics* **2012**, *13* (1), 646. doi: 10.1186/1471-2164-13-646.

(51) Wang, X.; Jiang, N.; Liu, J.; Liu, W.; Wang, G.-L. The Role of Effectors and Host Immunity in Plant–Necrotrophic Fungal Interactions. *Virulence* **2014**, *5* (7), 722–732. doi: 10.4161/viru.29798.

(52) Tresner, H. D.; Hayes, J. A. Sodium Chloride Tolerance of Terrestrial Fungi. *Appl Microbiol* **1971**, *22* (2), 210–213. doi: 10.1128/am.22.2.210-213.1971.

(53) Link, H. Observationes in Ordines Plantarum Naturales. *Dissertatio 1ma Magazin der Gesellschaft Naturforschenden Freunde Berlin* **1809**, No. 3, 3–42.

(54) Thom, C. The Evolution of Species Concepts in Aspergillus and Penicillium. *Ann N Y Acad Sci* **1954**, *60* (1), 24–34. doi: 10.1111/j.1749-6632.1954.tb39995.x.

(55) *Advances in Penicillium and Aspergillus Systematics*; Samson, R. A., Pitt, J. I., Eds.; Plenum Publishing Corporation, 1985; Vol. 102.

(56) Okuda, T. Variation in Colony Characteristics of *Penicillium* Strains Resulting from Minor Variations in Culture Conditions. *Mycologia* **1994**, *86* (2), 259–262. doi: 10.1080/00275514.1994.12026404.

(57) Christensen, M.; Frisvad, J. C.; Tuthill, D. Taxonomy of the Penicillium Miczynskii Group Based on Morphology and Secondary Metabolites. *Mycol Res* **1999**, *103* (5), 527–541. doi: 10.1017/S0953756298007515.

(58) Schoch, C. L.; Seifert, K. A.; Huhndorf, S.; Robert, V.; Spouge, J. L.; Levesque, C. A.; *et al*. Nuclear Ribosomal Internal Transcribed Spacer (ITS) Region as a Universal DNA Barcode Marker for *Fungi*. *Proceedings of the National Academy of Sciences* **2012**, *109* (16), 6241–6246. Doi: 10.1073/pnas.1117018109.

(59) Ogawa, H.; Sugiyama, J. Evolutionary Relationships of the Cleistothecial Genera with Penicillium, Geosmithia, Merimbla and Sarophorum Anamorphs as Inferred from 18S RRNA Sequence Divergence. In *Integration of Modern Taxonomic Methods for Penicillium and Aspergillus Classification*; Samson, R. A., Pitt, J. I., Eds.; CRC Press, 2000; pp 149–161.

(60) Nguyen, H. D. T.; McMullin, D. R.; Ponomareva, E.; Riley, R.; Pomraning, K. R.; Baker, S. E.; Seifert, K. A. Ochratoxin A Production by Penicillium Thymicola. *Fungal Biol* **2016**, *120* (8), 1041–1049. doi: 10.1016/j.funbio.2016.04.002.

(61) Frisvad, J. C. Halotolerant and Halophilic Fungi and Their Extrolite Production. In *Adaptation to Life at High Salt Concentrations in Archaea, Bacteria, and Eukarya*; Springer-Verlag: Berlin/Heidelberg; pp 425–439. doi: 10.1007/1-4020-3633-7_27.

(62) Twarużek, M.; Soszczyńska, E.; Kwiatkowska-Giżyńska, J. Molds in Food Spoilage. In *Encyclopedia of Mycology*; Elsevier, 2021; pp 208–214. doi: 10.1016/B978-0-12-809633-8.21048-0.

(63) Larsen, T. O.; Frydenvang, K.; Frisvad, J. C.; Christophersen, C. UV-Guided Isolation of Alantrypinone, a Novel *Penicillium* Alkaloid. *J Nat Prod* **1998**, *61* (9), 1154–1157. doi: 10.1021/np980056v.

(64) Ariza, M. R.; Larsen, T. O.; Petersen, B. O.; Duus, J. Ø.; Christophersen, C.; Barrero, A. F. A Novel Alkaloid Serantrypinone and the Spiro Azaphilone Daldinin D from *Penicillium Thymicola*. *J Nat Prod* **2001**, *64* (12), 1590–1592. doi: 10.1021/np0101550.

(65) Ma, L.-F.; Zheng, Y.; Qian, H.-Y.; Wang, Y.; Shan, W.-G.; Zhan, Z.-J. New Metabolites from Penicillium Thymicola IBT 5891. *J Chem Res* **2017**, *41* (2), 95–97. doi: 10.3184/174751917X14858862342188.

(66) Krain, A.; Siupka, P. Fungal Guttation, a Source of Bioactive Compounds, and Its Ecological Role—A Review. *Biomolecules* **2021**, *11* (9), 1270. doi: 10.3390/biom11091270.

(67) Sun, Y.-P.; Unestam, T.; Lucas, S. D.; Johanson, K. J.; Kenne, L.; Finlay, R. Exudation-Reabsorption in a Mycorrhizal Fungus, the Dynamic Interface for Interaction with Soil and Soil Microorganisms. *Mycorrhiza* **1999**, *9* (3), 137–144. doi: 10.1007/s005720050298.

(68) Aliferis, K. A.; Jabaji, S. Metabolite Composition and Bioactivity of *Rhizoctonia Solani* Sclerotial Exudates. *J Agric Food Chem* **2010**, *58* (13), 7604–7615. doi: 10.1021/jf101029a.

(69) Colotelo, N. Fungal Exudates. *Can J Microbiol* **1978**, *24* (10), 1173–1181. Doi: 10.1139/m78-191.

(70) Jennings, D. H. The Role of Droplets in Helping to Maintain a Constant Growth Rate of Aerial Hyphae. *Mycol Res* **1991**, *95* (7), 883–884. doi: 10.1016/S0953-7562(09)80054-3.

(71) Muñoz, K.; Vega, M.; Rios, G.; Geisen, R.; Degen, G. H. Mycotoxin Production by Different Ochratoxigenic Aspergillus and Penicillium Species on Coffee- and Wheat-Based Media. *Mycotoxin Res* **2011**, *27* (4), 239–247. doi: 10.1007/s12550-011-0100-0.

(72) Sica, V. P.; Rees, E. R.; Tchegnon, E.; Bardsley, R. H.; Raja, H. A.; Oberlies, N. H. Spatial and Temporal Profiling of Griseofulvin Production in Xylaria Cubensis Using Mass Spectrometry Mapping. *Front Microbiol* **2016**, *7*. doi: 10.3389/fmicb.2016.00544.

(73) Figueroa, M.; Jarmusch, A. K.; Raja, H. A.; El-Elimat, T.; Kavanaugh, J. S.; Horswill, A. R.; Cooks, R. G.; Cech, N. B.; Oberlies, N. H. Polyhydroxyanthraquinones as Quorum Sensing Inhibitors from the Guttates of *Penicillium Restrictum* and Their Analysis by Desorption Electrospray Ionization Mass Spectrometry. *J Nat Prod* **2014**, *77* (6), 1351–1358. doi: 10.1021/np5000704.

(74) Hutwimmer, S.; Wang, H.; Strasser, H.; Burgstaller, W. Formation of Exudate Droplets by *Metarhizium Anisopliae* and the Presence of Destruxins. *Mycologia* **2010**, *102* (1), 1–10. doi: 10.3852/09-079.

(75) Colotelo, N.; Sumner, J. L.; Voegelin, W. S. Chemical Studies on the Exudate and Developing Sclerotia of *Sclerotinia Sclerotiorum* (Lib.) DeBary. *Can J Microbiol* **1971**, *17* (9), 1189–1194. doi: 10.1139/m71-190.

(76) Cooke, R. C. Changes in Soluble Carbohydrates during Sclerotium Formation by Sclerotinia Sclerotiorum and S. Trifoliorum. *Transactions of the British Mycological Society* **1969**, *53* (1), 77–86. doi: 10.1016/S0007-1536(69)80009-4.

(77) dos Santos, A. G.; Marquês, J. T.; Carreira, A. C.; Castro, I. R.; Viana, A. S.; Mingeot-Leclercq, M.-P.; de Almeida, R. F. M.; Silva, L. C. The Molecular Mechanism of Nystatin Action Is Dependent on the Membrane Biophysical Properties and Lipid Composition. *Physical Chemistry Chemical Physics* **2017**, *19* (44), 30078–30088. doi: 10.1039/C7CP05353C.

(78) Bolard, J. How Do the Polyene Macrolide Antibiotics Affect the Cellular Membrane Properties? *Biochimica et Biophysica Acta (BBA) - Reviews on Biomembranes* **1986**, *864* (3–4), 257–304. doi: 10.1016/0304-4157(86)90002-X.

(79) Michel, G. W. Nystatin; 1977; pp 341–421. doi : 10.1016/S0099-5428(08)60349-4.

(80) Fjærvik, E.; Zotchev, S. B. Biosynthesis of the Polyene Macrolide Antibiotic Nystatin in Streptomyces Noursei. *Appl Microbiol Biotechnol* **2005**, *67* (4), 436–443. Doi: 10.1007/s00253-004-1802-4.

(81) Van Hoogevest, P.; De Kruijff, B. Effect of Amphotericin B on Cholesterol-Containing Liposomes of Egg Phosphatidylcholine and Didocosenoyl Phosphatidylcholine. A Refinement of the Model for the Formation of Pores by Amphotericin B in Membranes. *Biochimica et Biophysica Acta (BBA) - Biomembranes* **1978**, *511* (3), 397–407. doi: 10.1016/0005-2736(78)90276-6.

(82) Vardanyan, R. S.; Hruby, V. J. Antifungal Drugs. In *Synthesis of Essential Drugs*; Elsevier, 2006; pp 535–547. doi: 10.1016/B978-044452166-8/50035-2.

(83) Stanley, V. C.; English, M. P. Some Effects of Nystatin on the Growth of Four Aspergillus Species. *J Gen Microbiol* **1965**, *40* (1), 107–118. doi: 10.1099/00221287-40-1-107.

(84) Lackner, M.; de Hoog, G. S.; Verweij, P. E.; Najafzadeh, M. J.; Curfs-Breuker, I.; Klaassen, C. H.; Meis, J. F. Species-Specific Antifungal Susceptibility Patterns of Scedosporium and Pseudallescheria Species. *Antimicrob Agents Chemother* **2012**, *56* (5), 2635–2642. doi: 10.1128/AAC.05910-11.

(85) Al-Hatmi, A. M.; Hagen, F.; Menken, S. B.; Meis, J. F.; de Hoog, G. S. Global Molecular Epidemiology and Genetic Diversity of *Fusarium* , a Significant Emerging Group of Human Opportunists from 1958 to 2015. *Emerg Microbes Infect* **2016**, *5* (1), 1–11. doi: 10.1038/emi.2016.126.

(86) Slavin, M.; van Hal, S.; Sorrell, T. C.; Lee, A.; Marriott, D. J.; Daveson, K.; Kennedy, K.; *et al*. Invasive Infections Due to Filamentous Fungi Other than Aspergillus: Epidemiology and Determinants of Mortality. *Clinical Microbiology and Infection* **2015**, *21* (5), 490.e1-490.e10. doi: 10.1016/j.cmi.2014.12.021.

(87) Samson, R. A.; Hoekstra, E. S.; Frisvad, J. C.; Filtenborg, O. *Introduction to Foodborne Fungi*, 5th ed.; Samson, R. A., Hoekstra, E. S., Frisvad, J. C., Filtenborg, O., Eds.; Centraalbureau voor Schimmelcultures: Utrecht, 1996.

(88) Raper, K. B.; Thom, C. *A Manual of the Penicillia*; Williams & Wilkins Co.: Baltimore, Md, 1949.

(89) Beuchat, L. R. Influence of Water Activity on Growth, Metabolic Activities and Survival of Yeasts and Molds. *J Food Prot* **1983**, *46* (2), 135–141. doi: 10.4315/0362-028X-46.2.135.

(90) Reusser, F. Stability and Degeneration of Microbial Cultures on Repeated Transfer; 1963; pp 189–215. doi: 10.1016/S0065-2164(08)70011-X.

(91) Li, L.; Hu, X.; Xia, Y.; Xiao, G.; Zheng, P.; Wang, C. Linkage of Oxidative Stress and Mitochondrial Dysfunctions to Spontaneous Culture Degeneration in Aspergillus Nidulans. *Molecular & Cellular Proteomics* **2014**, *13* (2), 449–461. doi: 10.1074/mcp.M113.028480.

(92) Barreto, M. C.; Houbraken, J.; Samson, R. A.; Frisvad, J. C.; San-Romão, M. V. Taxonomic Studies of the Penicillium Glabrum Complex and the Description of a New Species P. Subericola. *Fungal Divers* **2011**, *49* (1), 23–33. doi: 10.1007/s13225-011-0090-4.

(93) Darwin, C. Natural Selection; or the Survival of the Fittest. In *The origin of species*; Books, Inc: New York; Boston, 1859; Vol. I, pp 97–163.

(94) Yang, Z.; Rannala, B. Molecular Phylogenetics: Principles and Practice. *Nat Rev Genet* **2012**, *13* (5), 303–314. doi: 10.1038/nrg3186.

(95) Pedersen, J. S.; Bejerano, G.; Siepel, A.; Rosenbloom, K.; Lindblad-Toh, K.; Lander, E. S.; Kent, J.; Miller, W.; Haussler, D. Identification and Classification of Conserved RNA Secondary Structures in the Human Genome. *PLoS Comput Biol* **2006**, *2* (4), e33. doi: 10.1371/journal.pcbi.0020033.

(96) Kellis, M.; Patterson, N.; Endrizzi, M.; Birren, B.; Lander, E. S. Sequencing and Comparison of Yeast Species to Identify Genes and Regulatory Elements. *Nature* **2003**, *423* (6937), 241–254. doi: 10.1038/nature01644.

(97) Wang, Z.; Gudibanda, A.; Ugwuowo, U.; Trail, F.; Townsend, J. P. Using Evolutionary Genomics, Transcriptomics, and Systems Biology to Reveal Gene Networks Underlying Fungal Development. *Fungal Biol Rev* **2018**, *32* (4), 249–264. doi: 10.1016/j.fbr.2018.02.001.

(98) Ballester, A.-R.; Marcet-Houben, M.; Levin, E.; Sela, N.; Selma-Lázaro, C.; Carmona, L.; Wisniewski, M.; Droby, S.; González-Candelas, L.; Gabaldón, T. Genome, Transcriptome, and Functional Analyses of *Penicillium Expansum* Provide New Insights Into Secondary Metabolism and Pathogenicity. *Molecular Plant-Microbe Interactions®* **2015**, *28* (3), 232–248. doi: 10.1094/MPMI-09-14-0261-FI.

(99) Brady, A.; Salzberg, S. PhymmBL Expanded: Confidence Scores, Custom Databases, Parallelization and More. *Nat Methods* **2011**, *8* (5), 367.

(100) Xu, J. Fungal Species Concepts in the Genomics Era. *Genome* **2020**, *63* (9), 459–468. doi: 10.1139/gen-2020-0022.

(101) Sanger, F.; Nicklen, S.; Coulson, A. R. DNA Sequencing with Chain-Terminating Inhibitors. *Proceedings of the National Academy of Sciences* **1977**, *74* (12), 5463–5467. Doi: 10.1073/pnas.74.12.5463.

(102) Grada, A.; Weinbrecht, K. Next-Generation Sequencing: Methodology and Application. *Journal of Investigative Dermatology* **2013**, *133* (8), 1–4. doi: 10.1038/jid.2013.248.

(103) Slatko, B. E.; Albright, L. M.; Tabor, S.; Ju, J. DNA Sequencing by the Dideoxy Method. *Curr Protoc Mol Biol* **1999**, *47* (1). doi: 10.1002/0471142727.mb0704as47.

(104) Hagemann, I. S. Overview of Technical Aspects and Chemistries of Next-Generation Sequencing. In *Clinical Genomics*; Elsevier, 2015; pp 3–19. doi: 10.1016/B978-0-12-404748-8.00001-0.

(105) Kircher, M.; Kelso, J. High-throughput DNA Sequencing – Concepts and Limitations. *BioEssays* **2010**, *32* (6), 524–536. doi: 10.1002/bies.200900181.

(106) Slatko, B. E.; Kieleczawa, J.; Ju, J.; Gardner, A. F.; Hendrickson, C. L.; Ausubel, F. M. "First Generation" Automated DNA Sequencing Technology. *Curr Protoc Mol Biol* **2011**, *96* (1). doi: 10.1002/0471142727.mb0702s96.

(107) Collins, F. S.; Fink, L. The Human Genome Project. *Alcohol Health Res World* **1995**, *19* (3), 190–195.

(108) Quail, M. A.; Kozarewa, I.; Smith, F.; Scally, A.; Stephens, P. J.; Durbin, R.; Swerdlow, H.; Turner, D. J. A Large Genome Center's Improvements to the Illumina Sequencing System. *Nat Methods* **2008**, *5* (12), 1005–1010. doi: 10.1038/nmeth.1270.

(109) Hu, T.; Chitnis, N.; Monos, D.; Dinh, A. Next-Generation Sequencing Technologies: An Overview. *Hum Immunol* **2021**, *82* (11), 801–811. doi: 10.1016/j.humimm.2021.02.012.

(110) Liu, L.; Li, Y.; Li, S.; Hu, N.; He, Y.; Pong, R.; Lin, D.; Lu, L.; Law, M. Comparison of Next-Generation Sequencing Systems. *J Biomed Biotechnol* **2012**, *2012*, 1–11. doi: 10.1155/2012/251364.

(111) Nilsson, R. H.; Anslan, S.; Bahram, M.; Wurzbacher, C.; Baldrian, P.; Tedersoo, L. Mycobiome Diversity: High-Throughput Sequencing and Identification of Fungi. *Nat Rev Microbiol* **2019**, *17* (2), 95–109. doi: 10.1038/s41579-018-0116-y.

(112) Payne, A.; Holmes, N.; Rakyan, V.; Loose, M. BulkVis: A Graphical Viewer for Oxford Nanopore Bulk FAST5 Files. *Bioinformatics* **2019**, *35* (13), 2193–2198. doi: 10.1093/bioinformatics/bty841.

(113) Delahaye, C.; Nicolas, J. Sequencing DNA with Nanopores: Troubles and Biases. *PLoS One* **2021**, *16* (10), e0257521. doi: 10.1371/journal.pone.0257521.

(114) Wick, R. R.; Judd, L. M.; Holt, K. E. Assembling the Perfect Bacterial Genome Using Oxford Nanopore and Illumina Sequencing. *PLoS Comput Biol* **2023**, *19* (3), e1010905. Doi: 10.1371/journal.pcbi.1010905.

(115) Samson Robert A.; Seifert, K. A.; Kujipers, A. F. A.; Houbraken, J. A. M. P.; Frisvad, J. C. Phylogenetic Analysis of Penicillium Subgenus Penicillium Using Partial B-Tubulin Sequences. *Stud Mycol* **2004**, *49*, 175–200.

(116) Varga, J.; Frisvad, J. C.; Samson, R. A. Two New Aflatoxin Producing Species, and an Overview of Aspergillus Section Flavi. *Stud Mycol* **2011**, *69*, 57–80. doi: 10.3114/sim.2011.69.05.

(117) Houbraken, J.; Due, M.; Varga, J.; Meijer, M.; Frisvad, J. C.; Samson, R. A. Polyphasic Taxonomy of Aspergillus Section Usti. *Stud Mycol* **2007**, *59*, 107–128. doi: 10.3114/sim.2007.59.12.

(118) Stielow, J. B.; Lévesque, C. A.; Seifert, K. A.; Meyer, W.; Irinyi, L.; Smits, D.; Renfurm, R.; *et al*. One Fungus, Which Genes? Development and Assessment of Universal Primers for Potential Secondary Fungal DNA Barcodes. *Persoonia - Molecular Phylogeny and Evolution of Fungi* **2015**, *35* (1), 242–263. doi: 10.3767/003158515X689135.

(119) Houbraken, J.; Samson, R. A. Phylogeny of Penicillium and the Segregation of Trichocomaceae into Three Families. *Stud Mycol* **2011**, *70*, 1–51. doi: 10.3114/sim.2011.70.01.

(120) Taylor, J. W.; Jacobson, D. J.; Kroken, S.; Kasuga, T.; Geiser, D. M.; Hibbett, D. S.; Fisher, M. C. Phylogenetic Species Recognition and Species Concepts in Fungi. *Fungal Genetics and Biology* **2000**, *31* (1), 21–32. doi: 10.1006/fgbi.2000.1228.

(121) Hibbett, D. S.; Taylor, J. W. Fungal Systematics: Is a New Age of Enlightenment at Hand? *Nat Rev Microbiol* **2013**, *11* (2), 129–133. doi: 10.1038/nrmicro2963.

(122) Zhao, Z.; Liu, H.; Luo, Y.; Zhou, S.; An, L.; Wang, C.; Jin, Q.; Zhou, M.; Xu, J.-R. Molecular Evolution and Functional Divergence of Tubulin Superfamily in the Fungal Tree of Life. *Sci Rep* **2014**, *4* (1), 6746. doi: 10.1038/srep06746.

(123) Rivera, K. G.; Seifert, K. A. A Taxonomic and Phylogenetic Revision of the Penicillium Sclerotiorum Complex. *Stud Mycol* **2011**, *70*, 139–158. doi: 10.3114/sim.2011.70.03.

(124) Visagie, C. M.; Hirooka, Y.; Tanney, J. B.; Whitfield, E.; Mwange, K.; Meijer, M.; Amend, A. S.; Seifert, K. A.; Samson, R. A. *Aspergillus* , *Penicillium* and *Talaromyces* Isolated from House Dust Samples Collected around the World. *Stud Mycol* **2014**, *78* (1), 63–139. doi: 10.1016/j.simyco.2014.07.002.

(125) Visagie, C. M.; Seifert, K. A.; Houbraken, J.; Samson, R. A.; Jacobs, K. Diversity of *Penicillium* Section *Citrina* within the Fynbos Biome of South Africa, Including a New Species from a *Protea Repens* Infructescence. *Mycologia* **2014**, *106* (3), 537–552. Doi: 10.3852/13-256.

(126) Visagie, C. M.; Houbraken, J.; Rodriques, C.; Pereira, C. S.; Dijksterhuis, J.; Seifert, K. A.; Jacobs, K.; Samson, R. A. Five New Penicillium Species in Section Sclerotiora: A Tribute to the Dutch Royal Family. *Persoonia - Molecular Phylogeny and Evolution of Fungi* **2013**, *31* (1), 42–62. doi: 10.3767/003158513X667410.

(127) Houbraken, J.; Frisvad, J. C.; Samson, R. A. Taxonomy of Penicillium Section Citrina. *Stud Mycol* **2011**, *70*, 53–138. doi: 10.3114/sim.2011.70.02.

(128) Houbraken, J.; Frisvad, J. C.; Samson, R. A. Fleming's Penicillin Producing Strain Is Not Penicillium Chrysogenum but P. Rubens. *IMA Fungus* **2011**, *2* (1), 87–95. doi: 10.5598/imafungus.2011.02.01.12.

(129) Stevens, F. C. Calmodulin: An Introduction. *Canadian Journal of Biochemistry and Cell Biology* **1983**, *61* (8), 906–910. doi: 10.1139/o83-115.

(130) Young, R. A. RNA POLYMERASE II. *Annu Rev Biochem* **1991**, *60* (1), 689–715. doi: 10.1146/annurev.bi.60.070191.003353.

(131) Sakurai, H.; Ishihama, A. Gene Organization and Protein Sequence of the Small Subunits of Schizosaccharomyces Pombe RNA Polymerase II. *Gene* **1997**, *196* (1–2), 165–174. doi: 10.1016/S0378-1119(97)00222-9.

(132) Akira, I.; Makoto, K.; Hiroshi, M. Subunits of Yeast RNA Polymerases: Structure and Function. *Curr Opin Microbiol* **1998**, *1* (2), 190–196. doi: 10.1016/S1369-5274(98)80010-6.

(133) Archambault, J.; Friesen, J. D. Genetics of Eukaryotic RNA Polymerases I, II, and III. *Microbiol Rev* **1993**, *57* (3), 703–724. doi: 10.1128/mr.57.3.703-724.1993.

(134) Möller, E. M.; Bahnweg, G.; Sandermann, H.; Geiger, H. H. A Simple and Efficient Protocol for Isolation of High Molecular Weight DNA from Filamentous Fungi, Fruit Bodies, and Infected Plant Tissues. *Nucleic Acids Res* **1992**, *20* (22), 6115–6116. doi: 10.1093/nar/20.22.6115.

(135) Dettman, J. R.; Eggertson, Q. Phylogenomic Analyses of *Alternaria* Section *Alternaria* : A High-Resolution, Genome-Wide Study of Lineage Sorting and Gene Tree Discordance. *Mycologia* **2021**, 1–15. doi: 10.1080/00275514.2021.1950456.

(136) Koren, S.; Walenz, B. P.; Berlin, K.; Miller, J. R.; Bergman, N. H.; Phillippy, A. M. Canu: Scalable and Accurate Long-Read Assembly via Adaptive *k* -Mer Weighting and Repeat Separation. *Genome Res* **2017**, *27* (5), 722–736. doi: 10.1101/gr.215087.116.

(137) Walker, B. J.; Abeel, T.; Shea, T.; Priest, M.; Abouelliel, A.; Sakthikumar, S.; Cuomo, C. A.; Zeng, Q.; Wortman, J.; Young, S. K.; Earl, A. M. Pilon: An Integrated Tool for Comprehensive Microbial Variant Detection and Genome Assembly Improvement. *PLoS One* **2014**, *9* (11), e112963. doi: 10.1371/journal.pone.0112963.

(138) Palmer, J. M.; Stajich, J. Funannotate v1.8.1: Eukaryotic Genome Annotation. Zenodo September 28, 2020. doi: 10.5281/zenodo.4054262.

(139) Gannibal, Ph. B. Polyphasic Approach to Fungal Taxonomy. *Biology Bulletin Reviews* **2022**, *12* (1), 18–28. doi: 10.1134/S2079086422010029.

(140) White, T. J.; Bruns, T.; Lee, S. Amplification and Direct Sequencing of Fungal Ribosomal RNA Genes for Phylogenetics. In *PCR protocols: a guide to methods and applications*; Innis, M. A., Gelfand, D. H., Shinsky, T. J., White, T. J., Eds.; Academic Press Inc.: New York, 1990; pp 315–322.

(141) Glass, N. L.; Donaldson, G. C. Development of Primer Sets Designed for Use with the PCR to Amplify Conserved Genes from Filamentous Ascomycetes. *Appl Environ Microbiol* **1995**, *61* (4), 1323–1330. doi: 10.1128/aem.61.4.1323-1330.1995.

(142) Hong, S.-B.; Cho, H.-S.; Shin, H.-D.; Frisvad, J. C.; Samson, R. A. Novel Neosartorya Species Isolated from Soil in Korea. *Int J Syst Evol Microbiol* **2006**, *56* (2), 477–486. doi: 10.1099/ijs.0.63980-0.

(143) Peterson, S. W.; Vega, F. E.; Posada, F.; Nagai, C. *Penicillium Coffeae,* a New Endophytic Species Isolated from a Coffee Plant and Its Phylogenetic Relationship to *P. Fellutanum, P. Thiersii* and *P. Brocae* Based on Parsimony Analysis of Multilocus DNA Sequences. *Mycologia* **2005**, *97* (3), 659–666. doi: 10.1080/15572536.2006.11832796.

(144) Liu, Y. J.; Whelen, S.; Hall, B. D. Phylogenetic Relationships among Ascomycetes: Evidence from an RNA Polymerse II Subunit. *Mol Biol Evol* **1999**, *16* (12), 1799–1808. doi: 10.1093/oxfordjournals.molbev.a026092.

(145) Houbraken, J.; Spierenburg, H.; Frisvad, J. C. Rasamsonia, a New Genus Comprising Thermotolerant and Thermophilic Talaromyces and Geosmithia Species. *Antonie Van Leeuwenhoek* **2012**, *101* (2), 403–421. doi: 10.1007/s10482-011-9647-1.

(146) Frisvad, J. C.; Filtenborg, O. Classification of Terverticillate Penicillia Based on Profiles of Mycotoxins and Other Secondary Metabolites. *Appl Environ Microbiol* **1983**, *46* (6), 1301–1310. doi: 10.1128/aem.46.6.1301-1310.1983.

(147) Nielsen, K. F.; Smedsgaard, J.; Larsen, T. O.; Lund, F.; Thrane, U.; Frisvad, J. C. Chemical Identification of Fungi: Metabolite Profiling and Metabolomics. In *Fungal Biotechnology in Agricultural, Food, and Environmental Applications*; Arora, D. K., Ed.; Marcel Dekker, Inc.: New York, 2004; pp 19–35.

(148) Schrimpe-Rutledge, A. C.; Codreanu, S. G.; Sherrod, S. D.; McLean, J. A. Untargeted Metabolomics Strategies—Challenges and Emerging Directions. *J Am Soc Mass Spectrom* **2016**, *27* (12), 1897–1905. doi: 10.1007/s13361-016-1469-y.

(149) Lu, W.; Bennett, B. D.; Rabinowitz, J. D. Analytical Strategies for LC–MS-Based Targeted Metabolomics. *Journal of Chromatography B* **2008**, *871* (2), 236–242. doi: 10.1016/j.jchromb.2008.04.031.

(150) De Vos, R. C.; Moco, S.; Lommen, A.; Keurentjes, J. J.; Bino, R. J.; Hall, R. D. Untargeted Large-Scale Plant Metabolomics Using Liquid Chromatography Coupled to Mass Spectrometry. *Nat Protoc* **2007**, *2* (4), 778–791. doi: 10.1038/nprot.2007.95.

(151) Gorrochategui, E.; Jaumot, J.; Lacorte, S.; Tauler, R. Data Analysis Strategies for Targeted and Untargeted LC-MS Metabolomic Studies: Overview and Workflow. *TrAC Trends in Analytical Chemistry* **2016**, *82*, 425–442. doi: 10.1016/j.trac.2016.07.004.

(152) Gorrochategui, E.; Jaumot, J.; Lacorte, S.; Tauler, R. Data Analysis Strategies for Targeted and Untargeted LC-MS Metabolomic Studies: Overview and Workflow. *TrAC Trends in Analytical Chemistry* **2016**, *82*, 425–442. doi: 10.1016/j.trac.2016.07.004.

(153) Esbensen, K. H.; Guyot, D.; Westad, F.; Houmoller, L. P. *Multivariate Data Analysis: In Practice: An Introduction to Multivariate Data Analysis and Experimental Design*, 5th ed.; 2002.

(154) Finking, R.; Marahiel, M. A. Biosynthesis of Nonribosomal Peptides. *Annu Rev Microbiol* **2004**, *58* (1), 453–488. doi: 10.1146/annurev.micro.58.030603.123615.

(155) Walsh, C. T.; O'Brien, R. V.; Khosla, C. Nonproteinogenic Amino Acid Building Blocks for Nonribosomal Peptide and Hybrid Polyketide Scaffolds. *Angewandte Chemie International Edition* **2013**, *52* (28), 7098–7124. doi: 10.1002/anie.201208344.

(156) Bushley, K. E.; Turgeon, B. G. Phylogenomics Reveals Subfamilies of Fungal Nonribosomal Peptide Synthetases and Their Evolutionary Relationships. *BMC Evol Biol* **2010**, *10* (1), 26. doi: 10.1186/1471-2148-10-26.

(157) Süssmuth, R. D.; Mainz, A. Nonribosomal Peptide Synthesis—Principles and Prospects. *Angewandte Chemie International Edition* **2017**, *56* (14), 3770–3821. doi: 10.1002/anie.201609079.

(158) Miller, B. R.; Gulick, A. M. Structural Biology of Nonribosomal Peptide Synthetases; 2016; pp 3–29. doi: 10.1007/978-1-4939-3375-4_1.

(159) Guo, H.; Rao, N. Chorismate-Mutase-Catalyzed Claisen Rearrangement. In *The Claisen Rearrangement: methods and applications*; Hiersemann, M., Nubbemeyer, U., Eds.; John Wiley & Sons, 2007; pp 1–23.

(160) Resende, D. I. S. P.; Boonpothong, P.; Sousa, E.; Kijjoa, A.; Pinto, M. M. M. Chemistry of the Fumiquinazolines and Structurally Related Alkaloids. *Nat Prod Rep* **2019**, *36* (1), 7–34. doi: 10.1039/C8NP00043C.

(161) Yan, D.; Chen, Q.; Gao, J.; Bai, J.; Liu, B.; Zhang, Y.; Zhang, L.; Zhang, C.; Zou, Y.; Hu, Y. Complexity and Diversity Generation in the Biosynthesis of Fumiquinazoline-Related Peptidyl Alkaloids. *Org Lett* **2019**, *21* (5), 1475–1479. doi: 10.1021/acs.orglett.9b00260.

(162) Wang, D.; Neupane, P.; Ragnarsson, L.; Capon, R.; Lewis, R. Synthesis of Pseudellone Analogs and Characterization as Novel T-Type Calcium Channel Blockers. *Mar Drugs* **2018**, *16* (12), 475. doi: 10.3390/md16120475.

(163) Netz, N.; Opatz, T. Marine Indole Alkaloids. *Mar Drugs* **2015**, *13* (8), 4814–4914. doi: 10.3390/md13084814.

(164) Campos, P.-E.; Pichon, E.; Moriou, C.; Clerc, P.; Trépos, R.; Frederich, M.; De Voogd, N.; Hellio, C.; Gauvin-Bialecki, A.; Al-Mourabit, A. New Antimalarial and Antimicrobial Tryptamine Derivatives from the Marine Sponge Fascaplysinopsis Reticulata. *Mar Drugs* **2019**, *17* (3), 167. doi: 10.3390/md17030167.

(165) Ames, B. D.; Haynes, S. W.; Gao, X.; Evans, B. S.; Kelleher, N. L.; Tang, Y.; Walsh, C. T. Complexity Generation in Fungal Peptidyl Alkaloid Biosynthesis: Oxidation of Fumiquinazoline A to the Heptacyclic Hemiaminal Fumiquinazoline C by the Flavoenzyme Af12070 from *Aspergillus Fumigatus*. *Biochemistry* **2011**, *50* (40), 8756–8769. doi: 10.1021/bi201302w.

(166) Ames, B. D.; Walsh, C. T. Anthranilate-Activating Modules from Fungal Nonribosomal Peptide Assembly Lines. *Biochemistry* **2010**, *49* (15), 3351–3365. doi: 10.1021/bi100198y.

(167) Ames, B. D.; Liu, X.; Walsh, C. T. Enzymatic Processing of Fumiquinazoline F: A Tandem Oxidative-Acylation Strategy for the Generation of Multicyclic Scaffolds in Fungal Indole Alkaloid Biosynthesis. *Biochemistry* **2010**, *49* (39), 8564–8576. doi: 10.1021/bi1012029.

(168) Haynes, S. W.; Ames, B. D.; Gao, X.; Tang, Y.; Walsh, C. T. Unraveling Terminal C-Domain-Mediated Condensation in Fungal Biosynthesis of Imidazoindolone Metabolites. *Biochemistry* **2011**, *50* (25), 5668–5679. doi: 10.1021/bi2004922.

(169) Walsh, C. T.; Haynes, S. W.; Ames, B. D.; Gao, X.; Tang, Y. Short Pathways to Complexity Generation: Fungal Peptidyl Alkaloid Multicyclic Scaffolds from Anthranilate Building Blocks. *ACS Chem Biol* **2013**, *8* (7), 1366–1382. Doi: 10.1021/cb4001684.

(170) Samson, R. A.; Pitt, J. I. Advances in Penicillium and Aspergillus Systematics; Samson, R. A., Pitt, J. I., Eds.; NATO ASI series. Series A, Life sciences; v. 102; Plenum Press: New York, 1985.

(171) Witte, T. E.; Overy, D. P. Untargeted Metabolomic Profiling of Fungal Species Populations; 2022; pp 349–365. doi: 10.1007/978-1-0716-2124-0_24.

(172) Larsen, T. O.; Franzyk, H.; Jensen, S. R. UV-Guided Isolation of Verrucines A and B, Novel Quinazolines from *Penicillium v Errucosum* Structurally Related to Anacine from *Penicillium a Urantiogriseum*. *J Nat Prod* **1999**, *62* (11), 1578–1580. doi: 10.1021/np990251p.

(173) Zhelifonova, V. P.; Antipova, T. V; Kozlovskiĭ, A. G. [Biosynthesis of Fumiquinazolines by the Fungus Penicillium Thymicola]. *Prikl Biokhim Mikrobiol* **2012**, *48* (3), 334–339.

(174) Tang, M.; Zou, Y.; Yee, D.; Tang, Y. Identification of the Pyranonigrin A Biosynthetic Gene Cluster by Genome Mining in *Penicillium Thymicola* IBT 5891. *AIChE Journal* **2018**, *64* (12), 4182–4186. doi: 10.1002/aic.16324.

(175) Ropars, J.; Didiot, E.; Rodríguez de la Vega, R. C.; Bennetot, B.; Coton, M.; Poirier, E.; Coton, E.; Snirc, A.; Le Prieur, S.; Giraud, T. Domestication of the Emblematic White Cheese-Making Fungus Penicillium Camemberti and Its Diversification into Two Varieties. *Current Biology* **2020**, *30* (22), 4441-4453.e4. doi: 10.1016/j.cub.2020.08.082.

(176) Blin, K.; Shaw, S.; Augustijn, H. E.; Reitz, Z. L.; Biermann, F.; Alanjary, M.; Fetter, A.; Terlouw, B. R.; Metcalf, W. W.; Helfrich, E. J. N.; van Wezel, G. P.; Medema, M. H.; Weber, T. AntiSMASH 7.0: New and Improved Predictions for Detection, Regulation, Chemical Structures and Visualisation. *Nucleic Acids Res* **2023**, *51* (W1), W46–W50. doi: 10.1093/nar/gkad344.

(177) Medema, M. H.; Blin, K.; Cimermancic, P.; de Jager, V.; Zakrzewski, P.; Fischbach, M. A.; Weber, T.; Takano, E.; Breitling, R. AntiSMASH: Rapid Identification, Annotation and Analysis of Secondary Metabolite Biosynthesis Gene Clusters in Bacterial and Fungal Genome Sequences. *Nucleic Acids Res* **2011**, *39* (suppl_2), W339–W346. doi: 10.1093/nar/gkr466.

(178) Yee, D. A.; Niwa, K.; Perlatti, B.; Chen, M.; Li, Y.; Tang, Y. Genome Mining for Unknown–Unknown Natural Products. *Nat Chem Biol* **2023**, *19* (5), 633–640. doi: 10.1038/s41589-022-01246-6.

(179) Butt, T. M.; Wang, C.; Shah, F. A.; Hall, R. DEGENERATION OF ENTOMOGENOUS FUNGI. In *An Ecological and Societal Approach to Biological Control*; Eilenberg, J., Hokkanen, H. M. T., Eds.; Springer Netherlands: Dordrecht, 2006; pp 213–226. Doi: 10.1007/978-1-4020-4401-4_10.

(180) Xie, H.; Ma, Q.; Wei, D.-Z.; Wang, F.-Q. Transcriptomic Analysis of Aspergillus Niger Strains Reveals the Mechanism Underlying High Citric Acid Productivity. *Bioresour Bioprocess* **2018**, *5* (1), 21. doi: 10.1186/s40643-018-0208-6.

(181) Jin, F. J.; Takahashi, T.; Matsushima, K.; Hara, S.; Shinohara, Y.; Maruyama, J.; Kitamoto, K.; Koyama, Y. SclR, a Basic Helix-Loop-Helix Transcription Factor, Regulates Hyphal Morphology and Promotes Sclerotial Formation in Aspergillus Oryzae. *Eukaryot Cell* **2011**, *10* (7), 945–955. doi: 10.1128/EC.00013-11.

(182) Zhong, Y.; Lu, X.; Xing, L.; Ho, S. W. A.; Kwan, H. S. Genomic and Transcriptomic Comparison of *Aspergillus Oryzae* Strains: A Case Study in Soy Sauce Koji Fermentation. *J Ind Microbiol Biotechnol* **2018**, *45* (9), 839–853. doi: 10.1007/s10295-018-2059-8.

(183) Martzy, R.; Mello-de-Sousa, T. M.; Mach, R. L.; Yaver, D.; Mach-Aigner, A. R. The Phenomenon of Degeneration of Industrial Trichoderma Reesei Strains. *Biotechnol Biofuels* **2021**, *14* (1), 193. doi: 10.1186/s13068-021-02043-4.

(184) Clutterbuck, P. W.; Lovell, R.; Raistrick, H. Studies in the Biochemistry of Micro-Organisms. *Biochemical Journal* **1932**, *26* (6), 1907–1918. doi: 10.1042/bj0261907.

(185) Douma, R. D.; Batista, J. M.; Touw, K. M.; Kiel, J. A.; Krikken, A. M.; Zhao, Z.; Veiga, T.; Klaassen, P.; Bovenberg, R. AL; Daran, J.-M.; Heijnen, J. J.; van Gulik, W. M. Degeneration of Penicillin Production in Ethanol-Limited Chemostat Cultivations of Penicillium Chrysogenum: A Systems Biology Approach. *BMC Syst Biol* **2011**, *5* (1), 132. doi: 10.1186/1752-0509-5-132.

(186) Righelato, R. C. Selection of Strains of *Penicillium Chrysogenum* with Reduced Penicillin Yields in Continuous Cultures. *Journal of Applied Chemistry and Biotechnology* **1976**, *26* (3), 153–159. doi: 10.1002/jctb.5020260309.

(187) Robin, J.; Lettier, G.; McIntyre, M.; Noorman, H.; Nielsen, J. Continuous Cultivations of a *Penicillium Chrysogenum* Strain Expressing the Expandase Gene from *Streptomyces Clavuligerus* : Growth Yields and Morphological Characterization. *Biotechnol Bioeng* **2003**, *83* (3), 361–368. doi: 10.1002/bit.10677.

(188) Künkel, W.; Berger, D.; Risch, S.; Wittmann-Bresinsky, B. Genetic Instability of Industrial Strains of Penicillium Chrysogenum. *Appl Microbiol Biotechnol* **1992**, *36* (4). doi: 10.1007/BF00170191.

(189) Kale, S.; Bennett, J. W. Strain Instability in Filamentous Fungi. In *Handbook of Applied Mycology: Volume 5: Mycotoxins in Ecological Systems*; Bhatnagar, D., Lillehoj, E. B., Arora, D. K., Eds.; Marcel Dekker: New York, 1991; Vol. 5, pp 311–331.

(190) Losada, L.; Ajayi, O.; Frisvad, J. C.; Yu, J.; Nierman, W. C. Effect of Competition on the Production and Activity of Secondary Metabolites in *Aspergillus* Species. *Med Mycol* **2009**, *47* (s1), S88–S96. doi: 10.1080/13693780802409542.

(191) Chatterjee, S.; Kuang, Y.; Splivallo, R.; Chatterjee, P.; Karlovsky, P. Interactions among Filamentous Fungi Aspergillus Niger, Fusarium Verticillioides and Clonostachys Rosea: Fungal Biomass, Diversity of Secreted Metabolites and Fumonisin Production. *BMC Microbiol* **2016**, *16* (1), 83. doi: 10.1186/s12866-016-0698-3.

(192) Horgen, P. A.; Carvalho, D.; Sonnenberg, A.; Li, A.; Van Griensven, L. J. L. D. Chromosomal Abnormalities Associated with Strain Degeneration in the Cultivated Mushroom,Agaricus Bisporus. *Fungal Genetics and Biology* **1996**, *20* (3), 229–241. doi: 10.1006/fgbi.1996.0038.

(193) Wang, C.; Skrobek, A.; Butt, T. M. Concurrence of Losing a Chromosome and the Ability to Produce Destruxins in a Mutant of *Metarhizium Anisopliae*. *FEMS Microbiol Lett* **2003**, *226* (2), 373–378. doi: 10.1016/S0378-1097(03)00640-2.

(194) Larsen, T. O.; Smedsgaard, J.; Nielsen, K. F.; Hansen, M. E.; Frisvad, J. C. Phenotypic Taxonomy and Metabolite Profiling in Microbial Drug Discovery. *Nat Prod Rep* **2005**, *22* (6), 672. doi: 10.1039/b404943h.

(195) Manni, M.; Berkeley, M. R.; Seppey, M.; Zdobnov, E. M. BUSCO: Assessing Genomic Data Quality and Beyond. *Curr Protoc* **2021**, *1* (12). doi: 10.1002/cpz1.323.

(196) Health Canada. *Information Document on Health Canada's Proposed Maximum Limits (Standards) for the Presence of Mycotoxin Ochratoxin A in Foods*; Ottawa, 2009.

(197) EU Commission. *Commission Regulation No 1881/2006 as Regards Maximum Levels of Ochratoxin A in Certain Foodstuffs*; European Food Safety Authority: Brussels, 2022; pp 1–4.

(198) IARC Working Groupe on the Evaluation of Carcinogenic Risks to Humans. OCHRATOXIN A. In *Some Naturally Occurring Substances: Food Items and Constituents, Heterocyclic Aromatic Amines and Mycotoxins*; International Agency for Research on Cancer: Lyon, 1993; Vol. 56.